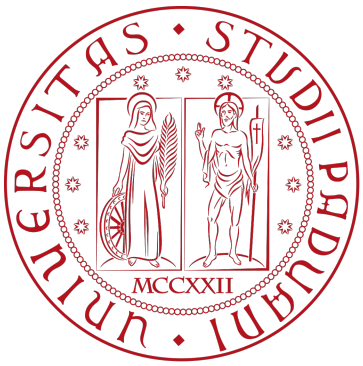

UNIVERSITÀ DEGLI STUDI DI PADOVA

Dipartimento di Fisica e Astronomia "Galileo Galilei"

Master Degree in Physics

Final Dissertation

Opto-microfluidic device in Lithium Niobate to investigate the proteins synthesis

Thesis supervisor

Prof. Cinzia Sada

Thesis co-supervisors

Dr. Leonardo Zanini

Dr. Annamaria Zaltron

Candidate

Enrico Turato

Academic Year 2020/2021

Abstract

Microfluidics is an interdisciplinary research field that deals with the production and the study of droplets on a micrometric scale. In the last decades microfluidics has gained an increasing interest by the scientific community. Microfluidics has arisen great attention since it controls the transport of small amounts of liquids inside which, for example, it is possible to make chemical reactions occur or through which is possible to transport biological samples or diagnostic markers. Their features, in combination with fast analysis tools, allow for the realization of Lab-on-a-Chips (LOCs) that is to say miniaturized and portable devices able to perform chemical, biological, environmental or medical analyses where bulky laboratory facilities lack. As a matter of fact in microfluidics' standards, imaging techniques are exploited to monitor the droplets generation and/or movement. In these cases, however, bulky microscopes eliminate the obtained advantages with miniaturization.

For this reason, it is important to integrate completely on a small scale the optical stage with the microfluidic one achieving a so called opto-microfluidic platform, an objective accomplished in the last few years, for example, through the realization of Lab-On-a-Chip in Lithium Niobate in the Physics and Astronomy department "Galileo Galilei", in Padua. This material has excellent optical properties that consent to host the realization of Ti-indiffused waveguides, by which it is possible to detect the produced droplets and their contents in the engraved microfluidic channel as it will be shown in this thesis.

This thesis presents a feasibility study on the use of integrated optics coupled to microfluidics circuitry to investigate the proteins synthesis. Since the process of the protein synthesis could be difficult and require several days, it is important to save as much as possible of the biological samples, by periodically monitoring its concentration both after the final purification process, and during the subsequent experiments. However, this usually implies the use (and waste) of a significant amount of the sample, so that often a compromise between these two aspects has to been found. On the contrary, in principle the use of the opto-microfluidic approach presented in this thesis would allow to comply with both the mentioned needs, since the monitoring of the protein concentration would be realized in a fast ways and without requiring large amount of the biological samples. Moreover, it can allow to monitor the effect of each update that can be introduced to the process to improve the synthesis or add extra elements into the proteins.

The work-plan of the thesis includes the realization and validation of the opto-microfluidic platform and the application to the detection of proteins. It consists of the characterization of various experimental setups until reaching the best configuration to monitor droplets containing proteins and a reagent called Bradford through a completely integrated opto-microfluidic device in Lithium Niobate. The study is aimed at understanding how proteins' synthesis can be monitored even in small amounts as some confined in a micrometric droplet.

The thesis aims to demonstrate that, by investigating how the protein-based droplet interacts with a light beam. It will be demonstrated that depending on the measurement of the optical transmission of such a droplet it is possible to detect if and when the protein has been synthesized. The final aim of the project, this thesis is included in, is the obtainment of a qualitative proteins detector.

The presence of the proteins in the dispersed phase is evaluated by means of the transmitted light using a systematic measurement protocol and having good control on the experimental apparatus thanks to the detailed characterization. The results obtained show that it is possible for our setup to detect qualitatively the presence of proteins in micrometric droplets.

Contents

List of Figures

List of Tables

Introduction

The lab-on-a-chip technology is changing the way of doing analysis in several application fields, from biology to chemistry and much more. The idea of holding a laboratory in our hands is representing a major technological breakthrough. Indeed, the possibility of having a diagnostic tool in our pockets could have a great impact on the life quality in the future.
It could be of significant interest the production and the detection of droplets containing various elements such as synthesized proteins. This could be a multidisciplinary research field that spans various sciences like chemistry, physics and engineering, with the aim of controlling matter at human cell-like dimensions. Many possible applications emerge thanks to the transition to the micro-scale; for more details on this regard see for example [2]. Talking about medical field, they can have important biomedical applications both at diagnostic level (identification of damaged tissues) and for selective therapy (drug transport).
Lab-on-a-chip can be described as a miniaturized device, where multiple tools are integrated together into a single chip. Since the emerging interest in Lab-On-a-Chip (LOC) applications, the demand for a high multi functional and portable device in order to increase the achievement of complex laboratories analysis on a small size chips has grown. This need pushed the research to integrate in the same substrate several tools with different tasks, and consequently, the requirements of the material exploited became rapidly more restricted. In particular, the performances of multiple toolkit device are related to its capabilities of combining and matching stages, thus avoiding any detrimental interference between the material properties needed for their realization.
During the last decades, several materials have been proposed for the combination of different tools on the same device, one of them being Lithium Niobate ($LiNbO_3$) as a valid possibility for a monolithic substrate in LOC applications [1], [2]. This material is well-known in the field of integrated optics due to its interesting optical properties that brought it to be the main component in optical modulators in the telecommunication devices. The excellent performances in this field can be combined to the microfluidics for the realization of reliable opto-microfluidic stages for LOC applications.
The development of these devices is driven by the various advantages provided by this technology compared to standard ones. Among these, one of the most evident is the compactness of a few centimeters chip in comparison to big laboratory instruments, guaranteeing more handling and the possibility to do complex operations and also an improved portability. These devices could be much more affordable than a full laboratory setup both in terms of cost and solutions consumption.
Moreover once a reliable build for the chip is reached the eventual sources of human errors could be greatly reduced due to the high automation of it. These features make lab-on-a-chips really interesting for different applications and in some of them they might even show superior performances than conventional systems.
By thinking for example to glucose monitoring devices or HIV detection and heart diagnostics we see that the commercialization of devices have already started. By the way it is clear that many lab-on-a-chips still have to be optimized to become commercially available.
In this framework, this thesis work is therefore part of a wide-ranging research program that aims to develop an integrated opto-microlfluidic platform thanks to which it is possible to identify, select and divide by size and characteristics objects of microscopic dimension immersed in a fluid. Another example of this kind of work can be found in [16]. This thesis is structured as follows:

Chapter 1 An explanation of the "biological problem" is inserted at the beginning of this chapter, in which I discuss about the biological problem and why microfluidic is important if related to biological applications and the possibility to obtain a qualitative detector to look for presence or absence of proteins in micrometric fluid volumes. Our physical solution to the biological problem is outlined, that is to say the motivation and the aim of this work. Finally some interesting information about the B.S.A. protein are included.

Chapter 2 The properties of Lithium Niobate are described in a general way: the chemical composition, the crystalline structure and all the physical properties that characterize this composite material that is to say the optical properties, the electro-optic, the piezoelectric, the pyroelectric, the photovoltaic effects and finally the photorefractive effect.

Chapter 3 All the steps that led to the fabrication of the microfluidic circuit in Lithium Niobate are mentioned here. First talking about all the procedures required for the realization of the Ti-indiffused wave guides. Then I describe the engraving of the microfluidic channel on the substrate and finally the enclosure and the functionalization of the chip are presented.

Chapter 4 Some general microfluidic notions are reported, like the various types of droplets generators, the many regimes of flowing and finally some theoretical information are exposed concerning the microfluidics and the formation of droplets inside a T-junction.

Chapter 5 The final configuration of the apparatus is presented. A section dedicated to the Bradford reagent and the Bradford assay method is included. Also the protocol for the detection of the protein with the chosen apparatus is described and some data are presented.

Chapter 6 In this chapter the conclusions to this thesis are inserted.

Chapter 7 Here some notions regarding possible steps towards a calibration of the apparatus are presented. In order to obtain a quantitative estimate of the concentration of proteins inside droplets some issues need to be addressed.

Appendix Other explored configurations of the setup for the production of droplets are described plus a detailed characterization for each of the setup is analyzed exposing advantages and drawbacks and the reasons for putting them aside.

Chapter 1

The "biological problem" and our physical solution to it

1.1 The problem and our solution

When making a synthesis of any protein, at the end of the preparation process it is important to quantify the amount of biological sample (protein) obtained, because this parameter plays a key role in carrying out the subsequent biochemical reactions and related analyzes.
Different methods can be used to determine the concentration of protein present in the solution: for example, gel staining with Coomassie Blue or with silver, which is however expensive and often dependent on the solution in which the protein is found; or instruments based on optical absorption by the sample, such as the ThermoFisher "nanodrop" or infrared spectrophotometers, which are however expensive and not compact.
A low cost alternative that is widely used for different types of proteins (usually larger than 3KDalton) is represented by colorimetric methods, such as the Bradford method [3], in which the biological sample containing the protein is "colored" by means of the addition of a suitable reagent and its optical absorption at a given wavelength is measured (more details regarding the Bradford reagent and the Bradford protein assay in the section 5.2).
In colorimetric techniques, which are particularly suitable for the case of proteins in solution, external standards are used to create a calibration curve which is then used to estimate the concentration of protein in the solution being studied. Specifically, the most widely used standard is the Bovine Serum Albumin protein (B.S.A.), because it is very stable and not very reactive.
The disadvantage of the Bradford method is that it requires the use of quantities of protein solution usually of several hundreds of μl, which then cannot be recovered, and of spectrophotometers for optical absorption measurements.
To test the correct functioning of our chip, the B.S.A. protein [4] was used, this being the universal standard used for quantitative measurements of protein concentration.
To provide for a solution to this problem, the use of an opto-microfluidic platform is proposed, in order to obtain a qualitative integrated proteins detector. The aim of the thesis is therefore the creation of an opto-microfluidic device that allows on the one hand to estimate the concentration of proteins in a solution via spectroscopic assays which need only a small amount of the biological sample (μl), thus reducing the wasting of the prepared protein, and on the other to carry out optical absorption measurements through a compact and portable chip that does not requires the use of bulky spectrophotometers.
To reach this goal, the characterization of various experimental setups until reaching the best configuration to monitor droplets containing proteins and a reagent called Bradford through a completely integrated opto-microfluidic device in Lithium Niobate is required.
The thesis aims to demonstrate that depending on the measurement of the optical transmission of such a droplet, so by investigating how the protein-based droplet interacts with a light beam, it is possible

to detect if and when the protein has been synthesized. The final aim of the project, within which this thesis is inserted, is the obtainment of a qualitative proteins detector and also the identification of a precise microfluidic protocol to facilitate the measures, that is to say the optimal microfluidic conditions under which protein detection is successfully achieved and optimized.
Since the process of the protein synthesis could be difficult and require several days, it is important to save as much as possible of the biological samples, by periodically monitoring its concentration both after the final purification process, and during the subsequent experiments. However, this usually implies the use (and waste) of a significant amount of the sample, so that often a compromise between these two aspects has to been found. On the contrary, in principle the use of the opto-microfluidic approach presented in this thesis would allow to comply with both the mentioned needs, since the monitoring of the protein concentration would be realized in a fast ways and without requiring large amount of the biological samples.

1.2 The B.S.A. protein

Serum albumin (SA) [4] is the most abundant plasma protein in mammals. When one refers to cattle, we talk about the Bovine Serum Albumine (B.S.A.); it is crystallized in a monoclinic crystal form and has a crystallization temperature of 16 °C.
Without entering too much in detail (for which one can refers to the paper [4]), it is synthesized in the liver and exported into the plasma, where it reaches a high concentration (ca. 0.6 mM).
Talking in general of Serum Albumine, it is a multifunctional protein with extraordinary ligand binding capacity, making it a transporter molecule for a diverse range of metabolites, drugs, nutrients, metals and other molecules.
Due to its ligand binding properties, albumins have wide clinical, pharmaceutical, and biochemical applications. Albumins are also allergenic, and exhibit a high degree of cross-reactivity due to significant sequence and structure similarity of SAs from different organisms. Albumins can act as allergens either through ingestion (meat, milk, eggs) or inhalation.
Talking a bit about the structure, Serum Albumins are relatively large (molecular weight of around 66 kDalton) and negatively charged proteins. Albumins are initially expressed in vivo, as preproalbumins. The bovine preproalbumin is 607 amino acids long; instead the corresponding mature protein is comprised of 583 amino acids. SAs are heart-shaped and comprise three helical domains, each comprising two subdomains, as can be seen in Figure 1.1.

Figure 1.1: The image (taken from [4]) represents the B.S.A. molecular structure, the domain and secondary structure element. Each domain is marked with a different color, and each subdomain is marked with a different shade.

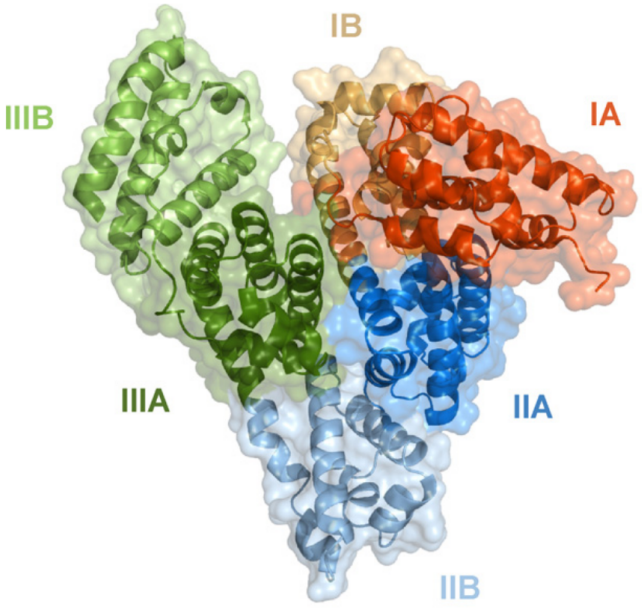

Chapter 2

Lithium Niobate

2.1 Introduction

In this chapter the summarized main characteristics and the physical properties of Lithium Niobate crystals are presented. For a description with much more details one can refer to the following works, from which what follows is based on: [1], [2], [6], [13].
The success gained by Lithium Niobate is due to the large variety of properties which allow for realizing platforms useful in a wide applications range. The combination of its optical properties with the microfluidic tools can lead to big development. Optofluidics fast development has carried to the realization of several lab-on-a-chips, which require the integration of multiple stages on the same compact substrate. This feature can be satisfied using for example a monolithic $LiNbO_3$ substrate.

2.2 Chemical composition

Lithium Niobate ($LiNbO_3$) is a synthetic material originating from the Li_2O - Nb_2O_5 system. It is colorless and insoluble both in water and in organic solvents; it has excellent chemical stability. As can be seen from the phase diagram in Figure 2.1 there is a wide range of solubility of the two oxides at high temperatures, whose solid-liquid curve shows a maximum at 48.38% of Li_2O. Crystals with this composition are called congruent and have a Li-deficient structure compared to stoichiometric crystals for which instead the percentages of Li_2O and Nb_2O_5 are equal to 50%.

Figure 2.1: Phase diagram of the Li_2O - Nb_2O_5 system near the congruent and stoichiometric composition of $LiNbO_3$.

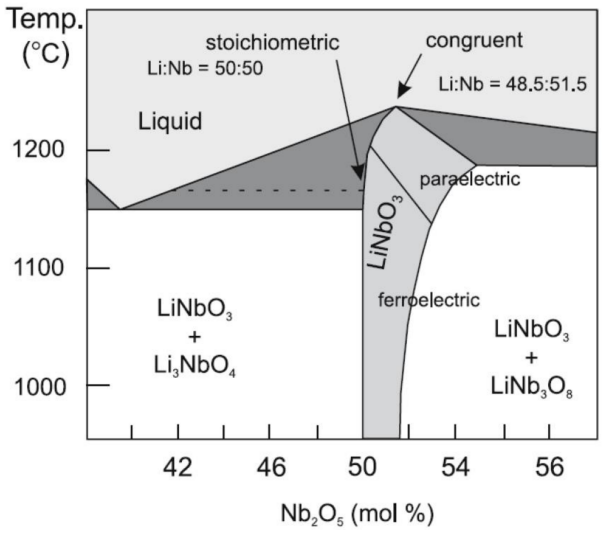

Talking about the congruent Lithium Niobate, the melted and the solid crystals have the same composition, which is advantageous because it allows to obtain the best possible uniformity in the product. This is important because many properties depend on the ratio between the concentrations of Li and Nb, e.g. phase transition temperature, phase matching temperature and position of the UV absorption edge [13]. As a result, due to the high sensitivity to compositional changes and due to the high stability achieved during the growth process, most commercial products are available in congruent composition.

2.3 A look at the crystal

To give a description of the structure of the crystal in the trigonal system, the definition of the crystallographic axes must be precise and not ambiguous so three different cells can be chosen: hexagonal, rhombohedral or orthohexagonal which are represented in Figure 2.2. In most applications the ortohexagonal is preferred for simplicity. In this configuration, the $\hat{z}$ axis is identified by the optical main axis $\hat{c}$, the $\hat{y}$ axis lies on a specular reflection plane and consequently the $\hat{x}$ axis is identified. The positive direction of the $\hat{z}$ and $\hat{y}$ axes is conventionally established as the one pointing towards the surface of the crystal that is negatively charged under a compressive action along the relative axes ($\hat{z}$ and $\hat{y}$ are therefore piezoelectric directions). Moreover, the $\hat{z}$ axis is pyroelectric and the positive direction is the one towards the surface that is positively charged by cooling the crystal [13].

Figure 2.2: Unitary hexagonal cell with symmetry planes and Cartesian reference system (left), rhombohedral cell (center) and orthohexagonal cell (right).

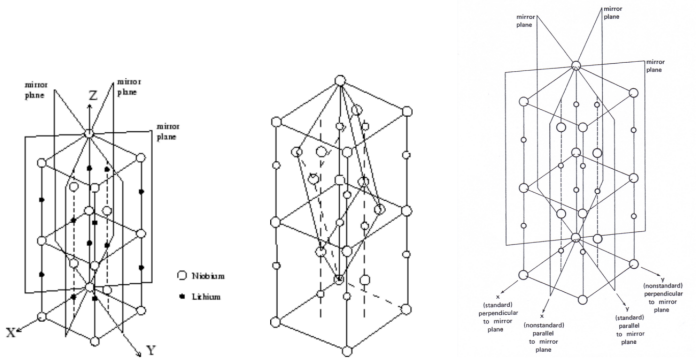

Lithium Niobate is a ferroelectric material, i.e. it has a spontaneous polarization that can be reversed by applying an electric field of certain magnitude. However, this property only exists below a critical temperature called Curie temperature, T≈ 1210 °C, beyond which the material, with the disappearance of spontaneous polarization, becomes paraelectric. The crystalline structure of Lithium Niobate is different depending on whether the material is above or below this critical temperature. As shown in Figure 2.3, in the para-electric phase ($T > T_C$) it consists in equidistant oxygen planes, where oxygen coordinates in triangular configurations rotated by approximately 180°; Li ions are located in the center of the oxygen triangle, while Nb ions are located at the center of an octahedron formed by two triangles. In the ferroelectric phase ($T < T_C$) the structure of the lattice is slightly different: ions move from the positions mentioned above along the optical axis $\hat{c}$ of the material giving rise to non-zero net electrical polarization within the material. In this phase the crystal exhibits a mirror symmetry about three planes that are 60° apart. The axis obtained by their intersection is the center for a three-fold rotational symmetry of the crystal. In the ferroelectric phase the interstitial sites of the octahedrons of oxygen are one third filled with Niobium atoms, one third with Lithium atoms and one third are empty, according to the sequence Nb-Li-V (where V stands for vacancy). In Lithium Niobate with congruent composition, moreover, some of the atoms of Nb in the material occupy the lattice site of Li remained empty because of the lower presence of Li in the material compared to the stoichiometric composition: these atoms are called Nb antisites, Nb_{Li}.

Figure 2.3: Compositional structure of Lithium Niobate and the sketched positions of Li and Nb atoms with respect to the oxygen planes for the paraelectric (left) and ferroelectric phase (right).

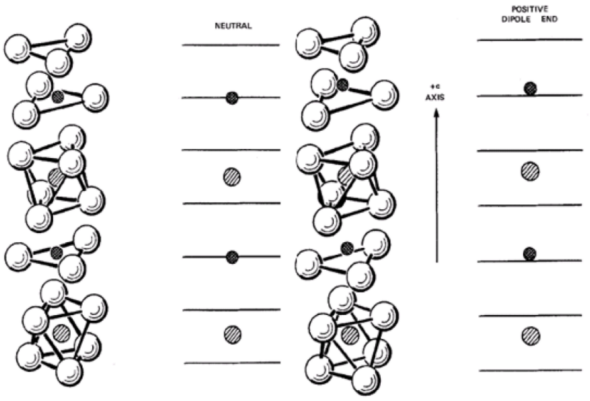

2.4 Physical properties

Lithium Niobate has many physical and optical properties. In the following the main features will be presented.

2.4.1 Optical properties

The peculiar structure of Lithium Niobate brings out a lot of physical properties. In particular, its optical unique features make it a well-known and widely exploited material in the field of optics. Pure material is almost transparent in the spectral region from 0.35 μm to 5 μm. In the standard orthohexagonal cell reference framework, the permittivity tensor points out its birefringence:

$$\bar{\bar{\epsilon}} = \begin{bmatrix} \epsilon_{11} & 0 & 0 \\ 0 & \epsilon_{11} & 0 \\ 0 & 0 & \epsilon_{33} \end{bmatrix} \tag{2.1}$$

where the two indices of refraction follows: the ordinary $n_0 = \sqrt{\frac{\epsilon_{11}}{\epsilon_0}}$ that is the index of refraction seen by light polarized in any direction perpendicular to the c-axis, and the extraordinary $n_e = \sqrt{\frac{\epsilon_{33}}{\epsilon_0}}$ seen by c-axis polarized light. Both indices axis, and the extraordinary depend strongly on extrinsic impurities, and this feature makes Lithium Niobate a flexible optical material with tailored properties. As optical material, the dispersion relationship of both index of refraction can be approximated by the Sellmeier equation. The accuracy depends on the range of the wavelength and the composition respectively.

2.4.2 Electro-optic effect

Both indices of refraction of the material can be modified by applying an electric field. The effect is described by a variation in the second order tensor $\Delta\left(\frac{1}{n^2}\right)_{ij}$:

$$\Delta\left(\frac{1}{n^2}\right)_{ij} = \Sigma_k r_{ijk} E_k + \Sigma_{kl} s_{ijkl} E_{kl} + ... \tag{2.2}$$

the two tensors r_{ijk} and s_{ijkl} depend on the material, i.e. structure and they refer to the linear or quadratic behavior of the material, usually called Pockels effect and Kerr-effect, respectively. Lithium Niobate exhibits only the Pockels effect and the Pockels' tensor can be simplified, due to its symmetric

structure, as follows:

$$r = \begin{bmatrix} 0 & -r_{22} & r_{13} \\ 0 & r_{22} & r_{13} \\ 0 & 0 & r_{33} \\ 0 & r_{42} & 0 \\ r_{42} & 0 & 0 \\ -r_{22} & 0 & 0 \end{bmatrix} \tag{2.3}$$

where the values of the coefficients are showed in the Table 2.1:

Table 2.1: This table contains the values of the coefficients of the tensor that summarize the properties of the Pockels effect.

r_{13}	$8.6 \cdot 10^{-12}$ mV^{-1}
r_{22}	$3.4 \cdot 10^{-12}$ mV^{-1}
r_{33}	$30.8 \cdot 10^{-12}$ mV^{-1}
r_{42}	$28 \cdot 10^{-12}$ mV^{-1}

2.4.3 Pyroelectric effect

The peculiar structure of Lithium Niobate is really sensitive to the temperature, as long as the position of Li and Nb sites are temperature dependent. The spontaneous polarization (ΔP) of the material changes accordingly with temperature (ΔT):

$$\Delta P = \hat{p}\Delta T \tag{2.4}$$

with $\hat{p}$=(0,0,p_3) where p_3 = -4 $\cdot$ 10^{-5} Cm^{-2}K and $\hat{p}$ is called the pyroelectric tensor. As expected, the only non-negligible component is the one corresponding to the direction where Li and Nb can easily shift respect to the paraelectric phase.

2.4.4 Piezoelectric effect

The spontaneous polarization $\vec{P}$ can also change by applying a stress. It emerges that (considering the orthogonal cell system):

$$P_i = \Sigma_{jk} d_{ijk} \sigma_{jk} \tag{2.5}$$

with

$$d = \begin{bmatrix} 0 & 0 & 0 & 0 & d_{15} & -2d_{22} \\ -d_{22} & d_{22} & 0 & d_{15} & 0 & 0 \\ d_{31} & d_{31} & d_{33} & 0 & 0 & 0 \end{bmatrix} \tag{2.6}$$

where P_i is the induced polarization in the i direction, σ_{jk} is the stress tensor and d_{ijk} is the piezoelectric one, which has only four independent components, due to the $LiNbO_3$ symmetry. The tensor d describes also the converse effect: i.e. the crystal shows a strain under the application of an external electric field.

2.4.5 Photovoltaic effect

The non-centrosymmetric structure leads typically to a photovoltaic effect, that is the current from the electrons excited from absorbing center in the material by way of optical interaction, and their movement to the neighboring ions in a preferential direction. The photovoltaic effect in $LiNbO_3$ was discovered in 1974, observing a stationary current in the material exposed to light. This current is proportional to the light intensity,the absorption coefficient and to the wavelength:

$$j_{phv,i} = \beta_{ijk} e_j e_k^* I = \alpha k_{G,ijk} e_j e_k^* I \tag{2.7}$$

where β_{ijk} is the complex photovoltaic tensor ($\beta_{ijk} = \beta_{ijk}^*$), e is the versor of the light field.

2.4.6 Photorefractive effect

The combination of electro-optic and photovoltaic effects leads the material to exhibit the peculiar mechanism of photorefractivity. This phenomenon consists of the change of the index of refraction of a material exposed to light illumination. If the material is illuminated by a non-uniform pattern of light, the photoinduced carries can freely move in the material. These carriers can be trapped in the interbands levels, like intrinsic or extrinsic impurities, resulting in a non uniform charge distribution, which leads to the rising up of an internal space-charge electric field. This photoinduced electric field modulates consequently the index of refraction by means of the electro-optic effect. The key role in observing this effect is therefore played by donor and acceptor centers in the material. In Lithium Niobate the niobium antisite has the double role of donor state, since Nb^{4+} acts as a donor state and Nb^{5+} as a acceptor state respectively. Indeed, it is crucial the presence of intrinsic or extrinsic impurities with two valence states for photorefractivity. One of the most common doping to enhance the effect is iron doping with the two states Fe^{2+} as a donor and Fe^{3+} as an acceptor.

Chapter 3

Microfluidic circuit fabrication in Lithium Niobate

3.1 Introduction to the fabrication of the chip

The chip reported in Figure 3.1 is an example of the real opto-microfluidic sample in Lithium Niobate which integrates completely on the same substrate a microfluidic stage, consisting of two microfluidic channels arranged in a cross, and an optical stage, represented by an array of light guides. Such light guides are parallel to each other and placed near the surface (with depth of a few μm), perpendicular to the longest microfluidic channel such that they are interrupted in the middle as can be seen in Figure 3.2.

Figure 3.1: An example of the opto-microfluidic chip after the fabrication process and ready to be installed in the final setup.

Figure 3.2: A scheme of the chip in which can be distinguished the array of light guides (not in scale). The black cross refers to the fact that one of the arm of the T-junction has been closed during each of our measurements.

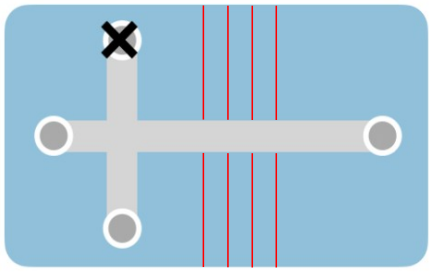

In order to obtain the opto-microfluidic device in question (Figure 3.1) there is a precise protocol to follow based on various steps. In the following a short summary of the optimized platform will be reported as the following previous works [1], [2] and [16]. The steps turn out to be in succession:

- creation of a parallel array of light guides;
- creation of a cross junction of microfluidic channels;
- sealing (either with glass or other cases) of the sample;
- functionalization of the channel to make its walls hydrophobic.

The samples on which the waveguides are made are obtained starting from a commercial wafer of congruent Lithium Niobate (Crystal Technology) orthogonally cut to the crystallographic x-axis with a thickness of 1 mm and polished on both sides. The wafer is cut using a South Bay 540 cutting machine equipped with a diamond-coated copper alloy blade. A graduated goniometer allows you to align the sample with precision to make cuts along the crystallographic axes. The samples thus obtained, once cleaned with ethanol, are suitably cataloged by marking their crystallographic orientations (the direction of the optical z-axis) on the x face of the sample.

3.2 Wave guides realization

Before explaining the detailed fabrication procedure for the realization of the channel waveguides it is useful to present a brief list of its main steps that can be also visualized in Figure 3.3:

Figure 3.3: Graphic scheme of the light guide manufacturing.

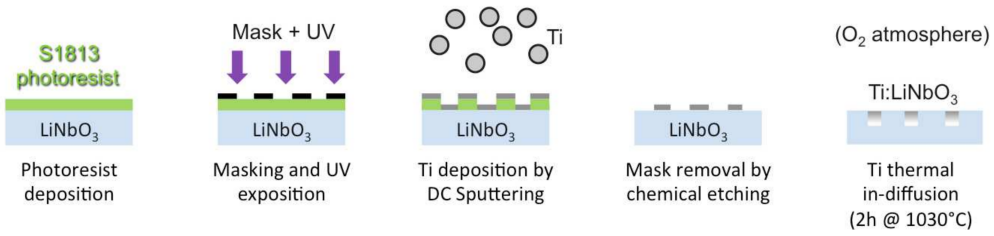

- a photoresist layer is deposited on the surface of the substrate;
- a mask is kept in contact with the photoresist layer while the substrate is illuminated with a UV lamp in order to impose degradation of the unmasked regions;
- a titanium thin film was deposited on the patterned surface by sputtering deposition;
- the photoresist layer is removed in a solvent bath in order to leave on the crystal surface only the desired titanium stripes;
- the titanium is diffused into the crystal by high temperature thermal annealing in an oxygen atmosphere.

This is a standard procedure. In the following the detailed steps for the fabrication of channel wave guides are presented.

3.2.1 Photolithoghraphy

To ensure high surface cleaning and a low level of dust, the of photolithography is carried out entirely in an ISO 7 class clean-room, funded by MISCHA project (Microfluidics laboratory for scientific and technological applications). After initially cleaning the samples with acetone and ethanol, they are placed in a medium vacuum environment (P≈0.6 mbar, reached with a rotary pump), in which oxygen is partially fluxed inside. With a discharge, a plasma is then triggered to clean further the surface, exploiting the interaction of the ions with the residues present. Once the cleaning phase is completed, the primer is deposited and then the photoresist. The primer is a substance (Hexamethyldisilazane,

HMDS) which is intended to favor the adhesion of the photoresist to the oxides of Lithium Niobate, releasing bonds and permitting that the photoresist interacts with them. The photoresist chosen is S1813 from the Microposit series S1800 G2, positive and compatible with the emission spectrum of the UV lamp supplied in dotation. To distribute them evenly and homogeneously, both the primer and the photoresist are deposited on the sample using a spin coater where the sample is placed and turned over immediately after the deposit of each of the two. For the primer is used a speed of 2000 rpm for 30 seconds, while for the photoresist of 6000 rpm for 30 seconds. These parameters have been previously optimized to obtain the thickness of photoresist that is necessary to have the best possible transmission in the light guides. The sample, after photoresist deposition, is then covered in direct contact with a chrome mask on quartz with strips of nominal width of 3 μm and exposed to the highly collimated UV lamp supplied with a power of 6300 $\frac{\mu W}{cm^2}$ for 13 seconds. The mask is positioned such that the strips are parallel to the crystallographic z-axis of Lithium Niobate. Subsequently, the sample is subjected to an immersion for 60 seconds in a basic solvent (Microposit MF-300) which reacts with the photoresist illuminated and deteriorated by removing it. Finally the sample is rinsed in distilled water for 30 seconds. The quality of the removed photoresist strips is observed with a transmission microscope and investigated with a contact profilometer.

3.2.2 Titanium sputtering

Sputtering deposition consists in the deposition on the sample surface of atoms which are removed from a metallic or insulating target after bombardment by the ions of a plasma. Titanium is deposited on the x-face of the sample with magneto-sputtering. For this reason the sample is placed in a vacuum chamber at a pressure of about 1.6×10^{-6}mbar, achieved with a rotary pump (medium vacuum) and a turbomolecular pump (high vacuum). An Argon plasma (accelerated with a potential difference of about 300 V) deteriorates a Titanium target to obtain the release of neutral Ti atoms with which to make the deposition. Initially, for the duration of 5 minutes, the target is covered by a screen to allow plasma to remove the titanium oxide present from the surface. After this stage, the target is exposed and for 22 minutes it gets titanium sputtering. Magnetic fields close to the target confine secondary electrons produced in plasma-target collisions, allowing a higher sputtering rate. The position of the sample in the chamber is in front of the target, with the surface to be covered perpendicular to the trajectories of the Ti atoms. At the end of the process the Titanium layer on the sample is equal to about 40 nm.

3.2.3 Lift-off

The lift-off is a chemical etching technique with which the strips of Titanium are removed if they have a non-illuminated photoresist underneath. The sample is immersed at the temperature of 60 °C in a bath of a photoresist positive solvent, SVC (TM)-14, which penetrates inside the surface it causes the detachment of the portions to be removed after a few hours. Sonification may also be required for a few seconds to speed up the process.

3.2.4 Annealing

The thermal diffusion of the Titanium strips left after the Lift-off inside the Lithium Niobate takes place in a Hochtemperaturofen Gmbh tubular furnace (model F-VS 100-500 / 13, Gero). A quartz bar allows you to place the sample in the center of the oven: between the quartz and the sample there is a platinum sheet to prevent contamination. Once the sample is allocated, the oven is heated at a rate of 300 °C per hour, then for two hours the temperature is maintained at 1030 °C. The subsequent cooling has a speed of 400 °C/h. The cooling and heating rates are chosen to avoid thermal stress of the crystals. The annealing process takes place in a oxygen fluxed atmosphere in the oven chamber at a 50 Nl/h flow rate, to favor the diffusion of Titanium, thanks to its oxidation, inside the Lithium Niobate. The diffusion process, which follows Fick's law, generates, once that the whole film is completely diffused, a Gaussian profile of the concentration of Titanium inside the sample in a direction orthogonal to the surface. In this way, light guides with a graduated refractive index are obtained, with modulation given by the concentration of Titanium. As a result, the shape of the guides, seen in

the frontal direction with respect to the propagation (crystallographic z-axis), is typically that of an ellipsoid flattened towards the surface of the sample.

3.2.5 Lapping and polishing

To obtain lateral surfaces with roughness compatible with those required for an optical stadium (such as a light guide), specimens should be polished laterally by lapping and polishing. Lapping is an abrasion process aimed at obtaining a controlled roughness: it uses coarse-grained particles (about 1-10 μm) which ruin by rubbing the surface thus modifying its roughness. Polishing works the same, but it must be done after lapping: in this case the particles have nanometric dimensions in order to decrease the roughness, obtaining typical values of optical surfaces (less than 1/10 of the wavelength). For lapping the lateral surface of interest is put into contact to the treatment with a rotating disk (rotation speed 40 rpm), by means of a suitable support that brings down the sample by gravity. The disk is then wetted with a aqueous solution containing aluminum oxide particles of size 9 μm and subsequently 3 μm. Then it proceeds in a similar way with polishing, in this case using nanometric particles until a completely transparent surface is obtained.

3.3 Microchannels realization with self-polishing saw

The microchannels of this work have been all realized with the same machine DISCO DAD 3350 precision saw (Disco Corporation, Tokyo, Japan), in collaboration with Femto-St Institute and University of Franche-Comté in Besançon. The machine can be equipped with different blade depending on the material to cut. Several study have been done by our group in, where the machine was equipped with a polymeric blade coated with diamond particle with 56 mm of diameter and 200 μm of thickness. The best surface quality was achieved with a rotation speed of 10000 rpm. The Figure 3.4 shows sharp edges, even in corners of the cross which is the most stressed part.

Figure 3.4: Microfluidic channels sections; image taken from [2].

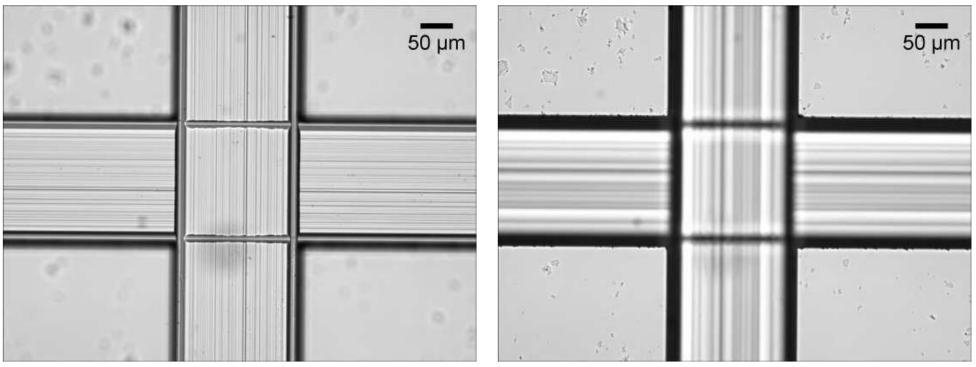

3.4 Glass enclosure

After engraving the channel, the $LiNbO_3$ samples have to be sealed with a top cover, which should allow the connection of fluidic inlets/outlets. The cover material needs specific requirements: firstly, it must be compatible with $LiNbO_3$ substrate, secondly it has to transparent in visible range for applications the imaging system, and thirdly it should be compatible with standard microfluidic fluids.
Once the light guides and microfluidic channels have been created, the device must be sealed with a top cover (in this case of glass) above the cross junction, thus obtaining a solid and compact chip. First one cut the lid with the cutting machine supplied (South Bay 540) such that it has the same sample size. On the glass lid, then, one digs four holes in correspondence of the four ends of the cross composed of the channels with a sandblaster, which constitute the entrances and the microfluidic junction outputs. After an appropriate cleaning of both, it is done a sandwich of the sample with the lid on top enclosed between two slides and locked by means of two clamps on the sides. Then keeping everything under

pressure, with a syringe it is injected a liquid polymer glue into the lateral gap between the sample and the lid, Norland Optical Adhesive 68 (NOA68, Norland Products Incorporation), which solidifies after UV irradiation. Due to capillarity, NOA spreads over the whole sample-lid interface in about 24 hours, stopping due to surface tension once the edges of the channels are reached.

3.5 OTS functionalization

The formation of droplets occurs using as a dispersed and continuous phase liquids that are immiscible to each other, such as oil (continuous phase) and water (dispersed phase). The functionalization of the microfluidic channels, in this case, is a process aimed at making hydrophobic the internal surfaces of the walls of them, both for the three sides in Lithium Niobate and for the side consisting of the glass lid. In particular, untreated Lithium Niobate has a contact angle with water of about 62°. In droplet microfluidics in fact it is necessary that, unlike the continuous phase, the dispersed phase never wet the walls of the channel, such that between the latter and the droplet there is always a thin continuous phase film. The creation of the droplets is thus more controllable, depending mainly on the interaction between the two phases. Furthermore, this is also related to the possible applications of the device, for example in the biological field, to preserve the content of the droplet from the interaction with the materials present on the sample surfaces. Functionalization is then obtained by fluxing a solution into the channel for 15 minutes 5 mM/L of OTS (= Octadecyltrichlorosilane) in Toluene by a syringe pump with a flow of 20μL/min. The effect of the functionalization can be seen in the following Figure 3.5 and Figure 3.6 (I am referring, as already mentioned, to previous works like [1], [2] and [16] from which the images are taken and the text is based).
OTS is a molecule composed of a long carbon chain hydrophobic and a polar head consisting of the -$SiCl_3$ group, which binds to the oxygen of Lithium Niobate forming Si-O bonds (Chlorine instead separates and goes into solution as HCl). In this way a monolayer (self-assembled monolayer) is formed on the surfaces of the canal walls such as to make them hydrophobic. Similarly functionalization with OTS also makes the glass lid wall hydrophobic. To rinse the channel of remaining OTS residues, pure Toluene is always fluxed at 20μL/min for another 15 minutes, and then the sample is heated at 65 °C for another 30 minutes in order to evaporate all the remaining Toluene. At the end of this process, the measurement of the water-niobate contact angle, for which we refer to previous works, turns out to be about 100°. As already said, Figure 3.5 and Figure 3.6 show a comparison of droplets production in microfluidic channel before and after functionalization: only after functionalization it is possible to produce droplets properly.

Figure 3.5: Examples of droplet production in T-junction configuration, using hexadecane with SPAN80 as continuous phase and water as dispersed one. Here no droplet are produced because of the absence of OTS functionalization.

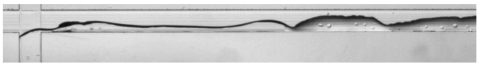

Figure 3.6: Here, thanks to OTS functionalization, droplet are properly produced.

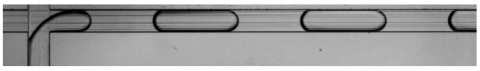

Chapter 4

Microfluidics basics

4.1 Droplets generators and regimes of flowing

Since the early years of the microfluidic growth, several droplets generators configurations have been developed and studied [11]: they can be divided in two main general categories the active and passive generators. The first requires an external source to achieve the complete droplet break-up, the second does not, and they are based only on geometry, fluxes and properties of the fluids. In most of the cases active generators are based on a passive ones with an additional active control, in order to enable additional handles for on-demand droplets generation. In this section I focus only on passive generators, among which one has been used for this thesis. The extension to an active version from a passive generator device is straightforward, in particular in Lithium Niobate which offers several properties for this purpose, such as piezoelectricity or inducing field properties respectively.
The most characteristic feature of a passive droplets generator is its geometry, which is commonly based on a junction where the interface between two immiscible fluids reaches the Rayleigh-Plateau instability [17] [18] and the break-up of the droplet happens. The two liquids are usually referred as dispersed phase, which is the droplet liquid, and the continuous phase. Thanks to the non-miscibility of these two it is possible to produce droplets, as we will see. For the rest of this work the "c" and "d" subscriptions refer respectively to these two phases. An overview of most common configurations is reported in Figure 4.1, that has been taken from [2] and the same is true for what I am going to describe.

Figure 4.1: The three main passive droplet generators geometries, a) is the co-flowing, b) is the flow- focusing and c) cross flowing. For each of the three junctions the three regimes are reported.

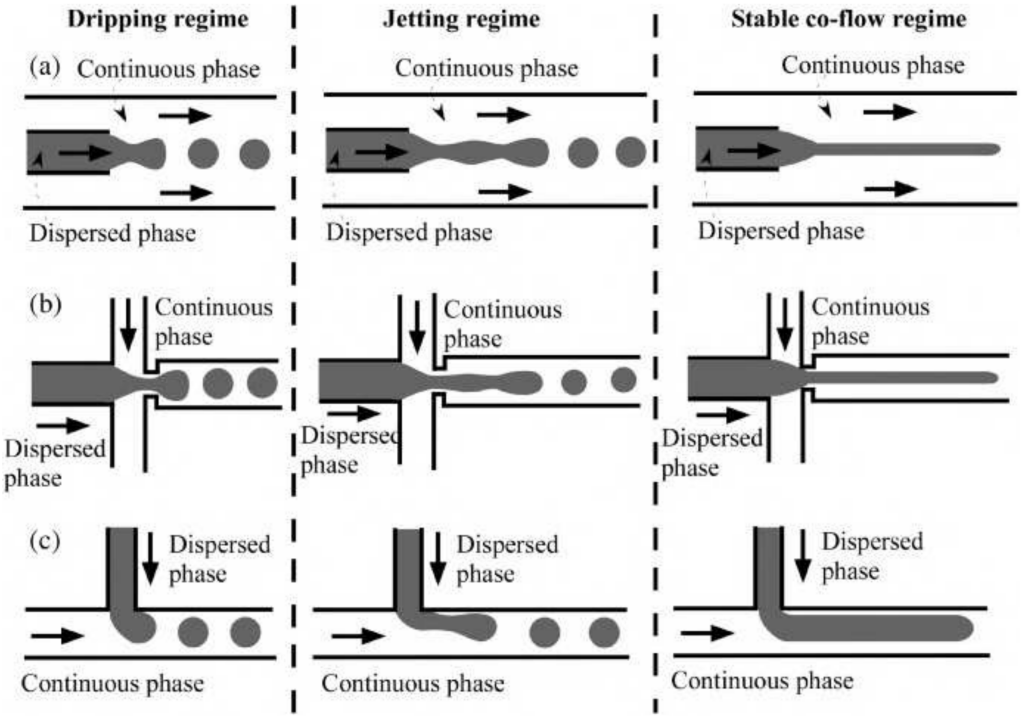

Co-flowing The two liquids interact by means of two coaxial tubes. This is one of first method ever proposed, however nowadays it is not so spread because it cannot be integrated in a chip in a straightforward way as other configurations.

Cross-flow The break-up is forced in this geometry by a T-junction, the dispersed phase obstructs the channel shrinking the continuous phase stream. This configuration is one of the simplest to be integrated, due to its simple geometry. Indeed this is the configuration used in this thesis.

Flow-focusing The dispersed phase stream is squeezed by the continuous liquid in two orthogonal channels, in a cross junction configuration. In this case the total flux of the continuous phase Q_c is divided in two halves, one for each channel $Q_c/2$.

For every passive configuration there are two interesting properties of the droplet, that have to be handled: the frequency and the volume. Both depend on several parameters of the system like the densities, the viscosities, interfacial tensions and fluxes of continuous and dispersed phases. These parameters influence drastically the droplet break-up as far as the Rayleigh-Plateau instability. Three main working regimes can be identified:

Co-flow In this regime, neither the Rayleigh-Plateau instability nor droplets break- up occur. Two phases flow parallel to each other. This regime is usually characterized by small fluids velocities, high interfacial tension, which makes unfavorable the creation of new interface, and similar viscosities of fluid to decrease any drag.

Jetting The main feature of this regime is a dispersed phase thread, that connects the junction to the droplet breakup. The Rayleigh-Plateau instability occurs far from the junction. Typically this regime is not the most stable, due to the thread instability. However fast production frequency can be achieved.

Dripping This is the standard regime for droplets production. Droplets breakup occurs at the junction. The performance of such regime is optimal for most of the applications, in terms of monodispersity of the droplets and production frequency respectively.
Moreover, other two regimes can be considered:

Squeezing This is an extension of the dripping regime. While the droplet does not fill completely the exit channel during the detachment, the regime is still called dripping regime. Instead, if the pressure dominates in the break-up and the droplet clogs the output channel we refer to it as the Squeezing regime. This regime is the one largely used in this thesis for the final measurements. For an extensive study on the squeezing-to-dripping transition in T-shaped microfluidic junctions one can see [15].

Balloon This is a novel regime discovered by Tarchichi. It is a peculiar regime of the T-junction configuration at low velocity of the continuous phase, and the droplet generation depends mainly on the geometry features of the junction and not on the velocities of the two phases.

4.2 Some details on the microfluidics of a T-junction

As we already said, by referring to what has been said in the work [16] and also to [1] (for many more details), microfluidics is a field of research that studies the control and manipulation of extremely small amounts of fluids (up to volumes of the order of picoliters or nanoliters), with applications ranging from biology and medicine to chemistry. These small volumes of fluid are obtained thanks to very confined geometries, with length scales typically of the order of a few tens of micrometers.
A parameter that is very important in fluid dynamics is the Reynolds number

$$Re = \frac{\rho v l}{\mu} \tag{4.1}$$

with ρ and μ respectively the density and the dynamic viscosity of the fluid of interest (different from the cinematic viscosity usually called $\nu = \frac{\mu}{v}$); with l that is the characteristic dimension of the system. The Reynolds number indicates the relationship between the inertial and viscous forces in the fluid: due to the very small lengths typical of microfluidic channels, this parameter has very low values ($\mathrm{Re} < 100$), associated with laminar flows of fluid that are easily controllable. In particular, droplet microfluidics consists in the production of small quantities of a fluid (called dispersed phase) confined within a microfluidic channel in another fluid immiscible with the first one (continuous phase).
An important feature of microfluidic channels is that the dispersed phase must never wet their walls, unlike the continuous phase, ensuring greater control over the transport and generation of the droplet. In this way the droplets never come into contact with the walls of the channel and so it protects what is contained in the droplet from interacting with external substances. This last thing we said is very relevant in some applications for example from a biological and chemical point of view, such as transport of chemical reagents, molecules or biological samples.
In this thesis a T-junction droplet generator is used that is, as said, a passive production method, whose name derives from the T configuration with which the microfluidic channels cross, as it is represented in the Figure 4.2.
Two immiscible liquids (such as oil and water) flow inside the channels and from the meeting between the two phases in the junction droplets can be generated, depending on the characteristics of the incoming fluids (density, viscosity, surface tension, wettability) and the fluxes of the dispersed (Q_d) and continuous (Q_c) phase. In more details, the break-up mechanism that leads to the formation of a droplet in a T-junction can be described in the following steps, helping with the Figure 4.2:

1 the two phases present an interface at the junction between the two channels, with the flow of the dispersed phase that penetrates the main channel causing the interface to grow;

2 the flow of the continuous phase distorts the interface of the dispersed phase at the junction in the direction of flow;

3 the neck that connects the inlet channel with the droplet breaks and the droplet flows into the main channel.

Figure 4.2: T-junction section with a schematic of the formation of a droplet in squeezing regime (image taken from [1]).

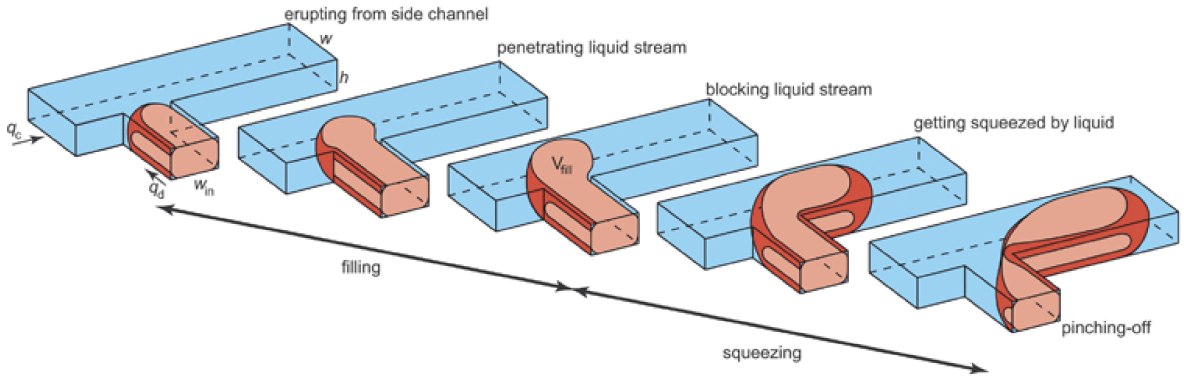

For these reasons, the production of the droplets and their size is determined by a competition between the resistance to deformation by the capillary pressure, on one hand, and the viscous forces and pressure due to the continuous phase, on the other.
The capillary number is defined as

$$Ca = \frac{\mu_c v_c}{\sigma} \tag{4.2}$$

with μ_c that is the viscosity of the continuous phase, v_c is the mean velocity of such phase and σ is the superficial tension. Ca expresses the relationship between the viscous forces and the capillary pressure and it is a parameter that provides information on the type of droplet production rate. In particular, for large Ca the viscous force is the main responsible for the separation process of the dispersed phase which leads to the formation of a droplet: the dispersed phase does not obstruct the main channel and therefore the droplets thus obtained are small and with asymmetrical terminal parts, with shape independent of the geometry of the channel. This droplet production regime is called dripping. For small Ca, the process is dominated by the pressure of the continuous phase: in this case the dispersed phase is able to obstruct the entire main channel and the rupture is caused by the greater resistance to flow encountered by the continuous phase, leading to longer droplets. and with more symmetrical ends, linked to the geometry of the channel. This regimen is denoted as squeezing and Garstecki et al. [12] have proposed a scaling law to describe it, verified with experimental data, which links the length of the droplets to the ratio between the flows, based on the relationship:

$$\frac{L}{w_c} = 1 + \alpha \frac{Q_d}{Q_c} \tag{4.3}$$

where L is the length of the droplet, w_c is the width of the principal channel (the one where the continuous phase originates) and α a parameter to be determined by fitting procedures.

Chapter 5

Final experimental setup and proteins detection

5.1 "Bi-phase" setup for proteins detection inside droplets

5.1.1 Mention to the other setups tested

Many experimental configurations have been tested for the protein detection. They are based on different approaches to achieve the best parameters control (for example stable droplets length and production frequency). To this aim it is mandatory to control the physical quantities that determine the droplet quality. This preliminary experimental work allowed to conclude that:

- after studying both flux controlled droplets production methods and pressure controlled ones, emerged that the first are better in our case;
- among the various setups studied, the double flow-meters controlled setup is the most accurate, but is limited by the problem of adding particles or objects into the dispersed phase since flow meters can't accept particles;
- still using the flux to control the droplets production, we replaced one flow-meter with a syringe pump (to allow the later insertion of particles like proteins). By the way the problem of oscillations of the fluxes values due to the step motor of the pump showed up resulting in the method being discarded;
- the solution found is in the use of the double flow-meters controlled setup with the addition of an important part in series with one of those (the one that controls the dispersed phase) that, acting like a reservoir, allows for proteins to be stored in solution before being injected as dispersed phase in the chip. For more details see the next section.

For more details about this topic see the Appendix A .

5.1.2 "Bi-phase" flow controlled droplet production

The droplet measurements are carried out using two immiscible liquids contained in two different test tubes and by activating a different pressure (mbar) on each of them with the Elveflow OBI Mk3 Pressure Controller, pressure which is then converted into a flux (μl/min) and kept monitored thanks to the presence of two flow meters.
One of the two flow meters, the one containing hexadecane with 3% of SPAN80 (that is a surfactant), is connected directly to the chip and forms the continuous phase. The second flow meter, which controls the flow of pure hexadecane, has a double units-based object at the tail end with two empty units glued through each edge of the base to the edges of a central empty cylindrical section (in Figure 5.1 the new component is represented by a box with a question mark; further details on the specifications can't be provided in this context because patent is pending). This part allowed us to solve the problem

of introducing objects in the dispersed phase without passing them through the flow meters but in this way we weren't renouncing to the usage of the latter as they are fundamental components of the apparatus that gave us the best result for the production of droplets.

Figure 5.1: Diagram of the final experimental apparatus used for the droplet measurements.

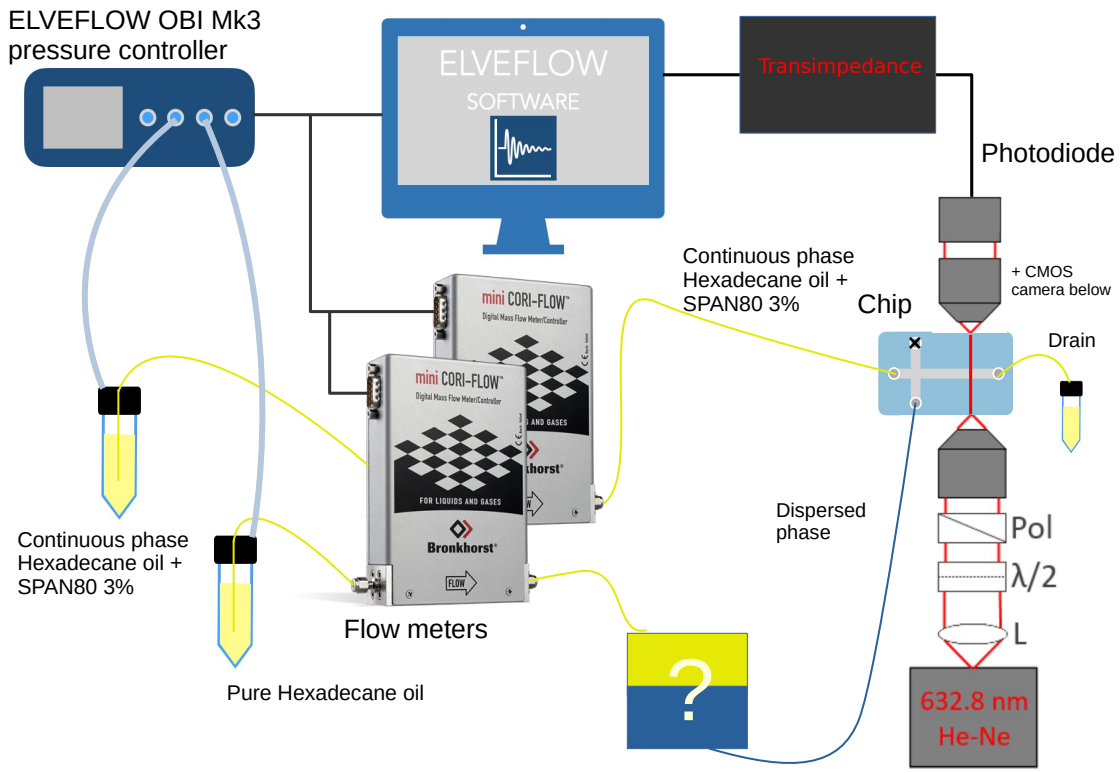

This is the core of the so-called "Bi-phase" setup. Pure hexadecane has been used, controlled in flow by this second flow meter, to push the dispersed phase to be introduced into the chip. The so-called "double phase" is characterized by the presence of a meniscus that is created inside this double units-based system. Clearly, this special test tube is first filled from below with the dispersed phase of interest, and then begins to be filled from above with pure hexadecane, such as to facilitate the creation of the meniscus and to avoid the presence of air bubbles. So, as one can understand, it gets connected in a second time to the chip with respect to the filling phase because the microfluidic tube used for filling is the same that is used to inject later the dispersed phase in the T-junction. Of course a third test tube is connected to the ELVEFLOW OBI Mk3 pressure controller and used for the filling procedure.
Through studies carried out by dr. L. Zanini (L. Zanini, unpublished), it was ensured that this new device responded well to variations in flow, set through the LabView interface, and controlled by the feedback circuit of the flow meters. In fact, in principle it is neither said that the response of the system arrives immediately to the variation of the value in the interface nor that the value perceived by the dispersed phase is precisely the one set rather than a shifted value due to this meniscus, for example. Both of these criticalities have been studied and their non-pathologicality has been verified. It should be noted that the data acquisition is performed each time, only when the meniscus of the double phase entered a "good area" which consists of the cylindrical portion of conjunction between the two cones. This is to avoid elastic responses of the system that would worsen the response time and the precision of the flow set due to the variation of the meniscus size and other edge effects.
As already mentioned, the droplets are produced using the cross junction in T-junction configuration, closing an inlet of the short channel and fluxing the continuous and dispersed phases as in the Figure 4.2. One microfluidic channel inlet (the longest) is reserved as a chip drain.
For the detection apparatus, in this case, the photodiode is connected to a transimpedance which

converts the photogenerated current into a voltage, which is sent directly to the acquisition system. The variation over time of the transmitted signal is collected by the photodiode at the passage of the microfluidic droplets produced in the channel. The light signal associated with the passage of the droplet is linked to its shape and composition and is extremely reproducible and periodic along the whole train of droplets detected in a single measure.
An example of a transmission signal associated with a train of microfluidic droplets is shown in the Figure 5.2, and then the Figure 5.3 shows the image of a droplet associated with the signal and taken with the Basler acA800-510μm camera (images taken from [16]). Note that the latter, that is to say the imaging system, is synchronized with the photodiode to grant the maximum number of information on the same droplets.

Figure 5.2: The signal associated with a train of droplets is detected by the photodiode.

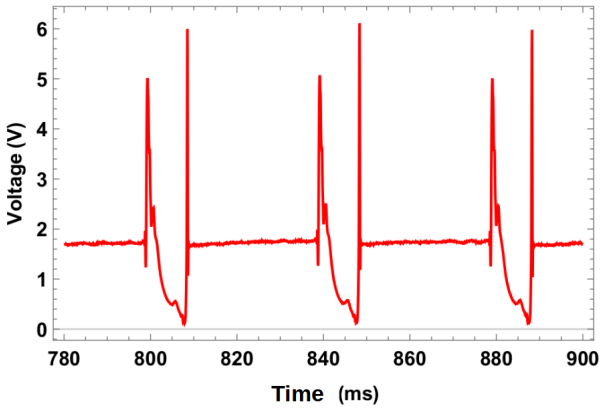

Figure 5.3: An image taken with the Basler camera of a droplet of the train with the position of the light guide visible.

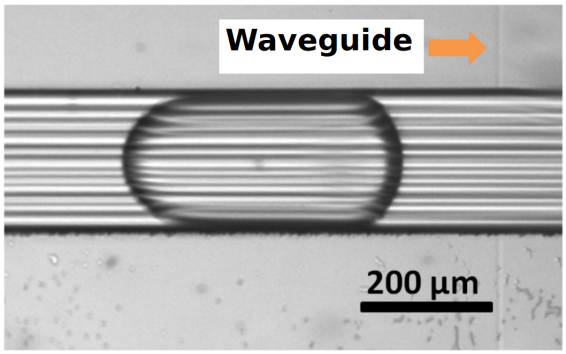

5.1.3 Real time acquisition with photodiode and CCD

The opto-microfluidic sample used in this thesis has the desired detection geometry with two collinear light guides that focus on the same micrometric channel. This aspect determines that the light intensity that the receiving guide can pick up is linked to the coupling that the guides have with the channel and therefore to the fluid that fills it. In fact, the beam transmitted by the input guide disperses by refractive effect at the point where it is interrupted with a opening angle θ_0 which is a function of the refractive index of the fluid in the channel.
For a light guide with graduated index, as for an optical fiber, the numerical aperture NA of the beam in correspondence with the interruption of the guide itself is:

$$NA = n_0 sin(\theta_0) = constant = \sqrt{n_{core}^2 - n_{cladding}^2} \approx 0.13 \tag{5.1}$$

where n_0 is in the case in question the refractive index of the channel and θ_0 is the beam opening (in our case that value results ≈ 0.13).

The numerical aperture NA, as the equation indicates, is a constant and is linked to the refractive indices of the inside and outside of the guide (for a fiber the terms core and cladding are used). Consequently, changing the refractive index n_0 changes the beam opening θ_0: if for example n_0 grows, the bundle shrinks.
Before talking about the real time acquisition we mention briefly the technique used to couple the already mentioned Ti-indiffused wave guides with the laser. One of the best method, required for a lab-on-a-chip realized in $LiNbO_3$ to couple laser light inside a waveguide, is the End Butt Coupling method. This is the technology used also for this thesis since it is permanent, stable and portable.

Figure 5.4: Diagram of the optical experimental apparatus in the right configuration for real-time measurements.

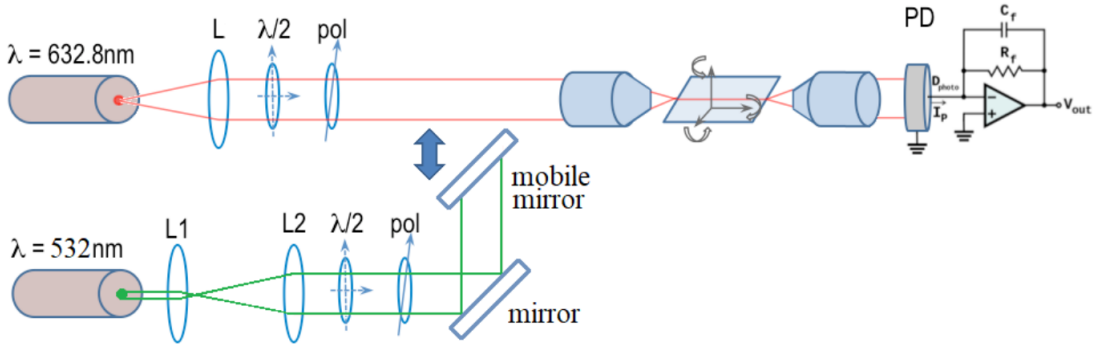

In order to measure real time the passage of the droplets a specific experimental setup was used. The setup is sketched in Figure 5.4 and includes:

- a He-Ne laser with a wavelength of 632.8 nm (red color), measured power (1.30 ± 0.03) mW and preferential polarization (22.8 ± 0.6)° with respect to the vertical axis clockwise (all these values were measured prior to this work);
- a laser diode with a wavelength of 532 nm (green color), measured power (5.30 ± 0.03) mW and preferential polarization (134.5± 0.6)° with respect to the vertical axis clockwise (not used in this thesis);
- on the red laser line, a long focal length collimating lens (f = 2 m) of the Rayleigh range of the laser beam ($z_0 \approx 20$ cm) and placed at a distance equal to f to obtain a collimating effect;
- on both laser lines, a $\frac{\lambda}{2}$ sheet and a polarizer needed to rotate the preferred laser polarization and select a TE or TM polarization for the beam to be conveyed to the sample (TE polarization used in this thesis);
- a movable mirror to select the wavelength of interest during the measure, directing the chosen laser beam towards the sample (not used since the red beam was the only laser required);
- a 20× objective (f = 1.2 mm, NA = 0.4) to focus the beam on the entrance guide;
- a 50× objective lens which collects the output of the collecting light guide in the focus;
- a sample holder that allows to move the sample to make the coupling sample objectives with End-Butt-Coupling technique;
- a photodiode with a circuit to connect it to a transimpedance which converts the photogenerated current into a voltage that is sent directly to the acquisition system. The variation in time of the signal transmitted by the guides and collected by the photodiode as the microfluidic droplets produced in the channel is passed. Note that the light signal associated with the passage of the droplet is linked to its shape and composition and it is extremely reproducible and periodic along the whole train of droplets detected in one single measure. The circuit to which the photodiode is connected is also used to amplify the signal (amplification used in this thesis $G = 10^7$);

- a CCD camera called Basler acA800-510μm which allows to perform video acquisitions simultaneously with the photodiode.

5.2 The Bradford reagent and the Bradford protein assay

The Bradford protein assay [21] was developed by Marion M. Bradford in 1976. It is used to measure the concentration of proteins in a solution. The reaction is independent on the amino acid composition of the measured proteins.
The Bradford assay, that is a colorimetric protein assay, is based on an absorbance peak shift of the dye Coomassie Brilliant Blue G-250. When the dye binds to the protein, it causes a shift from λ = 465 nm to λ = 595 nm, which is why the absorbance readings are generally taken at λ = 595 nm. In an acidic environment, proteins bind to Coomassie dye and thus results in a spectral shift from the reddish-brown form of the dye (with absorbance maximum at λ = 465 nm) to the blue form (with absorbance maximum at λ = 595 nm). The difference between the two dye forms is greatest at λ = 595 nm, making it the optimal wavelength to measure the blue color from the Coomassie dye-protein complex.
If desired, the blue color can be measured at any wavelength between λ = 575 nm and λ = 615 nm. At the two extremes there is an approximate 10% decrease [19] in the measured amount of absorbance compared to that obtained at λ = 595 nm.
Notice that for my measurements, I have used the laser light available originated from an He-Ne laser with a nominal λ = 632.8 nm (red light).
The Coomassie brilliant blue G-250 dye exists in three forms [20]: under acidic conditions, Coomassie G-250 is cationic and red, whereas in neutral condition the dye is green, and the anionic form is blue. The Bradford reagent is an acidified solution of Coomassie G-250; the dye is thus red.
Under acidic conditions, the red form of the dye is converted into its blue form, binding to the protein being assayed. If there is no protein to bind to, then the solution will remain brown. The increase of absorbance at λ = 595 nm is proportional to the amount of bound dye, and thus to the amount (concentration) of protein present in the sample.
The dye forms [21] a strong, noncovalent complex with the protein's carboxyl group by van der Waals force and amino group through electrostatic interactions.
The Bradford protein assay is less susceptible, with respect to some other types of assay, to interference by various chemical compounds such as sodium, potassium or carbohydrates, that may be present in the samples. An exception is elevated concentrations of detergents.
Other than the usual Bradford reagent, one can also use the "Detergent Compatible Bradford Assay" [19] that is a ready-to-use modification of the Bradford Assay with additional additives to make it compatible with 1% or higher concentration of commonly used detergents; or even the "Coomassie Plus (Bradford) Protein Assay" [19] that is a ready-to-use, reducing agent-compatible Bradford assay reagent that provides increased linearity of response and only half the protein-to-protein variation of other commercial Bradford assay formulations.

By referring to what is written in the Bradford reagent *Technical Bulletin* of Sigma-Aldrich®[22]: *"the standard 3.1 ml Bradford assay consists of mixing 1 part of the protein sample with 30 parts of the Bradford Reagent. The sample may be a blank, a protein standard, or an unknown sample. The blank consists of buffer with no protein. The protein standard consists of a known concentration of protein, and the unknown sample is the solution to be assayed."*

Standard 3.1 ml Assay Protocol *(0.1 ml of a 0.1-1.4 mg/ml protein sample is used) This assay is performed in test tubes. The assay uses 0.1 ml of the protein sample and 3 ml of the Bradford Reagent per tube. It is possible to do an assay directly in a cuvette by adding just 1.5 ml of Bradford Reagent to 0.05 ml of sample. Note: It is necessary to create a standard curve during each assay, regardless of the format used.*

1 Gently mix the Bradford Reagent in the bottle and bring to room temperature.

2 *Prepare protein standards of appropriate concentrations in the same buffer as the unknown samples. The standards should be created by serially diluting either the 2 mg/ml or 1 mg/ml BSA protein standard (Table 1). Deionized water may be substituted for the buffer, but any interference due to buffer components will not be compensated for in the protein standards. The protein standards can range from 0.1–1.4 mg/ml.*

3 *After adding 3 ml of Bradford Reagent to each tube, they should be vortexed gently for thorough mixing. The total liquid volume in each tube is 3.1 ml.*

4 *Let the samples incubate at room temperature for 5-45 minutes.*

5 *Transfer the samples into cuvettes.*

6 *Measure the absorbance at 595 nm. The protein-dye complex is stable up to 60 minutes. Theabsorbance of the samples must be recorded before the 60 minute time limit and within 10 minutes of each other.*

7 *Determine the protein concentration by comparison of the unknown samples to the standard curve prepared using the protein standards.*

5.2.1 Description of the dispersed and continuous phases

During the characterization I largely used as dispersed phase P.B.S. (Phosphate Buffered Saline) and as a continuous one a specific form of oil plus surfactant: Hexadecane plus SPAN80 at 3%. When I moved to the measurements regarding the detection of proteins I started using as dispersed phase the following two possibilities:

Baseline with the term "baseline" I indicate the dispersed phase injected in the chip made by distilled water (MilliQ with a certified resistivity of 18.2 MΩcm at 25 °C) plus the Bradford reagent in part of 1:30, that is to say that for each 100μl of water I must add 3 ml of Bradford reagent (see above for more details). The baseline is called in this way because this is the mixture used for the background subtraction since when the protein is not present the reagent should be in principle non-reactive.

Solution with the term "solution" I refer to the actual solution made by distilled water (MilliQ with a certified resistivity of 18.2 MΩcm at 25 °C) in a certain concentration with respect to the protein. For example, considering the maximum value of concentration of B.S.A. for which the behavior of the reagent is considered linear (1.4 mg/ml), I will have a concentration of 1:1 if I add 4.2 mg of B.S.A. at 3 ml of distilled water. Of course i can produce also dilution by starting from the 1:1 concentration to obtain 1:5 and 1:10 (0.14 mg/ml, that is instead the minimum value for which the behavior of the reagent is considered linear). This is exactly what I considered. As before, the Bradford reagent is added in part of 1:30, but this time with respect to the total mixture cited above, not only the part of distilled water. That is to say that for each 100μl of "water+protein" I must add 3 ml of bradford reagent.

5.2.2 Spectrophotometric analysis

Spectrophotometry [23] is a technique used in various biochemical experiments that involves for example proteins isolation. Samples in these applications are not usually available in large quantities, so analyzing them with non-destructive techniques, like this one, is of great importance.
In general, with a spectrophotometric analysis, you are comparing the absorbance of a blank sample that does not contain a colored compound to a sample that contains a colored compound. This coloring can be accomplished by a dye such as Coomasie Brilliant Blue G-250 dye measured at 595 nm, like in our case by using the Bradford reagent. The spectrophotometer is used to measure compounds in the visible region of light (between 300 nm and 800 nm), so it can be used to find more information about the substance being studied. Spectrophotometric data can also be used in conjunction with the Beer-Lambert Equation:

$$A = -\log_{10} T = \epsilon c l \tag{5.2}$$

where T is the transmittance (T=$\frac{I}{I_0}$), ϵ is the molar absorption coefficient, l is the length of solution the light passes through and c is the molar concentration of solution, in order to determine various relationships between transmittance and concentration, and absorbance and concentration (it is valid for diluted solutions). Because a spectrophotometer measures the wavelength of a compound through its transmittance, a dye binding substance can be added so that it can undergo a color change and be measured. Let's now see in detail the measurements I took with the spectrophotometer.
I focused the measurements into understanding mainly two things:

1 measuring the absorbance and looking at its variation in time of three different concentrations of B.S.A.: 1.4 mg/ml (1:1), 0.28 mg/ml (1:5) and 0.14 mg/ml (1:10), that are the ones used for this thesis. The question was to detect whether the solution changes in time after the incubation; if there is a linear trend between the absorbance and the concentration.

2 The possible interaction between the Bradford reagent and the continuous phase made by Hexadecane plus 3% SPAN80.

For this reasons I performed first the measurements for the three concentrations by acquiring data as follows. Each measurement is taken already referring to the empty cuvette (introduced as background into the spectrophotometer) but not referring to our baseline (that is in turn also referred to the empty cuvette) since I considered the zero concentration as a standalone measure. For this reason one might want to then subtract to each concentration measurement the values of the baseline. Talking again by the measures taken:

- a single measurement of the "zero" concentration (our baseline);
- concentration 0.14 mg/ml (1:10): measures at 20 minutes, 30 minutes, 40, 50, 100 and 120 minutes after incubation has started;
- concentration 0.28 mg/ml (1:5): measures at 10 minutes, 20 minutes, 30, 40, 50, 60 and 75 minutes after incubation has started;
- concentration 1.4 mg/ml (1:1): measures at 10 minutes, 45 minutes and 80 minutes after incubation has started;
- a double measurement with pure Hexadecane at 30 minutes and at 40 minutes after incubation;
- a single measurement with the Hexadecane plus 3% SPAN80 taken already after two minutes of mixing.

The results obtained are reported in the following; first the analysis for the zero concentration as can be seen in Figure 5.5:

Figure 5.5: The plot after the spectrophotometric analysis for the baseline.

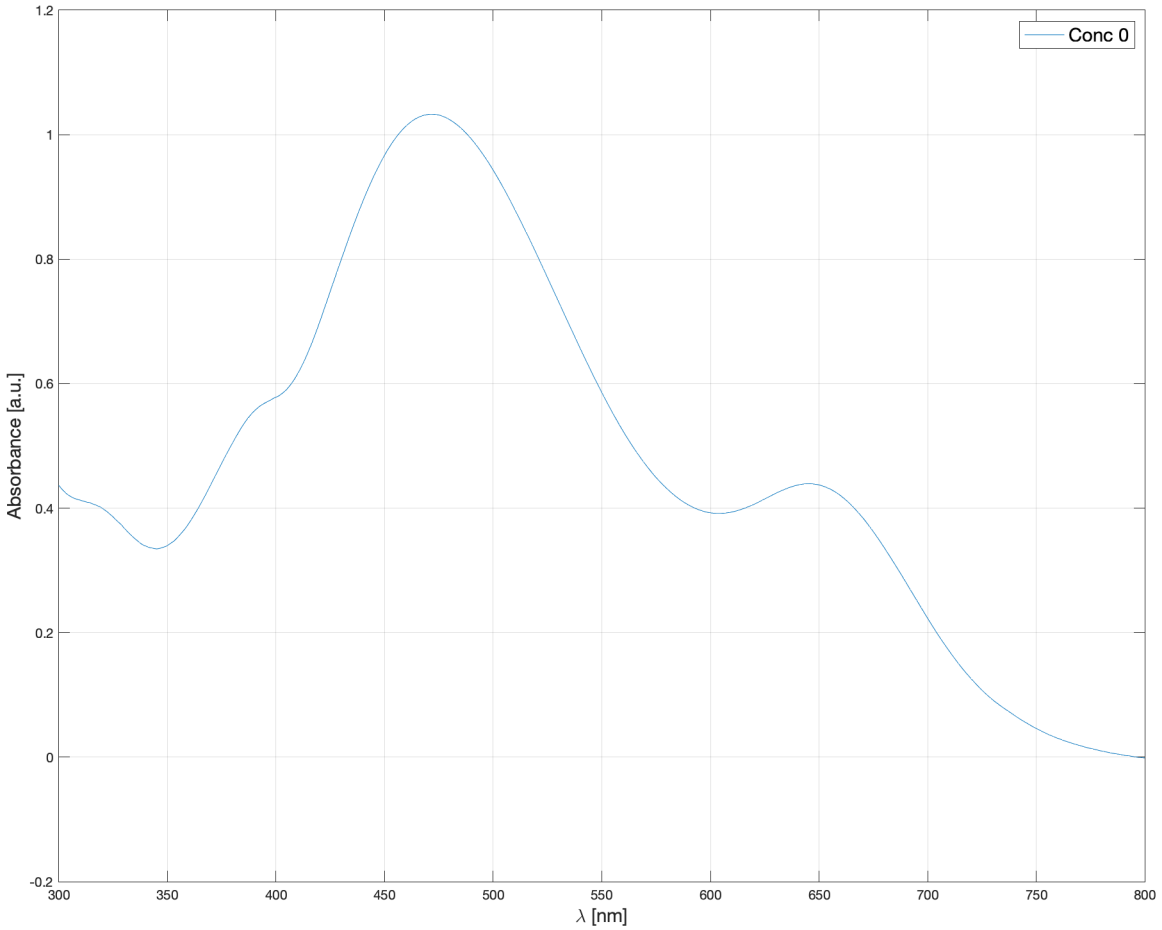

In Figure 5.6 the 1:10 concentration at various times has been plotted:

Figure 5.6: The plot after the spectrophotometric analysis for the concentration 1:10 at various times after the production (not the incubation).

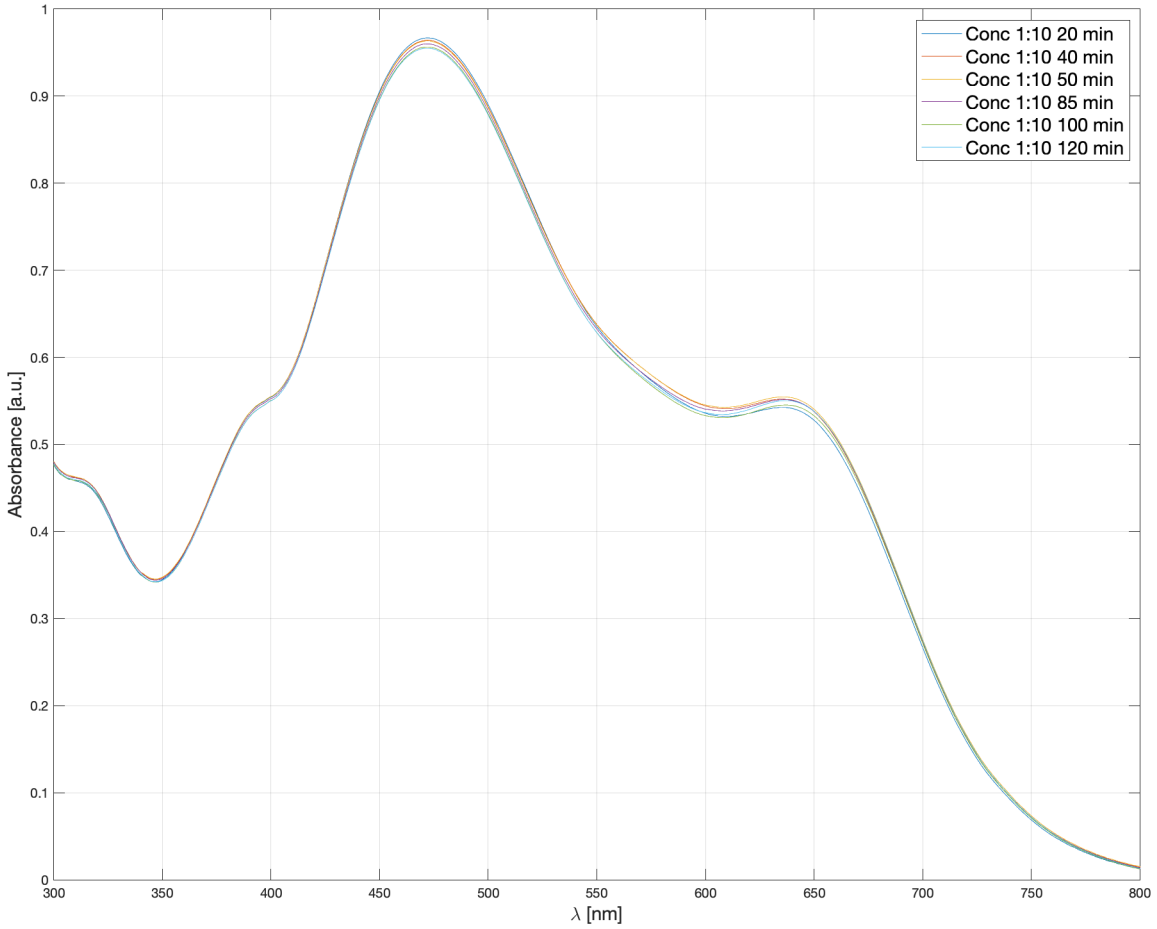

The 1:5 concentration at various times is presented in Figure 5.7:

Figure 5.7: The plot after the spectrophotometric analysis for the concentration 1:5 at various times after the production (not the incubation).

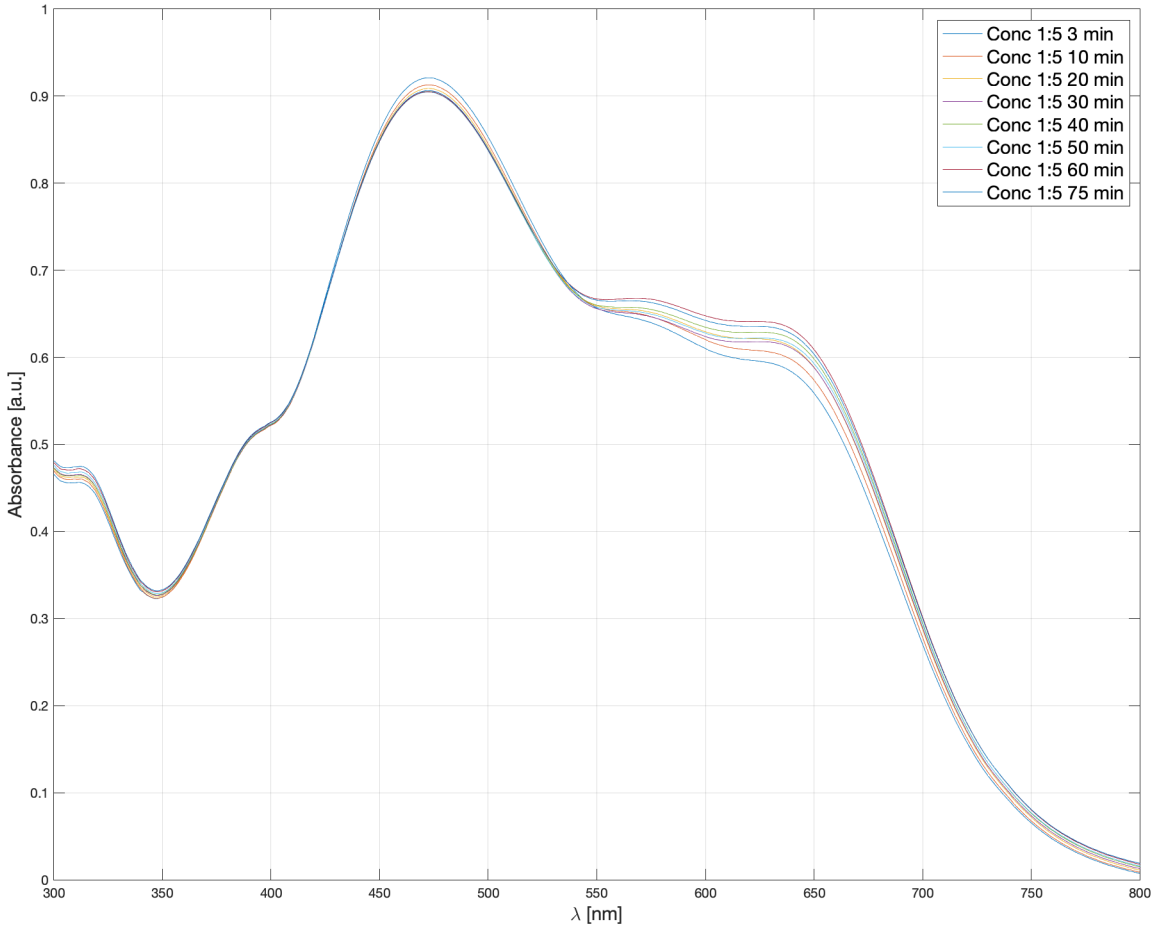

The 1:1 concentration at various times is reported in Figure 5.8:

Figure 5.8: The plot after the spectrophotometric analysis for the concentration 1:1 at various times after the production (not the incubation).

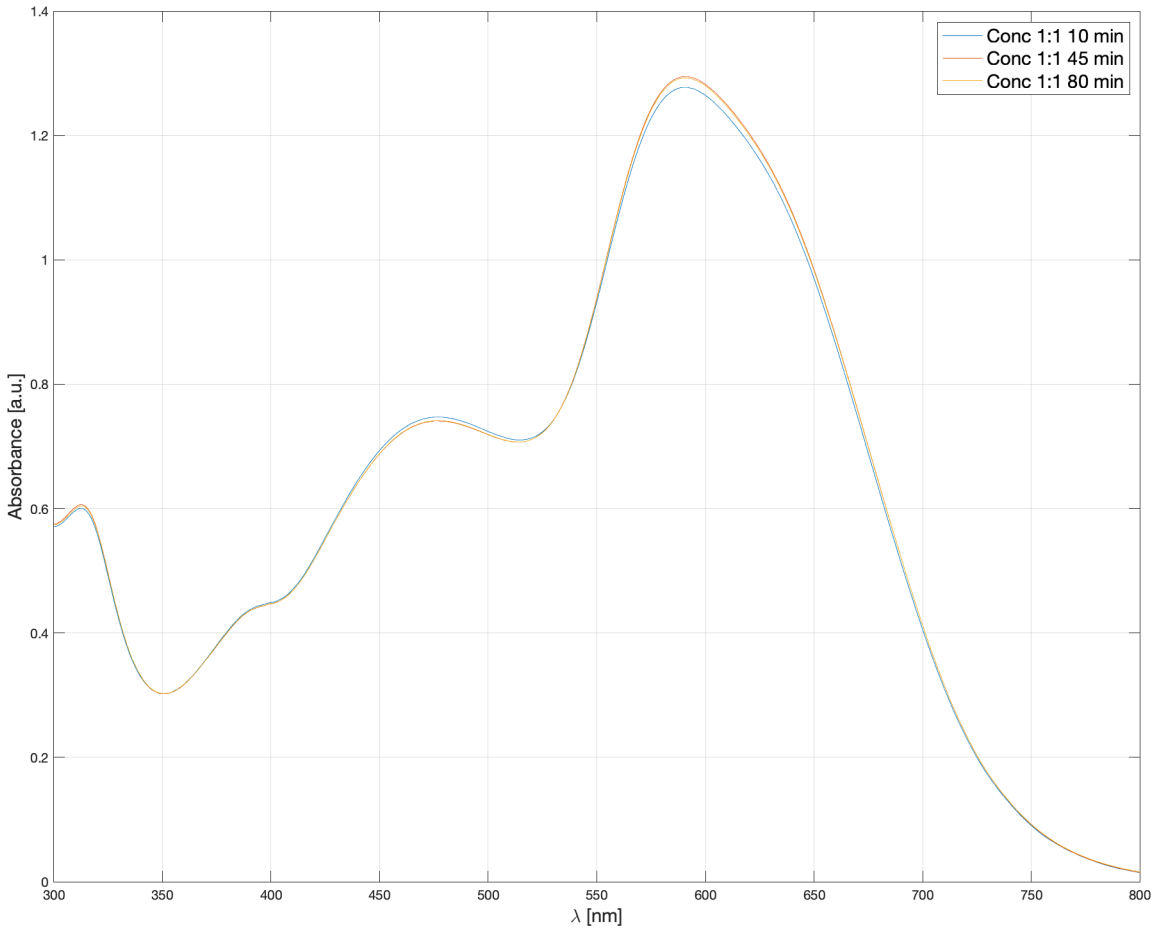

Finally all the concentrations together in order to compare the results (Figure 5.9):

Figure 5.9: The plot after the spectrophotometric analysis for all the concentrations at various times.

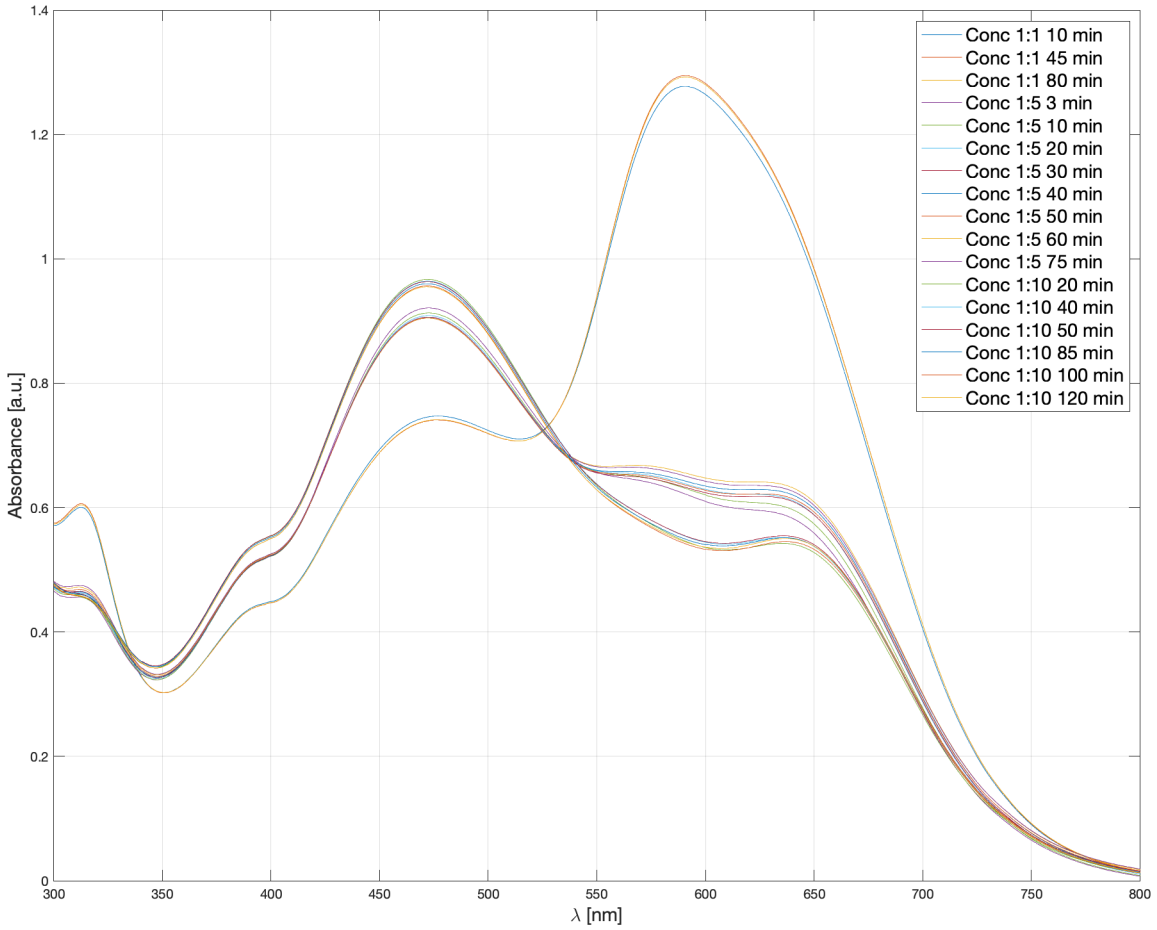

As far as the reaction of the Hexadecane with the Bradford reagent, in the following we will present the absorbance as detected by the spectrophotometer (Figure 5.10 and Figure 5.11):

Figure 5.10: Comparison between the reaction of pure Hexadecane and the Bradford reagent and Hexadecane with SPAN80 3% with the reagent.

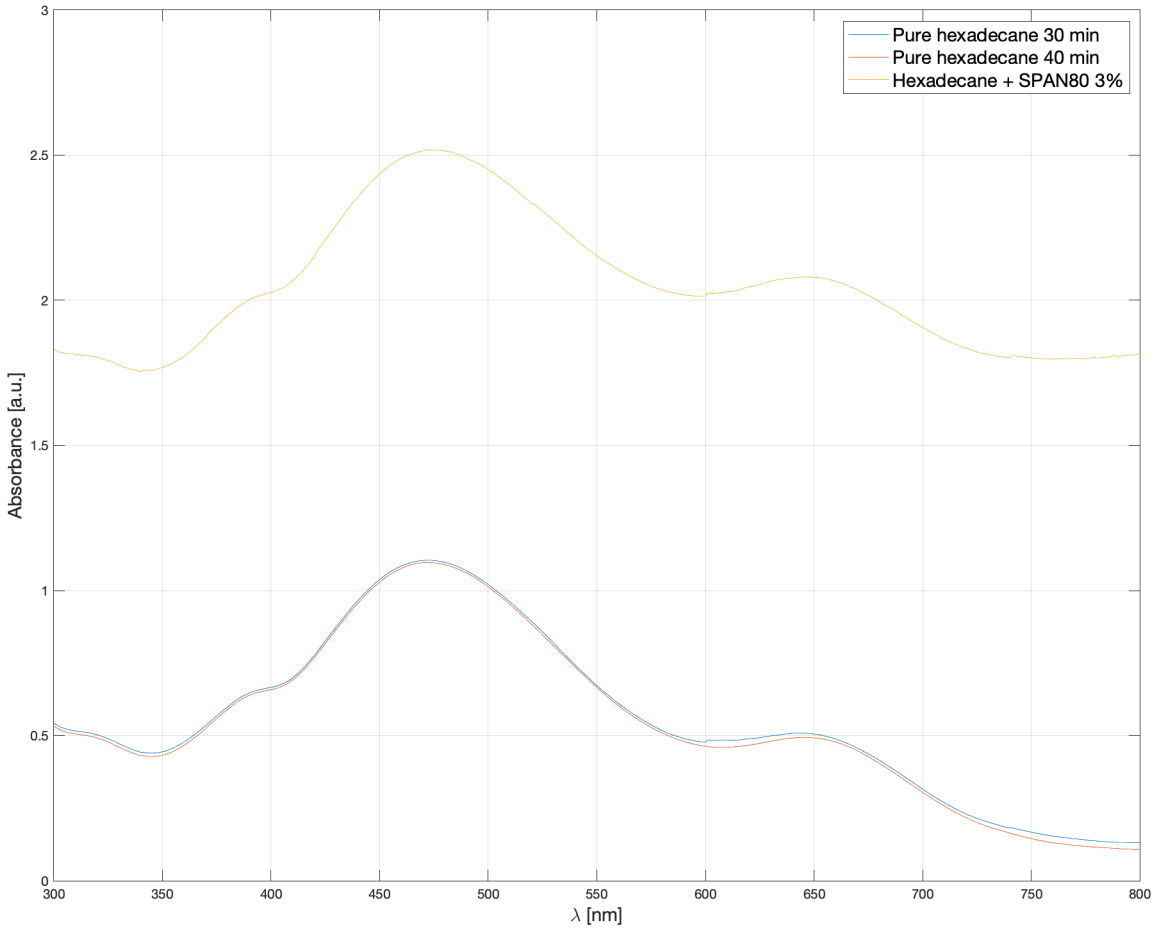

Figure 5.11: Comparison between the reaction of pure Hexadecane and the Bradford reagent and Hexadecane with SPAN80 3% with the reagent, together with concentration 1:1.

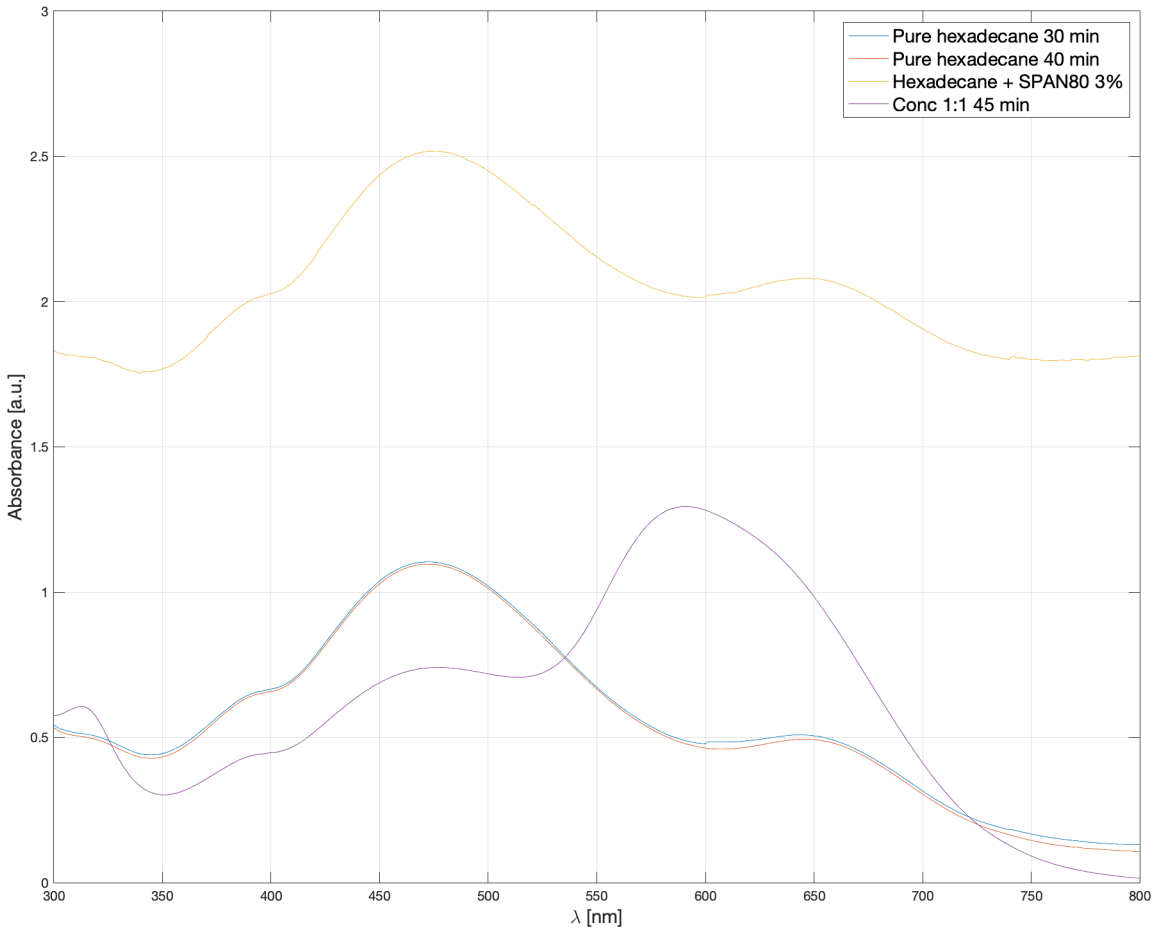

From these last two it is possible to understand that a reaction between the Bradford reagent and the Hexadecane plus SPAN80 at 3% occurs. By comparing with the pure Hexadecane curves one can see that the component responsible for the reaction is the surfactant. We can also notice that the absorbance in the case of the reaction between the Bradford reagent and the SPAN80 is significant compared to the ones when the solutions are involved. As we will see this proves the strength of measurements with droplets to confine the dispersed phase because without confinement there would have been a lot of reaction between the surfactant and the reagent such that the detection of the proteins would not have been possible (on the contrary to what we have observed as can be seen below).

5.3 Introduction to the measurements with droplets

Measurements of light transmission when a train of droplets passes through the microfluidic channel are carried out by means of the experimental apparatus described in section 5.1. In this case, the signal acquired by the photodiode is scanned over time in a reproducible way and periodic from the transit of the droplets. The variation in transmission induced by a droplet is linked to its shape and composition: the study that is presented is aimed at understanding how the collected intensity changes according to the presence of the protein inside the micrometric droplets. As already mentioned, the droplets are produced in a T-junction configuration, using as a continuous phase hexadecane (3% surfactant, SPAN80) and as dispersed phase distilled water plus the Bradford reagent plus the protein

(when considering the solution). See section 5.2 for much more details. The signals collected are normalized to the oil voltage making them independent on laser intensity and coupling. To have a qualitative estimate of the effects of the presence of proteins, a comparison of the signals alone for two droplets is not sufficient: then for this purpose it is necessary to consider a set of several droplet signals belonging to the same train and extrapolate an average parameter that expresses their light transmission. Applying the approach described (the same approach was used also in [16]), with this average parameter it is then possible to obtain a curve as a function of the length of the droplets of the train and thus carry out comparisons as the content of the dispersed phase used changes. A good comparison parameter must express the intensity transmitted by a droplet taking into account the variation in laser intensity and the coupling between the sample and optics. In fact, the coupling is not always regained in the same conditions and over time it decreases leading to a rescaling of signals in intensity but not in shape. This parameter must also be reproducible for all the droplets of the train, in order to obtain a mean value to be associated with the droplets of that specific length. The chosen parameter, which satisfies all these requirements, is the average value of the signal due to the transit of the droplet normalized to the average voltage associated with the hexadecane immediately before and after the signal change. With reference to the Figure 5.12, this is equivalent to carry out the integral of the signal between t_{start} and t_{end}, dividing it by t_{end} - t_{start} and normalizing it to the mean value of V_{hexa}. For a single droplet it results:

$$\bar{V}_{droplet} = \frac{I}{L(ms)} = \frac{1}{\bar{V}_{hexa} \cdot (t_{end} - t_{start})} \cdot \int_{t_{start}}^{t_{end}} V(t)\, dt \tag{5.3}$$

Figure 5.12: The integral of the signal associated with the transit of a droplet is calculated between t_{start} and t_{end} corresponding to the first and last minimum that are identified in the variation of the signal with respect to continuous oil voltage.

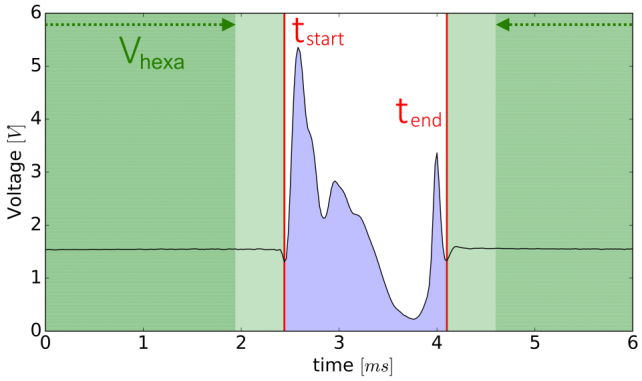

where L (ms) = t_{end} - t_{start} and "I" is the integral and $\bar{V}_{droplet}$ is the parameter called "INTn" (that is to say the normalized integral). The times t_{start} and t_{end} correspond to the first and last minimum that are identified in the variation of the signal with respect to the continuous oil voltage, chosen for reproducibility, as they are always present in each droplet type. Normalizing with respect to the oil tension (as also done in the Figure 5.12) makes the parameter independent from changes in the intensity of the laser and the coupling. The average of this parameter can be calculated over the entire train of droplets constituting a single measurement, returning an accurate statistical estimate.

5.4 Data acquisition

5.4.1 Overview

Most of the effort and time for the work of this thesis was spent to reach an optimal experimental apparatus to produce droplets in a controlled way, by also having the possibility of inserting objects inside the dispersed phase (for example like proteins as I did). Another important part was to obtain, in

conjunction with such controlled setup, the establishment of an efficient protocol of measure to ensure the minimal variation between measurement taken in different days but regarding the same subject. The part regarding the characterization of some setups configurations and the consequent discard of the non optimal ones upon reaching the final apparatus mentioned at the beginning of chapter 5 is discussed in a concise but complete way in Appendix A.
In the following I focus on the "final" measurements taken already having the necessary instruments ready as well as the method of measure and protocol. For this reason I will describe here the structure of the dataset, taken to understand if our device is able to detect the hypothetical presence of proteins inside the droplets in the dispersed phase.
As already mentioned the aim of this thesis was to obtain a controllable experimental apparatus to grant, at our best possibilities, reproducibility in the production of droplets and then applying the optimized protocol to detect proteins inside the dispersed phase by taking measurements in droplets rather than in continuous phase for the reasons already mentioned.
The data acquiring was spread over five days (one day of final calibration and study of the reagent plus four days of official measurements).

5.4.2 The datasets and the parameters

The following measurements have been taken:

- a single "measurement in time" for just one concentration (in particular the 1:1 so 1.4 mg/ml of B.S.A. with respect to water). With "measurement in time" I refer to the acquisition of various parameters related to the droplets passing in the chip at constant intervals in time without modifying anything in the starting configuration of the setup (values of the fluxes, composition, position, Temperature, etc...). This is used to see the evolution in time of the different parameters obtained from our data analysis to understand the degradation of the solution, for example, and much more. The same procedure has been applied both for the baseline (in the morning) and the solution (in the afternoon) to get in the same day both the useful signal and the necessary measures for the background subtraction;
- a "curve study" done both for the baseline and the solution, but also repeated in three days to get information (single points only, not repeated measures) for three different concentrations of B.S.A. that are the one cited above. With the term "curve study" I indicate the periodic acquisition of data by changing the dispersed phase flux value and waiting for the system to stabilize before taking the following measurement. The considered range of Q_d was (2-12) μl/min with fixed Q_c at 25 μl/min.

Now, talking about the physical quantities obtainable from our setup (thanks also to the data analysis done after the measurements), I report here the explanation of the ones that I will treat when showing the results.

Geometrical parameters:

- Length or L = simple average of the lengths of the droplets (front meniscus - rear meniscus) on all frames and for all droplets recorded with camera (measured in μm).
- Velocity or v = simple average of the velocity of the droplets over all frames and for all the droplets recorded with a camera considering the movement of the points both on the frontal and rear meniscus (measured in $\frac{\mu m}{ms}$)
- Transit time or T_t = average of transit time or time length (ms) obtainable from the photodiode that is to say the interval of time within which the droplet intercepts the guide of light.

Optical parameters:

- Integral or Int = average of the integral signal normalized to the previous oil voltage (measured in a.u.);

- INTn = Int/T_t = simple average of the integral normalized on the oil voltage and divided by the transit time of the signal. This corresponds to the average value of the signal associated with the transit of the droplet (measured in a.u./ms).
- Minimum or Min = simple average of the minimum intensity in the signal associated with the droplet normalized on the oil voltage (measured in a.u.).

5.5 Early results and data analysis

5.5.1 "Curve study"

Let's start by considering some results regarding the "curve study". This study was successfully performed for all three concentrations of B.S.A.: 1.4 mg/ml (1:1), 0.28 mg/ml (1:5) and 0.14 mg/ml (1:10).
First of all I consider the smaller concentration (0.14 mg/ml of B.S.A. with respect to the MilliQ water). I start by showing the obtained trend between the INTn and our parameters. INTn is the parameter that gives an estimate to the light reaching the photodiode (transmitted light) after passing through the droplets so it is the main parameter that will change by changing the dispersed phase.

Figure 5.13: The normalized integral as a function of the flux of the dispersed phase and the transit time .

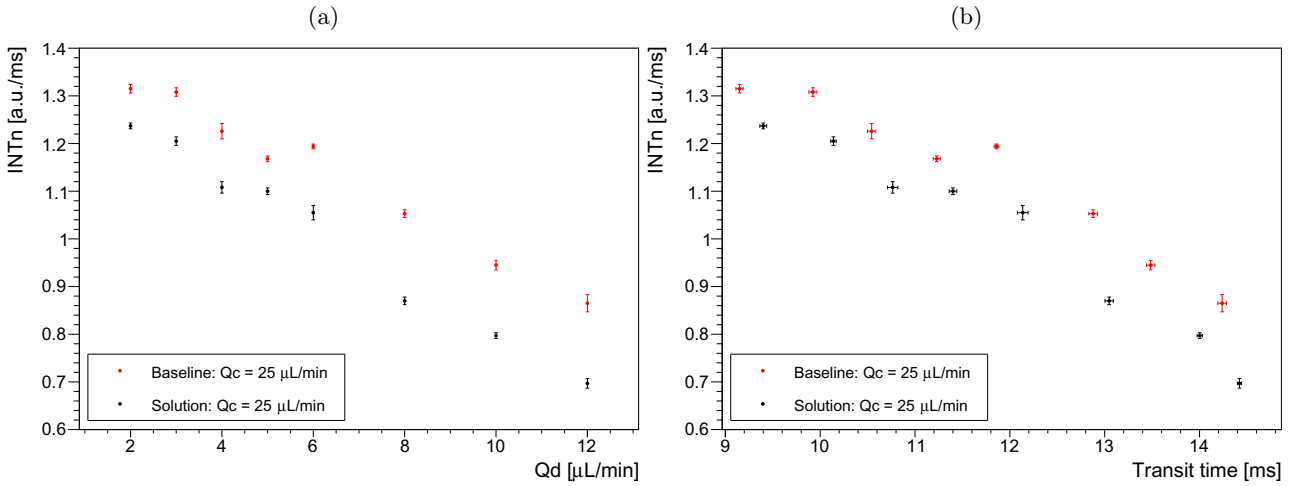

Figure 5.14: The normalized integral as a function of the velocity of the droplets and the length of the droplets, that are the most relevant parameters obtained from the camera.

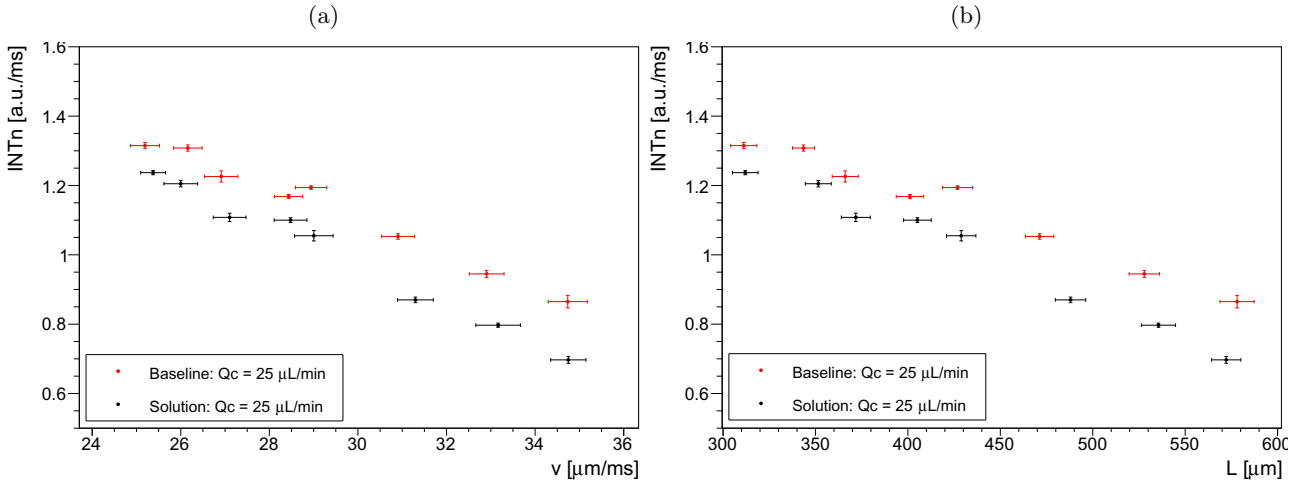

The observations one can make from these plots are the following:

- based on what we have just seen, our setup has been successful in the qualitative detection of the proteins inside the dispersed phase for the lowest concentration considered. This is true since there is a clear difference between our baseline (that is the background) and the solution, that is our signal of interest. Please note that usually the background lies below the signal to study but in our case we are looking at transmitted light and, since the reaction occurs with the insertion of proteins, the transmitted light (so INTn in this case) will be lower for the solution: visually the dispersed phase gets darker with the addition of B.S.A..
- It is worth mentioning that, although not fully reported in this thesis, all the data presented (here and also later in this work) deriving by the analysis coming from the measurements with the opto-microfluidic platform, have been also compared with the ones coming from the synchronous imaging processing (CCD). The overall amount of data analyzed is much larger than the one reported here, and no data have been discarded, even if not presented. Talking about the data just reported coming from the imaging processing, these data are consistent with what acquired with the opto-microfluidic platform. I am validating the use of the opto-microfluidic platform as a standalone device with respect to the addition of a CCD which is in fact not necessary in our case. It is important to note that the video analysis is also time and effort consuming so by removing it one can save both time and money.
  It is also possible to physically get the information of the length of the droplets and their velocity, too, by just considering the photodiode plus a prior calibration to relate, thanks to some fitting parameters, the transit time (and also the frequency that is another parameter that can be obtained from the photodiode) to the effective length of the droplets (in μm) and the velocity. To be clearer, by referring to the Figure 5.15:

Figure 5.15: Image (not in scale) of the revelation of the passage of the drop by the guide (taken from [16]).

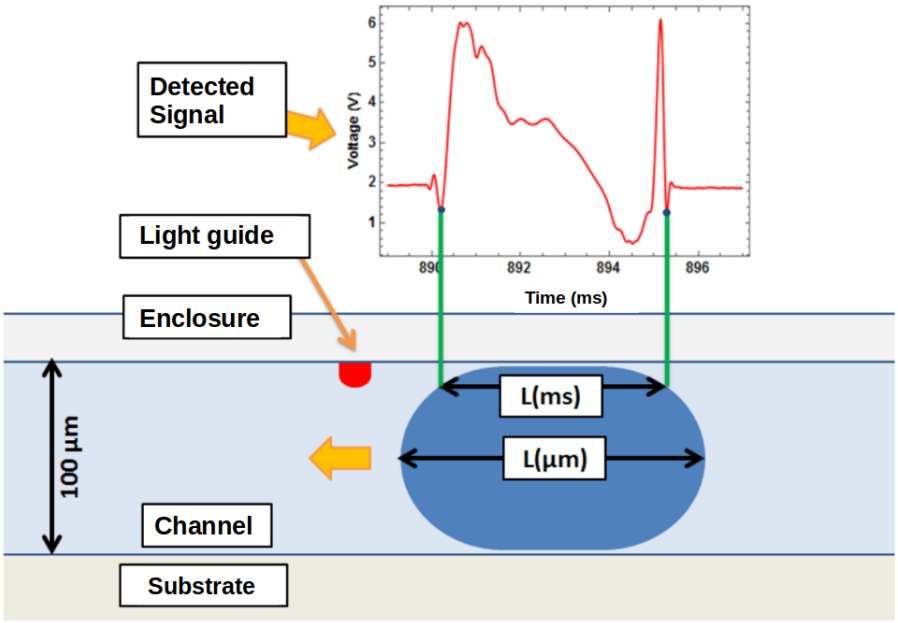

considering all the possible dependencies such as on the speed, transit time and droplet profile, the length L [μm] can be written as

$$L[\mu m] = v(L[\mu m]) \cdot L[ms] + k(L[\mu m]) \tag{5.4}$$

and after fitting the points obtained by associating the transit time to the length of the droplets for each measurement of interest, a fit for example of the type

$$L[\mu m] = a + b \cdot L[ms] + c \cdot L[ms]^2 \tag{5.5}$$

I can rewrite the above equation as

$$L[\mu m] = v(L[ms]) \cdot L[ms] + k(L[ms]) \tag{5.6}$$

exploiting the biunivocal correspondence just found. A more detailed explanation of such procedure can be found here [16].

Just to be a little more quantitative regarding the trends followed by the data in the plots just shown (Figure 5.13 and Figure 5.14), I performed some linear fits, both for the baseline and the solution, that are presented below (following the same presentation pattern as above).

Figure 5.16: Linear fits of the normalized integral as a function of the flux of the dispersed phase and the transit time.

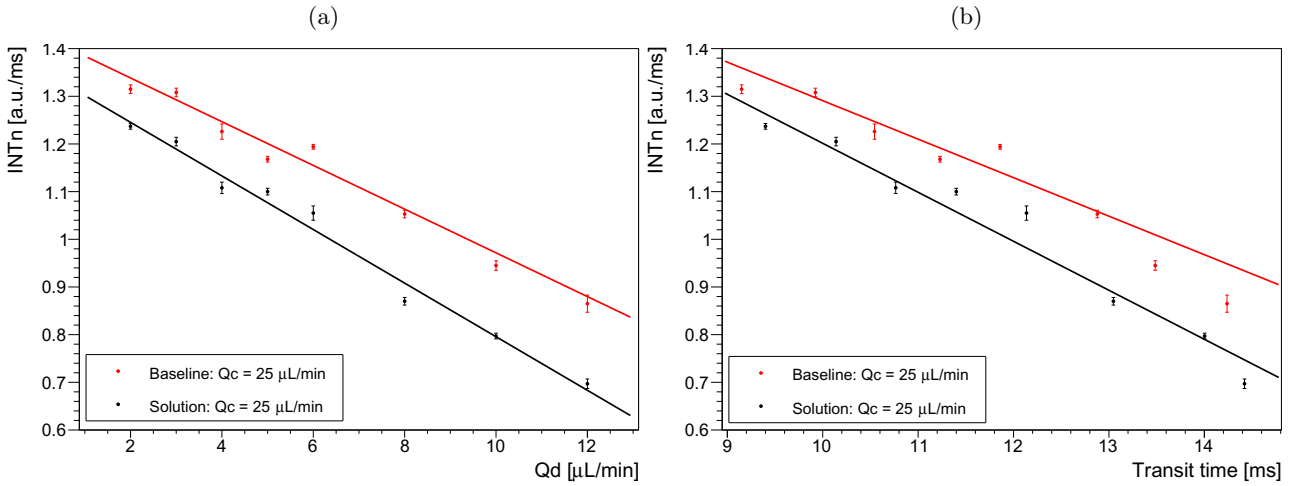

Figure 5.17: Linear fits of the normalized integral as a function of the velocity of the droplets and the length of the droplets.

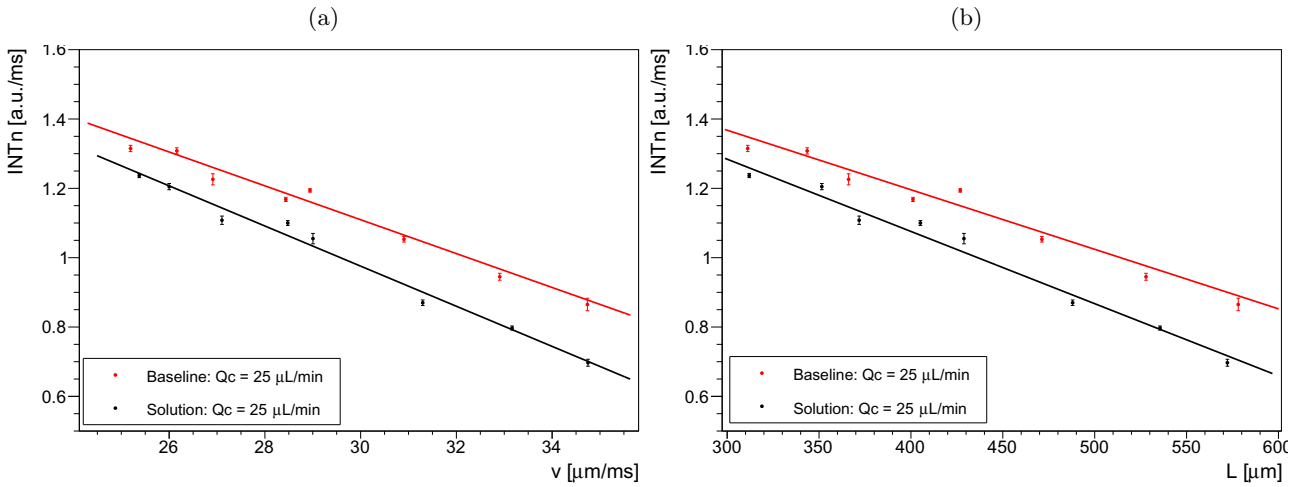

Then I calculated the residuals. Let's first focus on all the residuals plots for the baseline (Figure 5.18 and Figure 5.19):

Figure 5.18: Residuals of the fits (baseline) of the normalized integral as a function of the flux of the dispersed phase and the transit time.

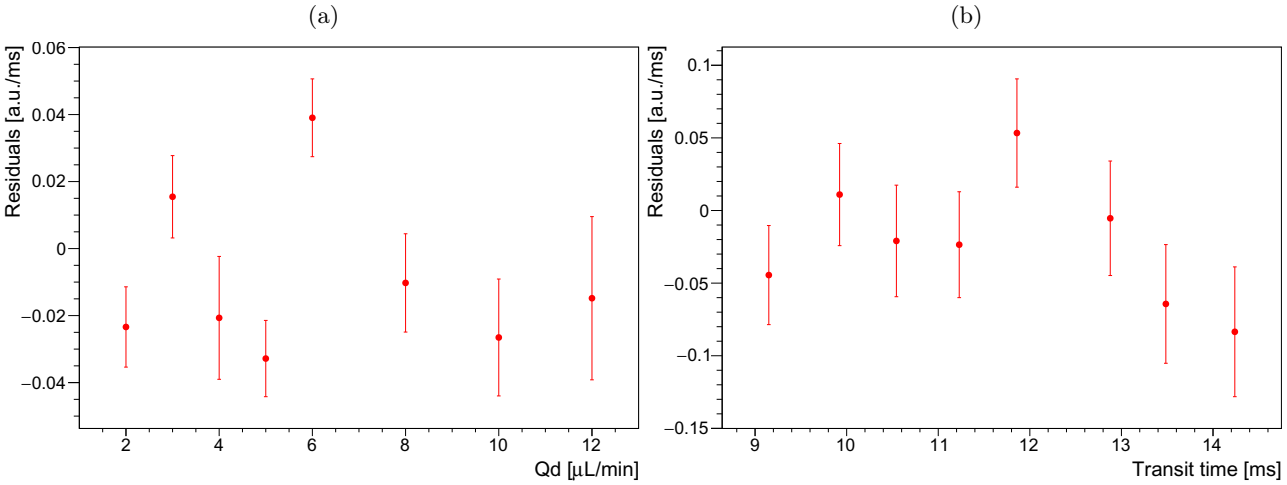

Figure 5.19: Residuals of the fits (baseline) of the normalized integral as a function of the velocity of the droplets and the length of the droplets.

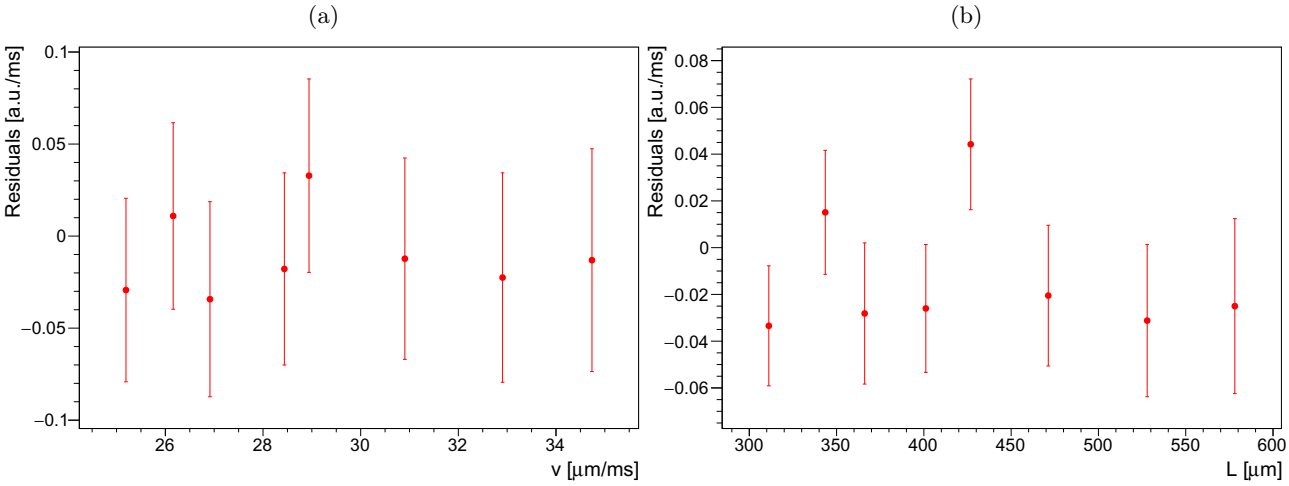

Now let's consider all the residuals plots for the solution (Figure 5.20 and Figure 5.21):

Figure 5.20: Residuals of the fits (solution) of the normalized integral as a function of the flux of the dispersed phase and the transit time.

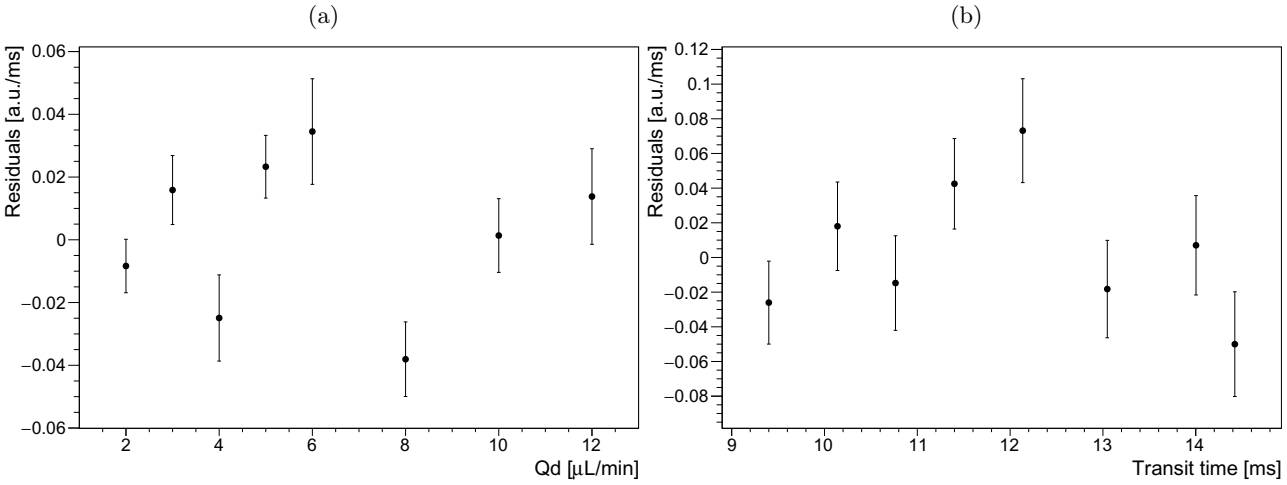

Figure 5.21: Residuals of the fits (solution) of the normalized integral as a function of the velocity of the droplets and the length of the droplets.

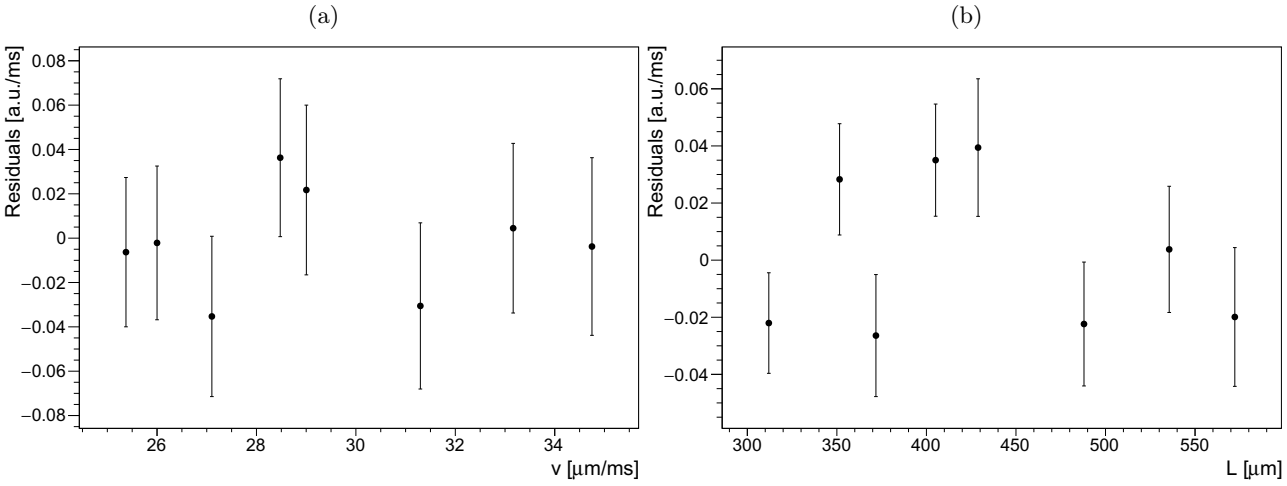

As can be seen, all the residuals are randomly distributed and near zero.
Now I can go back to the fits I showed above (Figure 5.16 and Figure 5.17)to describe the fitting functions used and all the parameters obtained. Note that all the parameters reported have been calculated thanks to a ROOT interface with MINUIT2 libraries [24] [25] and the MIGRAD method.
Talking about Figure 5.16(a) I have:

Baseline:

$$y = mx + q = -0.046\frac{a.u. \cdot min}{ms \cdot \mu l} \cdot x + 1.43\frac{a.u.}{ms} \tag{5.7}$$

Solution:

$$y = mx + q = -0.056\frac{a.u. \cdot min}{ms \cdot \mu l} \cdot x + 1.36\frac{a.u.}{ms} \tag{5.8}$$

Table 5.1: Tables containing the parameters of the linear fits of the plot INTn vs Q_d.

(a) Baseline.

m[$\frac{a.u.\cdot min}{ms\cdot\mu l}$]	σ_m[$\frac{a.u.\cdot min}{ms\cdot\mu l}$]	q[$\frac{a.u.}{ms}$]	σ_q[$\frac{a.u.}{ms}$]
-0.046	0.001	1.43	0.01

(b) Solution.

m[$\frac{a.u.\cdot min}{ms\cdot\mu l}$]	σ_m[$\frac{a.u.\cdot min}{ms\cdot\mu l}$]	q[$\frac{a.u.}{ms}$]	σ_q[$\frac{a.u.}{ms}$]
-0.056	0.001	1.36	0.01

Now focusing on the baseline I report the covariance and the correlation matrices:

	q	m
q	0.00006	-0.000008
m	-0.000008	0.000001

(a) Covariance matrix.

	q	m
q	1	-0.93
m	-0.93	1

(b) Correlation matrix.

Instead for the solution:

	q	m
q	0.00003	-0.000004
m	-0.000004	0.0000007

(a) Covariance matrix.

	q	m
q	1	-0.87
m	-0.87	1

(b) Correlation matrix.

Talking about Figure 5.16(b) I have[1]:

Baseline:

$$y = mx + q = -0.081\frac{a.u.}{ms^2}\cdot x + 2.10\frac{a.u.}{ms} \quad (5.9)$$

Solution:

$$y = mx + q = -0.103\frac{a.u.}{ms^2}\cdot x + 2.23\frac{a.u.}{ms} \quad (5.10)$$

Table 5.2: Tables containing the parameters of the linear fits of the plot INTn vs Transit time.

(a) Baseline.

m[$\frac{a.u.}{ms^2}$]	σ_m[$\frac{a.u.}{ms^2}$]	q[$\frac{a.u.}{ms}$]	σ_q[$\frac{a.u.}{ms}$]
-0.081	0.002	2.10	0.03

(b) Solution.

m[$\frac{a.u.}{ms^2}$]	σ_m[$\frac{a.u.}{ms^2}$]	q[$\frac{a.u.}{ms}$]	σ_q[$\frac{a.u.}{ms}$]
-0.103	0.002	2.23	0.02

Now focusing on the baseline I report the covariance and the correlation matrices:

	q	m
q	0.0007	-0.00006
m	-0.00006	0.000005

(a) Covariance matrix.

	q	m
q	1	-0.994
m	-0.994	1

(b) Correlation matrix.

[1]Note that for this fit I considered just the errors associated to the INTn, that is to say the quantity in ordinate.

Instead for the solution:

	q	m
q	0.0003	-0.00003
m	-0.00003	0.000002

(a) Covariance matrix.

	q	m
q	1	-0.988
m	-0.988	1

(b) Correlation matrix.

Talking about Figure 5.17(a) I have[2]:

Baseline:

$$y = mx + q = -0.0489\frac{a.u.}{\mu m} \cdot x + 2.58\frac{a.u.}{ms} \quad (5.11)$$

Solution:

$$y = mx + q = -0.058\frac{a.u.}{\mu m} \cdot x + 2.71\frac{a.u.}{ms} \quad (5.12)$$

Table 5.3: Tables containing the parameters of the linear fits of the plot INTn vs v.

(a) Baseline.

m$[\frac{a.u.}{\mu m}]$	$\sigma_m[\frac{a.u.}{\mu m}]$	q$[\frac{a.u.}{ms}]$	$\sigma_q[\frac{a.u.}{ms}]$
-0.049	0.001	2.58	0.04

(b) Solution.

m$[\frac{a.u.}{\mu m}]$	$\sigma_m[\frac{a.u.}{\mu m}]$	q$[\frac{a.u.}{ms}]$	$\sigma_q[\frac{a.u.}{ms}]$
-0.058	0.001	2.71	0.03

Now focusing on the baseline I report the covariance and the correlation matrices:

	q	m
q	0.001	-0.00005
m	-0.00005	0.000002

(a) Covariance matrix.

	q	m
q	1	-0.997
m	-0.997	1

(b) Correlation matrix.

Instead for the solution:

	q	m
q	0.0006	-0.00002
m	-0.00002	0.0000007

(a) Covariance matrix.

	q	m
q	1	-0.994
m	-0.994	1

(b) Correlation matrix.

Talking about Figure 5.17(b) I have[3]:

Baseline:

$$y = mx + q = -0.0017\frac{a.u.}{ms \cdot \mu m} \cdot x + 1.88\frac{a.u.}{ms} \quad (5.13)$$

Solution:

$$y = mx + q = -0.00208\frac{a.u.}{ms \cdot \mu m} \cdot x + 1.91\frac{a.u.}{ms} \quad (5.14)$$

[2]Note that for this fit I considered just the errors associated to the INTn, that is to say the quantity in ordinate.
[3]Note that for this fit I considered just the errors associated to the INTn, that is to say the quantity in ordinate.

Table 5.4: Tables containing the parameters of the linear fits of the plot INTn vs L.

(a) Baseline.

m[$\frac{a.u.}{ms\cdot\mu m}$]	σ_m[$\frac{a.u.}{ms\cdot\mu m}$]	q[$\frac{a.u.}{ms}$]	σ_q[$\frac{a.u.}{ms}$]
-0.0017	0.0001	1.88	0.02

(b) Solution.

m[$\frac{a.u.}{ms\cdot\mu m}$]	σ_m[$\frac{a.u.}{ms\cdot\mu m}$]	q[$\frac{a.u.}{ms}$]	σ_q[$\frac{a.u.}{ms}$]
-0.00208	0.00003	1.91	0.01

Now focusing on the baseline I report the covariance and the correlation matrices:

	q	m
q	0.0004	-0.0000009
m	-0.0000009	0.000000002

(a) Covariance matrix.

	q	m
q	1	-0.989
m	-0.989	1

(b) Correlation matrix.

Instead for the solution:

	q	m
q	0.0002	-0.0000004
m	-0.0000004	0.0000000009

(a) Covariance matrix.

	q	m
q	1	-0.978
m	-0.978	1

(b) Correlation matrix.

Recalling the observations previously exposed concerning the redundancy of the plots coming from the data analysis of the data obtained thanks to the CCD, from now on we will consider just the parameters that can be obtained from the opto-microfluidic platform thanks to the photodiode and without the camera.
Focusing on the smaller concentration, we can begin to try to understand what are the best conditions for our apparatus to detect the proteins. Before proceeding, the core of the data analysis will be outlined.
First of all I show the baseline values of INTn (background) and the solution ones to expose the difference between both transmitted lights.
In alternative the quotient of the two, can be considered instead.

Figure 5.22: Background subtraction-like procedure.

(a) *Difference of the signals.*

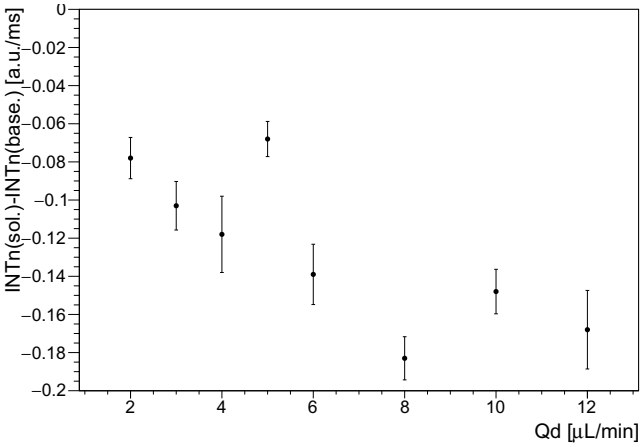

(b) *Quotient of the signals.*

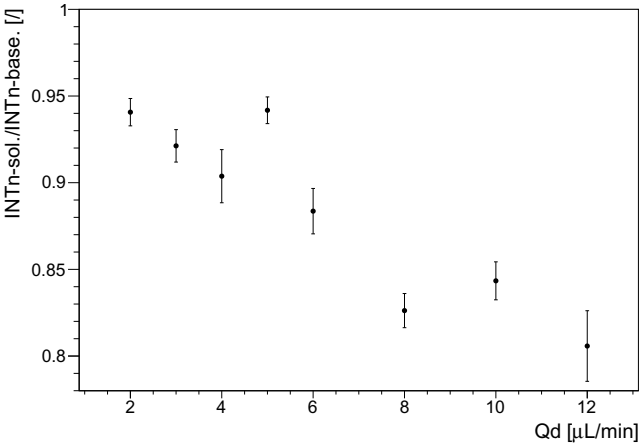

It clearly emerges that at bigger values of the flux, so Q_d, there is a bigger gap between the baseline and the solution which manifests itself in being "more negative" so smaller when looking at the difference, and "more near zero" when looking at the quotient. It starts to be clear that the detection of proteins

can be simplified for a certain range of Q_d or maybe for a certain value.
There are various advantages in fixing a single value of Q_d for the measurements rather than doing a full "curve study", some of which are:

1 from the perspective of the usage of this apparatus for biological investigations, it is easier to implement a single value of Q_d as a requirement for the measure rather than being necessary a "scan" across a big range of flux values;

2 it is not only cheaper, but also less time consuming. For such biological system, time is a very important parameter so having the ability to concentrate the measures in 10 second rather than being necessary forty minutes (like in the case of a full curve study) is crucial. As the time passes by, the aging of the solution in unavoidable and this leads to all types of artifacts like the formation of agglomerates that will mess up the measure.

So far we talked about the normalized integral as a good parameter since it contains the information of the transmitted light but actually there is also another important parameter: the "Min". As already said, the minimum is the simple average of the minimum intensity in the signal associated with the droplet and normalized to the oil voltage (measured in a.u.).
Let's see if we can see the separation between the baseline and the solution we saw by looking at the INTn plotted as a function of Q_d, also by looking at the Min as a function of Q_d (data will be presented for the 0.14 mg/ml concentration). As example:

Figure 5.23: Comparison between the INTn and the Min as a function of Q_d for the 0.14 mg/ml concentration.

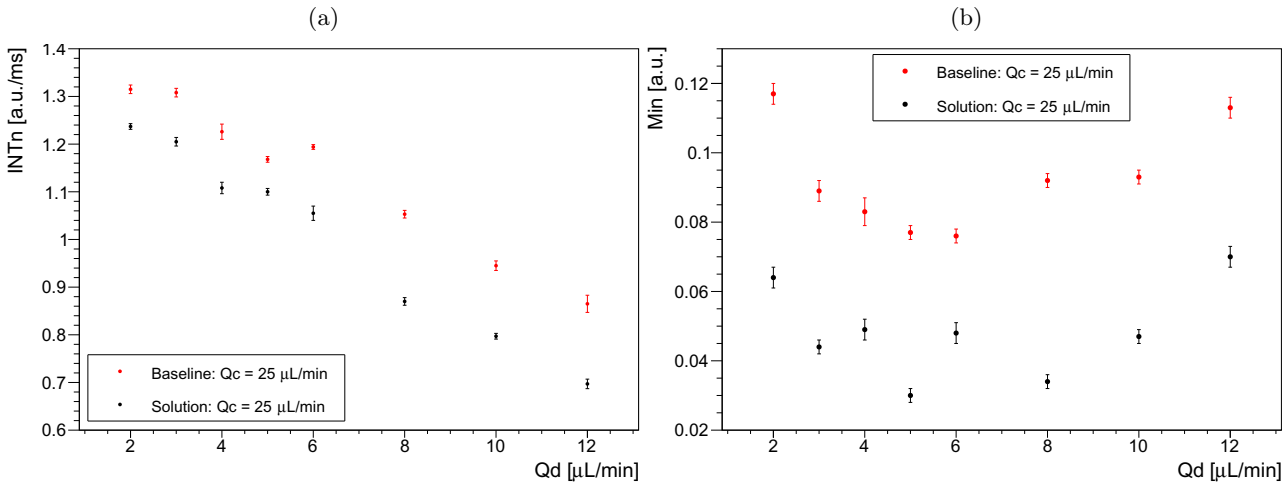

What can be noted is that the Min is a viable option to monitor the system since it shows a clear separation between the baseline and the solution as the normalized integral does.
Just for completeness, what we said regarding the information one can obtain from the photodiode compared to those obtainable from the camera is also true for the Min. As an example let's check the Figure 5.24:

Figure 5.24: The Minimum as a function of the transit time and the length of the droplets.

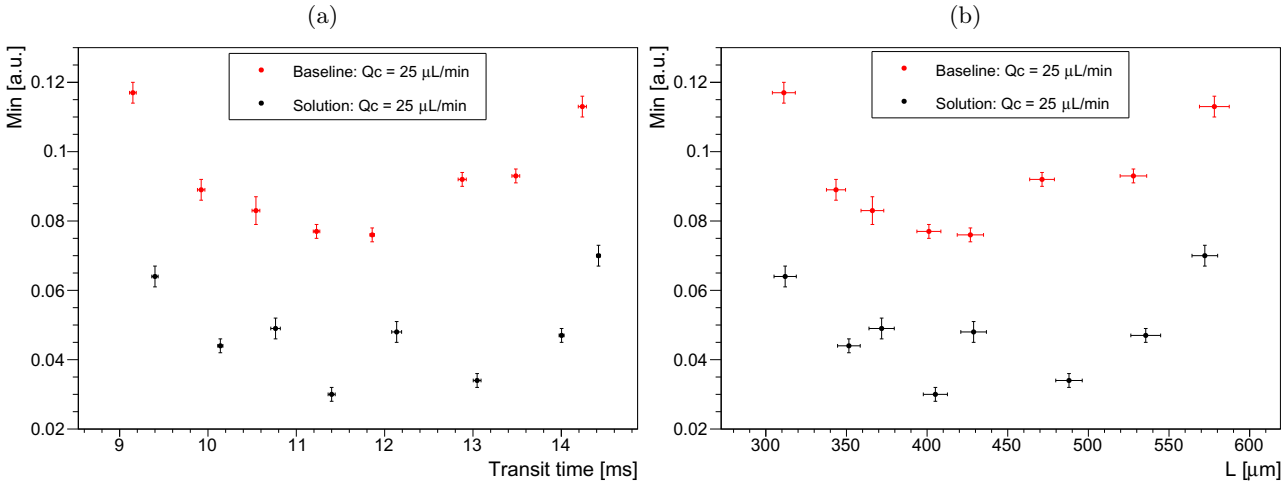

Again, we are validating the fact that camera can be removed under proper prior calibrations to obtain all the important parameters just from the photodiode.
Assessed that the opto-microfluidic platform is sensible to the protein, we will consider now also the other two concentrations: 0.28 mg/ml and 1.4 mg/ml. I want to start evaluating the effects of higher concentrations in small volumes of fluid and also taking a look at the possible presence of the concentration quenching.
First of all I start by showing the obtained trend between the INTn and the Q_d also for the other two concentrations (I stopped at $Q_d = 10$ μl/min):

Figure 5.25: The trend of INTn versus Q_d for the other two concentrations.

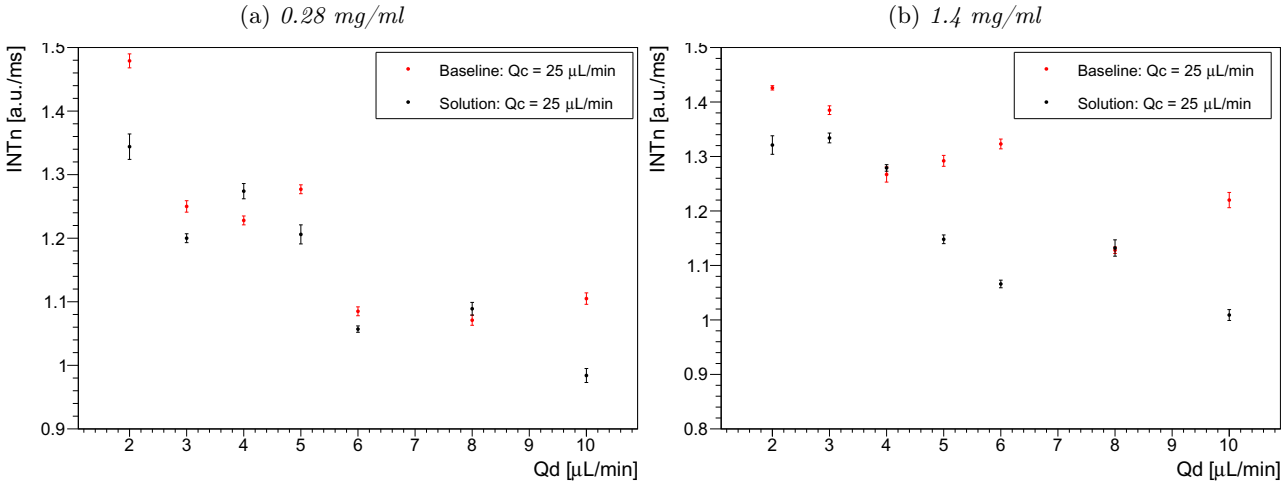

It is clear that moving towards higher concentrations could compromise a bit the system thus resulting into some artifacts that will affect the measurements. This can be evident in some "problematic points" (the ones where the transmitted light appears to be higher for the solution rather than the baseline) are consistent for both concentrations being Q_d=4 μl/min and Q_d=8 μl/min: this needs further investigations since it can be linked to the presence of some different regimes in the considered system.
However the gap between the baseline and the solution is clear: also with these concentrations I was successful in detecting the presence of the proteins with the apparatus.
Another important thing to notice is the fact that also here for these two concentrations, one of the bigger difference between background and signal is obtained for Q_d=10 μl/min, as it was for the 0.14 mg/ml concentration. A pattern starts to emerge, thus showing the possibility to find a single value

for which the detection is clearer.
It is useful to compare all three concentrations by plotting them in the same graph to understand for example if there is such consistent value of Q_d for which the detection of proteins is less affected by artifacts (concentration quenching is reduced, etc..).
Although information can be achieved by looking at INTn or Min, in the following we will focus on the INTn. Let's start by plotting both the difference between INTn of the solution and the baseline and also the respective values obtained with the ratio:

Figure 5.26: First comparison between all three concentrations.

(a) *Difference-based ordinate value.* (b) *Quotient-based ordinate value.*

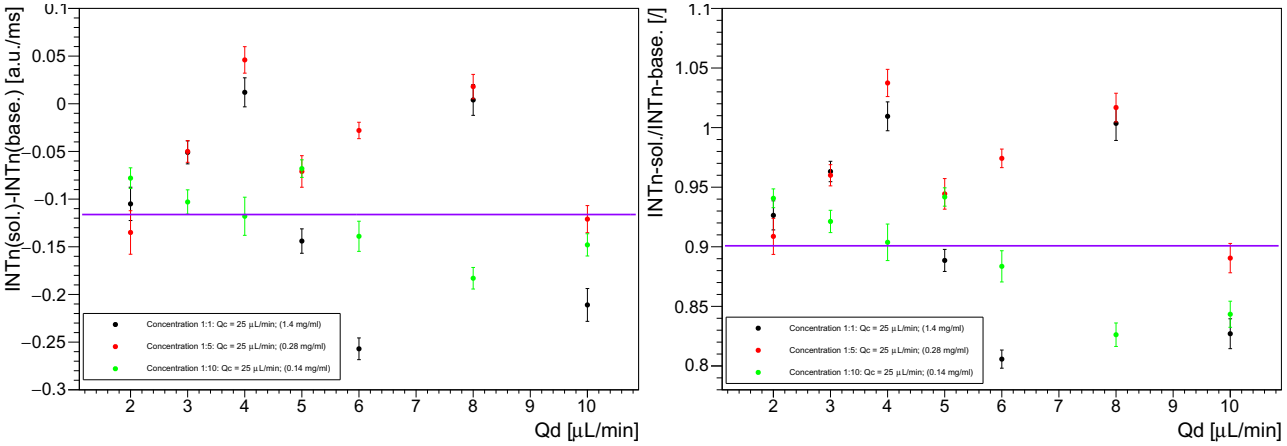

The meaning of the qualitative purple lines is just to have some graphical thresholds to help isolate some points. That is to say that there are no quantitative reasons for their position on the plots, but they have been placed there arbitrarily just for visualization sake. In particular I see that for Q_d=10 μl/min I consistently get in both cases the lowest possible values in ordinate by having at the same time also all the three points of the three concentrations close to each other. I am interested in the lowest possible values because what I am looking at in ordinate is basically the difference between the signal and the background. Since in this case the background is described by the baseline measures of transmitted light, whose values are bigger than the solution ones, we are interested in the lowest possible values, smaller than zero. Other than that we want all points below a certain value for consistency in the method. Both these requests get satisfied by the points corresponding to Q_d=10 μl/min.
We can say that to obtain a proper detection of proteins in the range of concentrations explored, the best conditions among the one I investigated are the following: the flux of the continuous phase Q_c=25 μl/min; the flux of the dispersed phase Q_d=10 μl/min; the concentration of B.S.A. with respect to the MilliQ distilled water [4] ranging from 0.14 mg/ml to 1.4 mg/ml; red laser light at 632.8 nm (He-Ne laser); the microfluidic channel of dimension 200 μm $\times$ 100 μm (width $\times$ height); hexadecane plus 3% SPAN80 as continuous phase.

It is worth mentioning that the transmitted light is actually dependent not only on the medium it passes through (and therefore on the content of the droplets in our case) but is also dependent on the geometry of the droplets. Due to effects related to diffraction and scattering of light, having longer rather than smaller droplets will make a difference, thus affecting the value of transmitted light detected by the photodiode.
This observation is an important hint towards the reaching of quantitative previsions regarding the concentrations of proteins inserted in the dispersed phase thus obtaining a calibration with our experimental apparatus in order to reach situations in which it is possible to predict the concentration of the dispersed phase of which the droplets are composed starting from measurements of transmitted light. Although this last subject is not an aim of my thesis work, here are some considerations on the effects

[4] Remember that to get the full solution one must add to those ml also thirty times that volume of Bradford reagent.

that the geometry of the droplets has had on my measurements of transmitted light.
A natural starting point to understand the possible contribution of the length of the droplets is by looking at the Figure 5.27 (I choose for simplicity the lowest concentration, but the same thing can be seen also for the others):

Figure 5.27: Transit time versus Q_d for the 0.14 mg/ml concentration.

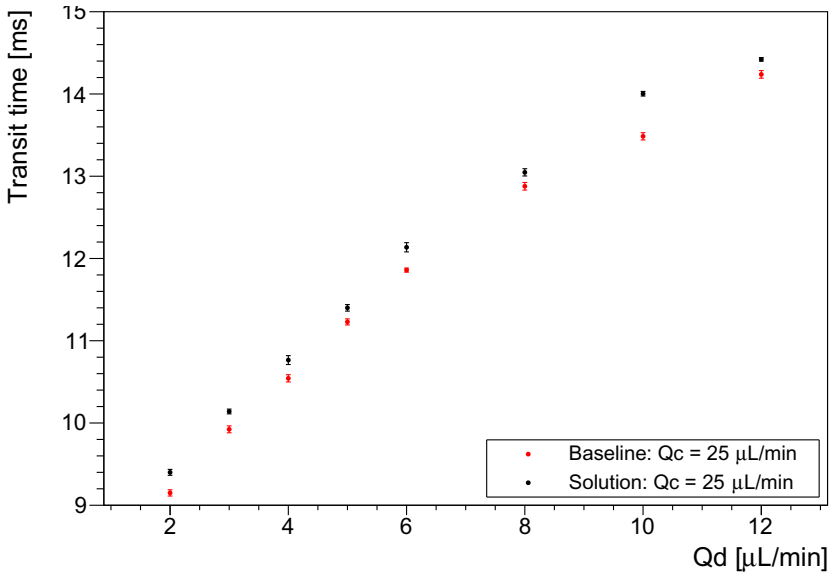

Here is reported the relation between the transit time (that is in bi-univocal correspondence to the length of the droplets under proper calibrations, as already underlined by Garstecki et al. in the squeezing regime) and the flux of the dispersed phase, that is the parameter I focused for my previous analysis.
One can see that the length of the droplets made by the solution is systematically bigger with respect to those composed by the baseline. So by comparing that plot to the graph I showed at the beginning regarding the variation of INTn as a function of Q_d, I can make an important observation.

Figure 5.28: INTn vs Q_d for 0.14 mg/ml concentration.

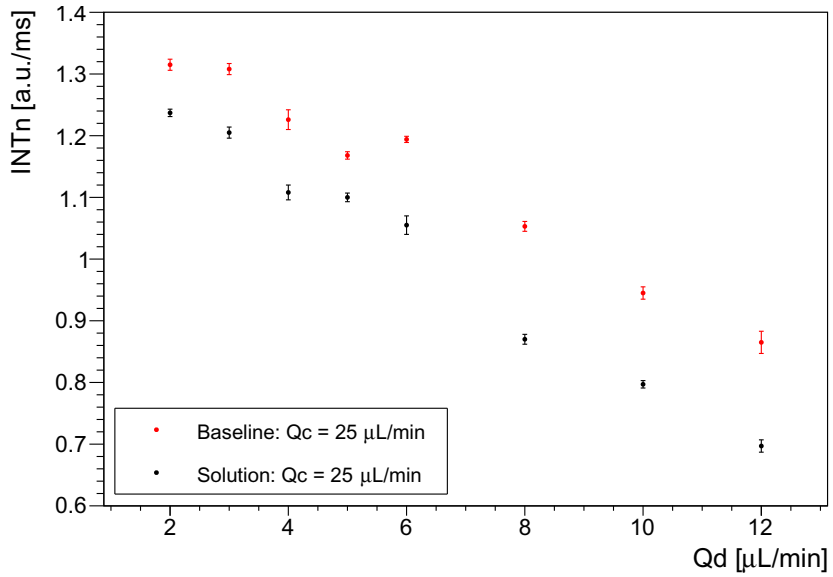

One might suspect that the difference in transmitted light between the solution and the baseline arises only from the geometrical difference between the droplets. It is clear that, since the INTn is built like that, there is a dependence on the length of it (represented here by the transit time but we have seen

that there is a correspondence between ms and μm). Just to be more quantitative in this case, I can calculate the Δ of those transit times and plot it as a function of Q_d. I obtain:

Figure 5.29: Difference between transit times as a function of Q_d in the case of the 0.14 mg/ml concentration.

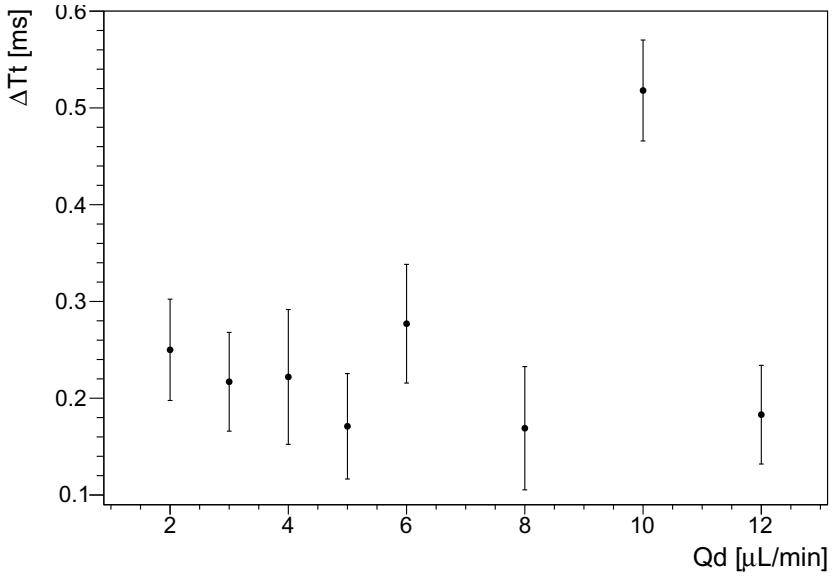

There is a peak on the value we underlined as the best one so this could be a problem. By the way, by taking a look at the same comparison graph as the ones we showed above between concentrations but this time not considering the INTn but the INT (thus removing partially the dependence on the transit time) I see that the $Q_d = 10$ μl/min seems to be still the best one for the reasons previously pointed out:

Figure 5.30: Comparison between the three concentrations with the difference of the transmitted light (using the non normalized integral, INT) and Q_d.

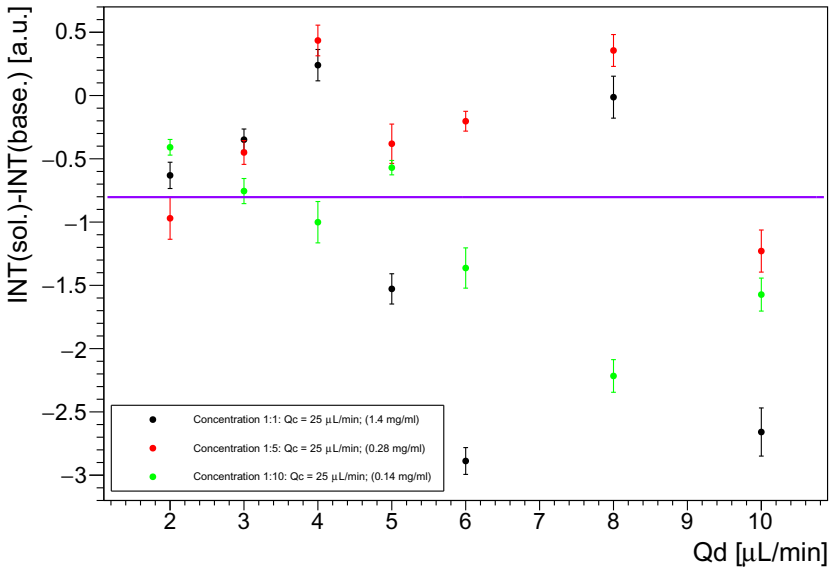

By referring to the Figure 5.27, we observe that there seems to be one trend for points below $Q_d = 7$ μl/min and one trend for points above. To further investigate qualitatively this behavior, some fits on the points of both the baseline and the solution on both ranges have been performed:

Figure 5.31: Fits on the points of both the baseline and the solution on both ranges: points below Q_d = 7 μl/min and above.

(a) Baseline fitted

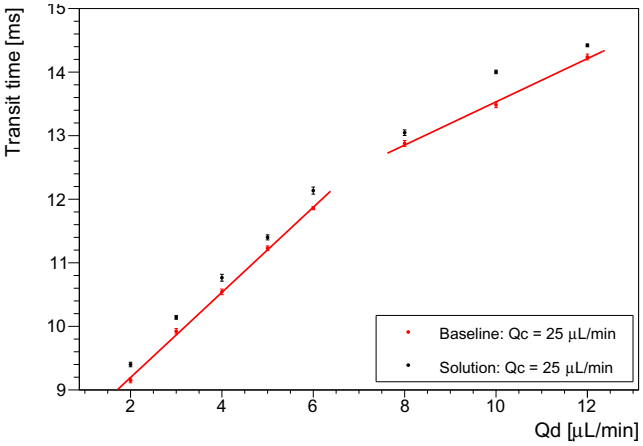

(b) Solution fitted

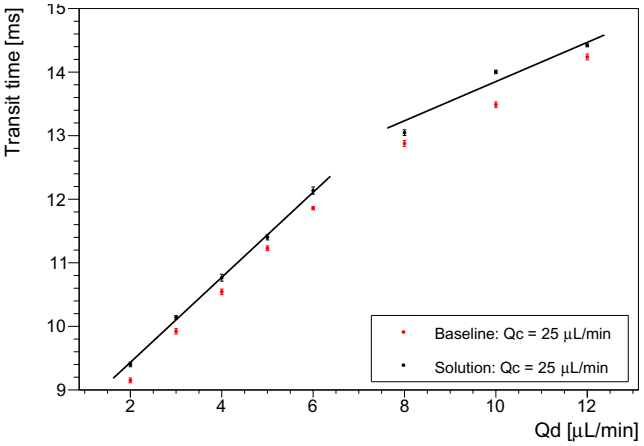

Now I describe the fitting functions used and all the parameters obtained. Note that, as above, all the parameters reported have been calculated thanks to a ROOT interface with MINUIT2 libraries [24] [25] and the MIGRAD method.
Talking about the baseline I have:

Q_d<7μl/min: Q_d>7μl/min:

$$y = mx + q = 0.67\frac{ms \cdot min}{\mu l} \cdot x + 7.86ms \quad (5.15) \qquad y = mx+q = 0.34\frac{ms \cdot min}{\mu l} \cdot x + 10.1ms \quad (5.16)$$

Table 5.5: Tables containing the parameters of the linear fits of the baseline for the plot Transit time vs Q_d.

(a) Points below Q_d = 7 μl/min.

m[$\frac{ms \cdot min}{\mu l}$]	σ_m[$\frac{ms \cdot min}{\mu l}$]	q[ms]	σ_q[ms]
0.67	0.01	7.86	0.05

(b) Points above Q_d = 7 μl/min.

m[$\frac{ms \cdot min}{\mu l}$]	σ_m[$\frac{ms \cdot min}{\mu l}$]	q[ms]	σ_q[ms]
0.34	0.02	10.1	0.2

Now focusing on the points below Q_d = 7 μl/min I report the covariance and the correlation matrices:

	q	m
q	0.002	-0.0005
m	-0.0005	0.0001

(a) Covariance matrix.

	q	m
q	1	-0.947
m	-0.947	1

(b) Correlation matrix.

Instead for the points above Q_d = 7 μl/min:

	q	m
q	0.03	-0.003
m	-0.003	0.0003

(a) Covariance matrix.

	q	m
q	1	-0.987
m	-0.987	1

(b) Correlation matrix.

Talking about the solution I have:

Q_d<7μl/min: Q_d>7μl/min:

$$y = mx + q = 0.67\frac{ms \cdot min}{\mu l} \cdot x + 8.09ms \quad (5.17) \qquad y = mx + q = 0.31\frac{ms \cdot min}{\mu l} \cdot x + 10.8ms \quad (5.18)$$

Table 5.6: Tables containing the parameters of the linear fits of the solution for the plot Transit time vs Q_d.

(a) Points below Q_d = 7 μl/min.

m[$\frac{ms \cdot min}{\mu l}$]	σ_m[$\frac{ms \cdot min}{\mu l}$]	q[ms]	σ_q[ms]
0.67	0.01	8.09	0.05

(b) Points above Q_d = 7 μl/min.

m[$\frac{ms \cdot min}{\mu l}$]	σ_m[$\frac{ms \cdot min}{\mu l}$]	q[ms]	σ_q[ms]
0.31	0.01	10.8	0.1

Now focusing on the points below Q_d = 7 μl/min I report the covariance and the correlation matrices:

	q	m
q	0.003	-0.0006
m	-0.0006	0.0002

(a) Covariance matrix.

	q	m
q	1	-0.939
m	-0.939	1

(b) Correlation matrix.

Instead for the points above Q_d = 7 μl/min:

	q	m
q	0.02	-0.001
m	-0.001	0.0001

(a) Covariance matrix.

	q	m
q	1	-0.991
m	-0.991	1

(b) Correlation matrix.

Focusing for example on the fit of the baseline, I see that the angular coefficient obtained by fitting, with a linear trend, points above Q_d = 7 μl/min is smaller than the angular coefficient obtained from the fit of points below Q_d = 7 μl/min. This can be interpreted as if the length of the droplets influences less the measures taken with Q_d > 7 μl/min thus reinforcing the estimate of Q_d = 10 μl/min as being the best based on our investigations.

5.5.2 Measurement in time

Some plots regarding the variation of some parameters of interest with the passing of time have been performed. As already said, I took measurements for just the 1.4 mg/ml concentration. With this type of measurement I refer to the acquisition of various parameters, in this case I chose to show the most relevant ones such as INTn, Min and the transit time, related to the droplets passing in the chip at constant intervals in time without modifying anything in the starting configuration of the setup. The time "zero" actually refers to forty minutes after the incubation has started, and I took measurements for eighty minutes for the baseline but I stopped at sixty-four for the solution.

Figure 5.32: Evolution in time of the INTn and the Min.

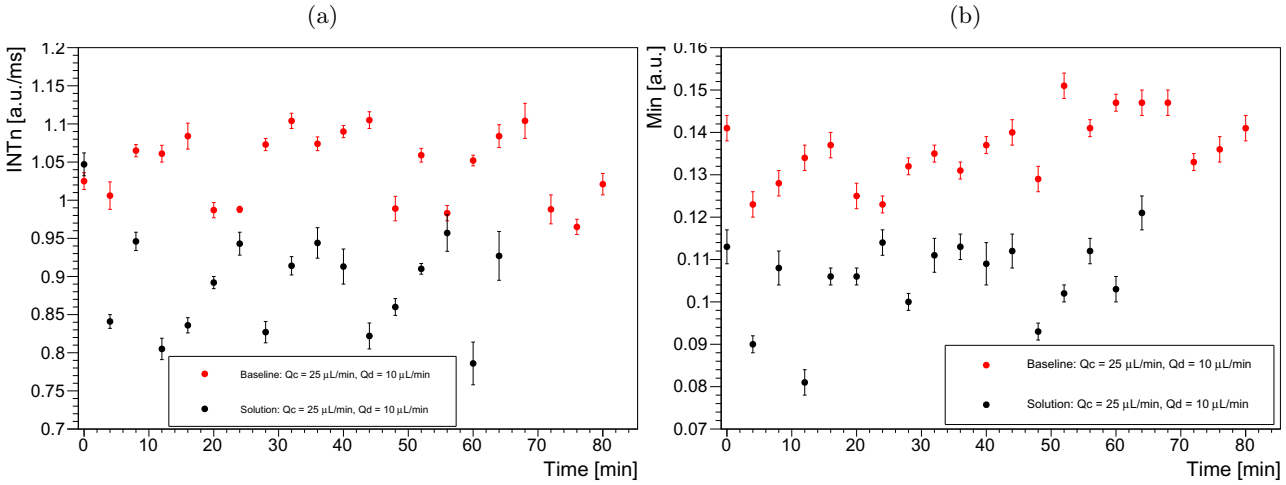

Figure 5.33: Evolution in time of the transit time.

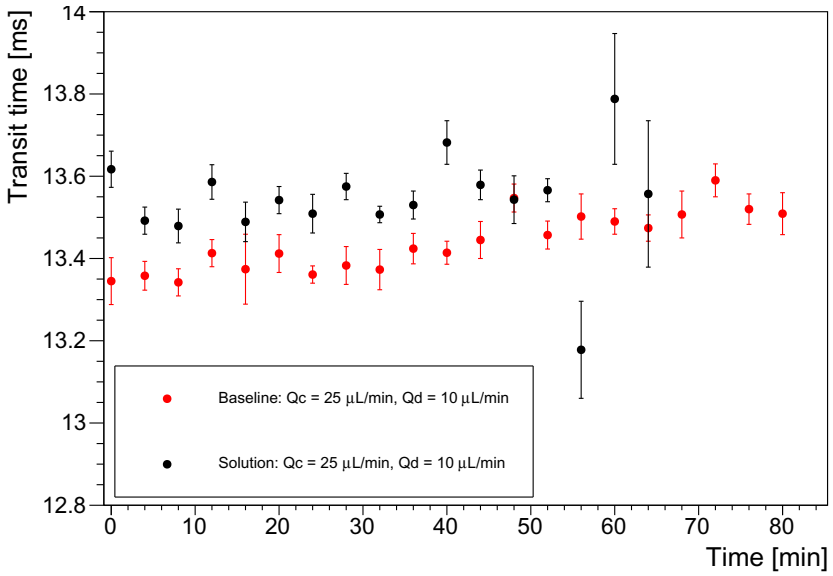

No systematic trend can be observed by looking at the graph that refers to the normalized integral. As regards the Minimum, on the other hand, a slight increase in the average value over time can be observed referring to the baseline and the solution. As far as the transit time is concerned, it can be seen that the greatest effect that the aging of the solution had on the system was realized both on the variation of the average value but also on the increase in the errors associated with the last three measurements related to the times of fifty-six minutes, sixty and sixty-four minutes (which, if the incubation time is also taken into account, correspond to 1h and 36 minutes, 1h and 40 minutes and 1h and 44 minutes).
The significance of such an increase in errors can be interpreted by understanding how they are calculated. Since each point (value) reported in the graph derives from the average over all the single droplet values for a train of about 150 droplets, the errors associated with these average values are calculated through dispersion. The increase in the error bars can be interpreted as an increase in the dispersion of the droplet size (in this case the transit time) due to the aging of the solution.
It should be noted that the measurements carried out for the curve study are completed in a time equal to 40 minutes (which correspond to a total of 80 minutes taking into account the forty minutes of incubation) well before the times that have been indicated here as problematic.

Chapter 6

Conclusions

In this thesis, the use of an opto-microfluidic device in Lithium Niobate for the detection of proteins within micrometric droplets has been studied. The main purpose of this work was to understand how proteins confined within droplets interact with a light beam, studying the intensity of the signal transmitted as a function of various parameters and concentrations of the proteins in the dispersed phase to understand if it was possible to detect the presence of those with our setup.
In this work it has been shown how our opto-microfluidic platform can be used to detect proteins inside micrometric volumes with a droplet-like shape. A reliable and reproducible measurement protocol has been used and verified. The method has been validated and the usage of the camera as redundant with respect to the platform has been pointed out. A successful qualification of the presence of the protein has been carried out. Three different concentrations were measured and a different behavior between baseline and solution was observed already for the lowest concentration of protein (0.14 mg/ml of B.S.A). The system is therefore suitable for use even at a given value of the flux of the dispersed phase (Q_d) because baseline and solution are distinguishable. The best value found, based on our studies, is $Q_d = 10$ μl/min.
The method is considered reliable as there are repeatable measurement conditions for which the solution is clearly distinct from the baseline. The objectives of the thesis have been fully achieved.
Furthermore the limits of detection and sensitivity were highlighted, in particular towards a more quantitative approach in order to predict in the future the concentration of proteins from transmitted light measurements. Indeed we pointed out the fact that the transmitted light is actually dependent not only on the medium it passes through (and therefore on the content of the droplets in our case) but is also dependent on the geometry of the droplets (see Figure 5.27 on this regard).
We have also seen that in our case this phenomenon did not affect much the measures (see Figure 5.30) despite being something that needs to be studied in detail in the future to obtain quantitative estimates.
Finally we saw that the length of the droplets influenced less the measures taken with $Q_d > 7$ μl/min (see Figure 5.31) thus reinforcing the estimate of $Q_d = 10$ μl/min as being the best value among the ones considered.

Chapter 7

Future perspectives

First of all, as far as the main topic of this thesis, some important perspectives have been highlighted by the results achieved in this work. To obtain an analysis and consequently more quantitative results, the approach used here of single measurements is not sufficient.
In order to provide for quantitative previsions regarding the concentrations of proteins inserted in the dispersed phase further upgrade to both the protocol of measurements and to the data analysis are required.
In order to achieve this aim, a calibration curve is mandatory to reach situations in which it is possible to predict the concentration of the dispersed phase of which the droplets are composed starting from measurements of transmitted light.
As already pointed out, in fact, the transmitted light is actually dependent not only on the medium it passes through (and therefore on the content of the droplets in our case) but also on the geometry of the droplets.
Due to effects related to diffraction and scattering of light, longer rather than smaller droplets will behave differently, thus affecting the value of transmitted light detected by the photodiode. For this reason this artifact will need to be considered and its influence on the measurements possibly reduced or isolated. It is also important to mention that the use of the Bradford reagent has led to some critical issues which can be worked on in the future in order to improve the detection. These are:

- its incompatibility with detergents. Although we saw that a strength of the measurements with droplet is that these allow to confine and separate the dispersed phase and the continuous phase, this might not be sufficient. Indeed interface effects between the two immiscible phases, for instance, have not been studied yet. Unwanted reactions could still occur at the interface. A possible solution is the usage of the already mentioned "Detergent Compatible Bradford Assay" [19];

- the Bradford protein assay is linear over a short range of concentrations. Dilutions of a sample have been necessary. This may have introduced some systematic errors that need to be further investigated in the future;

- the use of a dye, in general, leads to the problem of tube stains that can affect all the measurements;

- the management of incubation time is a critical aspect in this case. Due to the fact that this method is time sensitive all incubation times must be kept monitored and possibly the same when measurements are to be taken;

- the blue color can be measured at any wavelength between $\lambda = 575$ nm and $\lambda = 615$ nm. At the two extremes there is an approximate 10% decrease [19] in the measured amount of absorbance compared to that obtained at $\lambda = 595$ nm. The measurements taken for this work were based on the only good laser light available, that was originated by an He-Ne laser with a nominal $\lambda = 632.8$ nm (red light), so far beyond the ideal condition.

This thesis has therefore put the foundations towards obtaining a device for measuring protein concentrations have been laid.
Finally, after having obtained the possibility of making quantitative predictions regarding concentrations of proteins in the future, this new use of the Lithium Niobate opto-microfluidic platform would join all the other uses already verified: the optical control of droplet motion on Fe-doped Lithium Niobate crystals via photovoltaic effect [6], the Opto-microfludic pH titration [9] and [2], the integration of a photovoltaic tweezer and the integrated light-controlled Liquid crystals cell [2], the characterization of droplets with gold nano-particles in density and diameter [16] and much more.

Appendix A

Other explored setup possibilities for the droplets production

A.1 Double flow meter controlled production

A.1.1 Setup scheme

Figure A.1: Diagram of the experimental apparatus for droplet measurements with two flow meters.

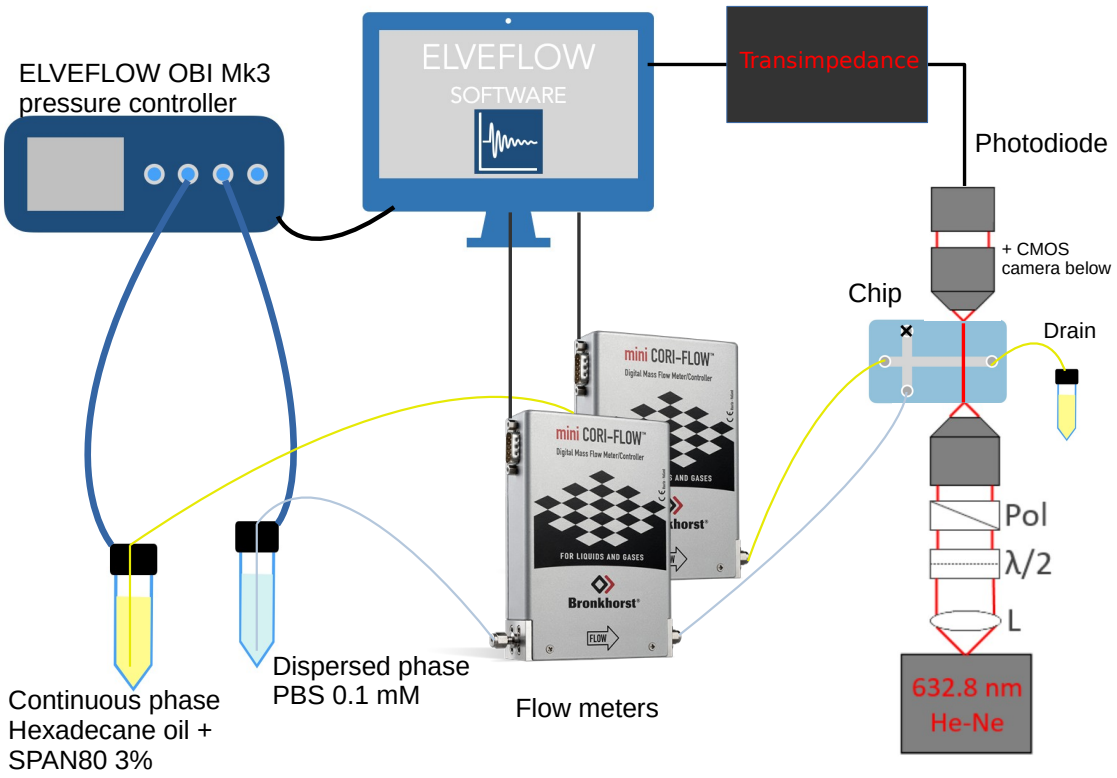

A.1.2 Characterization

With the sample in collinear guide configuration and using a T-junction as a droplets generator, I had to implement a droplets production control with optimal reproducibility at different times and days, comparing the production of droplets with flow control thanks to two flow meters with other production methods. To this end, I controlled both the continuous phase (hexadecane oil with 3% surfactant) and the dispersed phase (here PBS while for the measures suitable for detecting proteins MilliQ distilled water plus the Bradford reagent and, when necessary, Bovine serum albumine that is the protein considered) in flow with the two available flow meters. Then checked if the flow meters stabilized the production and in particular allowed good repeatability and reproducibility of curves as a function of length.
Different measures have been carried on and I specify these in the following.

Dependence on the height of the outlet I changed the height of the drain of the microfluidic chip (eight measures for each regime chosen) with fixed Q_c and Q_d, at the same levels. I studied the influence of the height of the drain on the system. Used two comparison schemes:

- $Q_c = 25\ \frac{\mu l}{min}$ and Q_d such that the length of the droplets (L) was approximately two times the width of the channel (squeezing regime) (12 $\frac{\mu l}{min}$). This was referred as the regime 1;
- $Q_c = 50\ \frac{\mu l}{min}$ and Q_d such that L was about twice the width of the channel (24 $\frac{\mu l}{min}$). This was referred as regime 2.

Considered the following drain heights for both regimes: Δh = (20 - 18 - 16 - 14 - 12 - 10 - 8 - 6) cm. As a procedure to follow, I proceeded as follows:

1 I entered the desired levels and set the height of the drain at 20 cm above the working table (taken as reference);

2 I carried out all the measurements for one of the two Q_d-Q_c flow regimes consecutively over about ten minutes, changing only the height of the drain and instantly recording the measurements. I neglected implicitly the temporal evolution since I stayed no longer than 10 minutes total;

3 I replaced liquids in the tubes;

4 I repeated the measurements with the other Q_d-Q_c flow regime consecutively in about ten minutes.

In the data analysis, I had to determine optical parameters from the measurements with photodiode (transit time, integral of the signal, etc...) associated with the signal. From the measurements with the CCD I had to look at the length and actual speed of the droplets associated with each train considered. Then plotting the optical parameters and L and v as a function of height of the drain, estimate the rate of change due to the height of the drain.
What follows are the result obtained. I report all the parameters obtained from the photodiode as a function of the drain height for both regime; then all the parameters obtained from the camera (always considering both regimes). Then at the end I make some observation on what can be seen.

Figure A.2: The transit time and the normalized integral as a function of the drain height for the double flow-meters controlled production method.

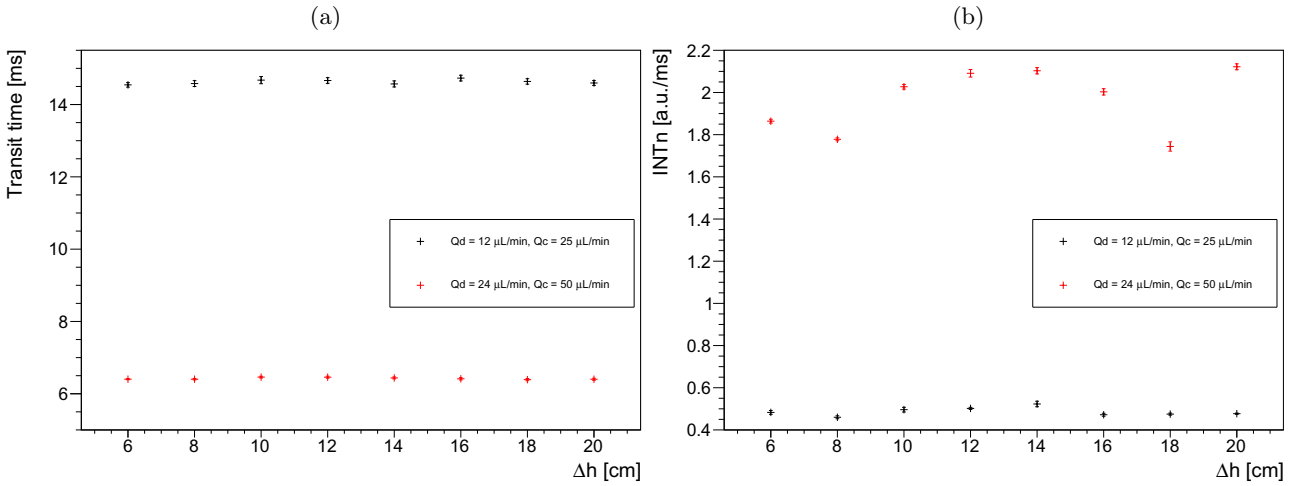

Figure A.3: The frequency and the integral as a function of the drain height for the double flow-meters controlled production method.

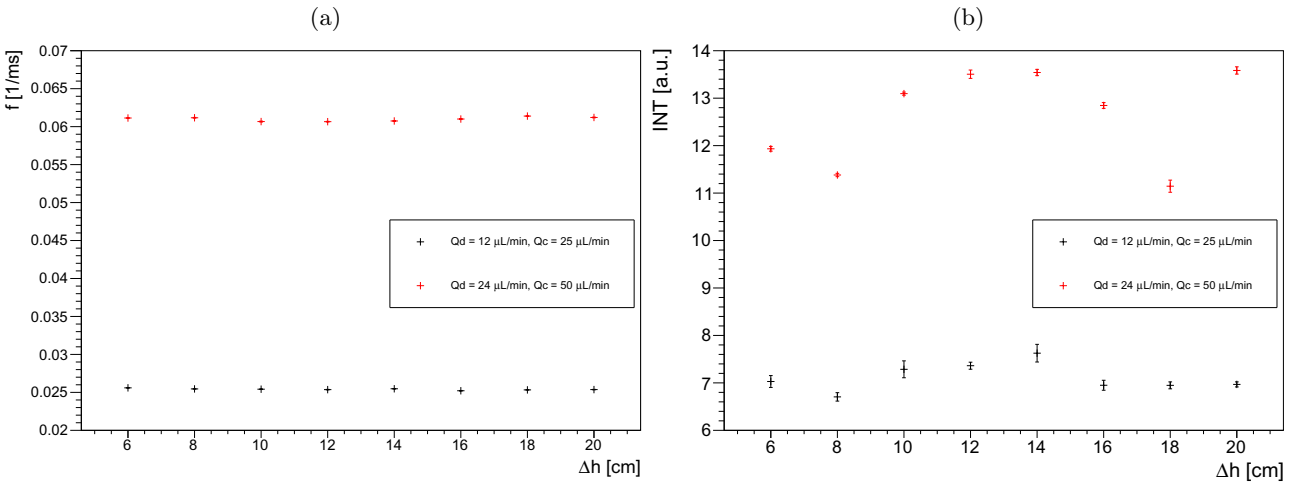

Figure A.4: The lenght of the droplets and the velocity as a function of the drain height for the double flow-meters controlled production method.

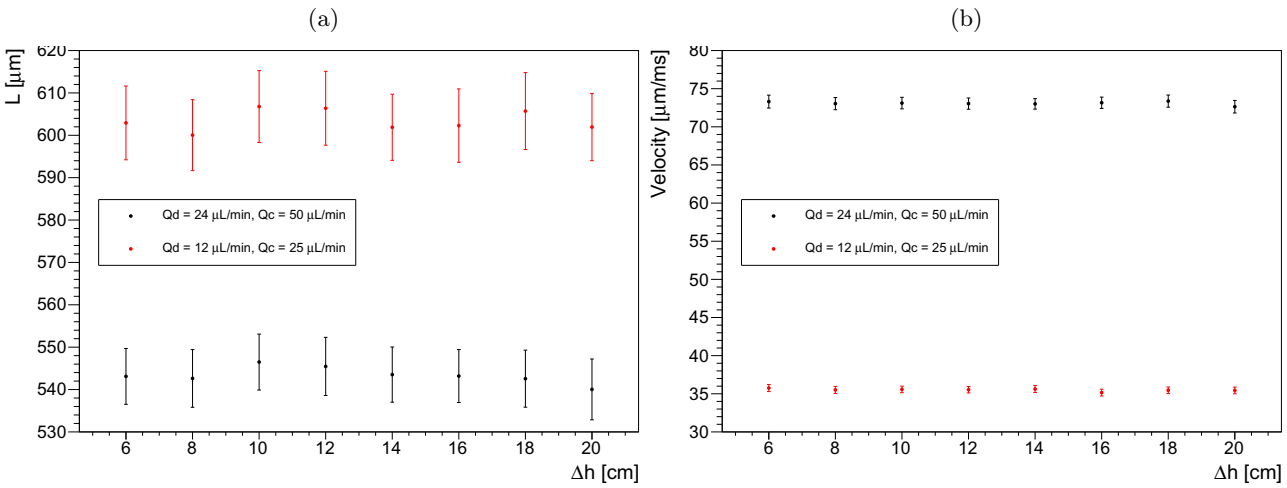

The drain height does not influence greatly the longitudinal dimension nor the velocity of the droplets; this is true for both regimes. The same can be said for the frequency of the droplets production. Talking about the normalized integral and the integral, instead, a noticeable perturbation of the system is observed: in particular the most affected regime is the second one, $Q_c = 50\ \frac{\mu l}{min}$ and $Q_d = 24\ \frac{\mu l}{min}$. This was one of the various hints that lead us later to choose the first regime ($Q_c = 25\ \frac{\mu l}{min}$ and $Q_d \approx 10\ \frac{\mu l}{min}$) for the consequent measures that involved the proteins. Just to mention, no official measurements have been taken regarding the levels of the fluids inside the test tubes (as we will see for the pressure controlled production method) because the usage of flow-meters allowed to monitor greatly the pressure and the fluxes of the system. By the way from an unofficial point of view, no effects of the volumes of fluids inside the test tubes on the system has been noted.

Curve study The study of the trend of the various parameters (both optical and geometrical) as a function of the flux of the dispersed phase (so as a function, also, of the length of the droplets since the correspondence between them; see [12]). Five curves spread over three days (three on a single day and another two on two different days) with both photodiode and camera, fixed Q_c and varying Q_d, with the same levels (starting) and height of the drain, have been taken (four curves, instead, for the regime 1). Used two comparison schemes:

- $Q_c = 25\ \frac{\mu l}{min}$ and varying Q_d along the whole droplet production range (avoiding extreme dripping on the lowest side of dispersed phase flux and avoiding co-flow on the other side, when $\frac{Q_d}{Q_c} \approx 1$).
- $Q_c = 50\ \frac{\mu l}{min}$ and varying Q_d along the whole droplet production range (same conditions as above).

Regarding the data analysis, I had to determine the optical parameters (transit time, integral of the signal, etc...) associated with the signal from the measurements with the photodiode. From the measurements with the camera, determine the length and the actual speed of the droplets associated with each train considered. Then plotting the optical parameters of the transit time sometimes expressed as T_t (ms) as a function of the parameters L and v, estimate the rate of dispersion in the curve.
Let's first focus on the regime 1:

Figure A.5: The transit time and the normalized integral as a function of the quotient between Q_d and Q_c, for the regime 1, for the double flow-meters controlled production method.

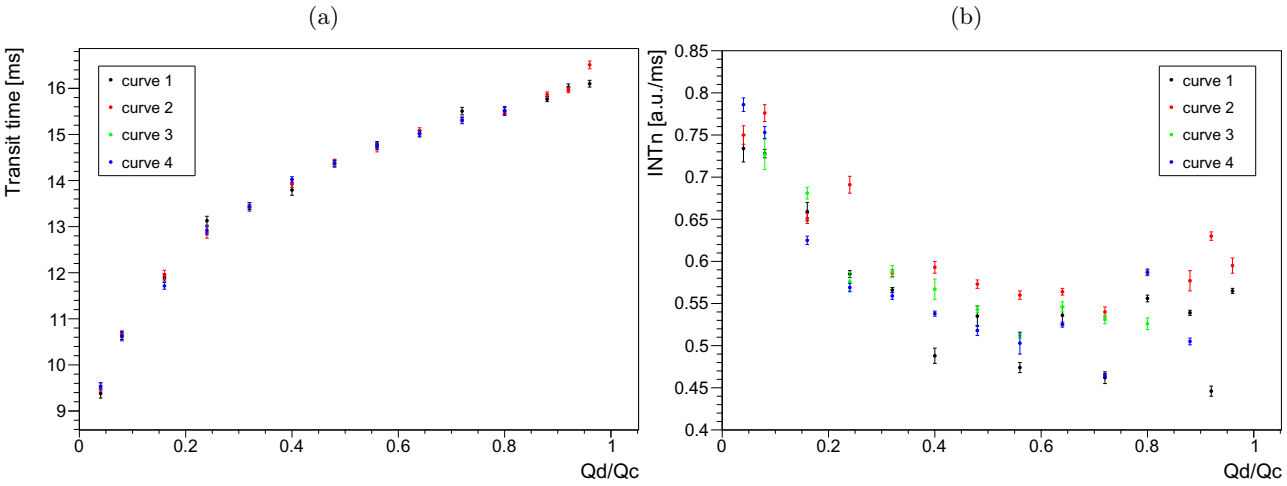

Figure A.6: The length of the droplets and the velocity as a function of the quotient between Q_d and Q_c, for the regime 1, for the double flow-meters controlled production method.

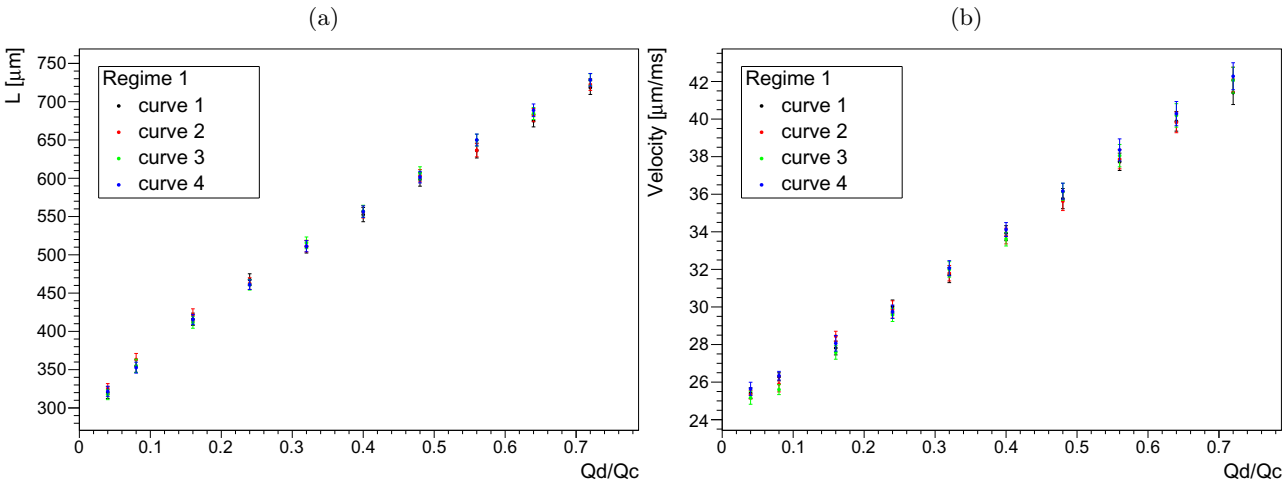

Now, talking about the regime 2:

Figure A.7: The transit time and the normalized integral as a function of the quotient between Q_d and Q_c, for the regime 2, for the double flow-meters controlled production method.

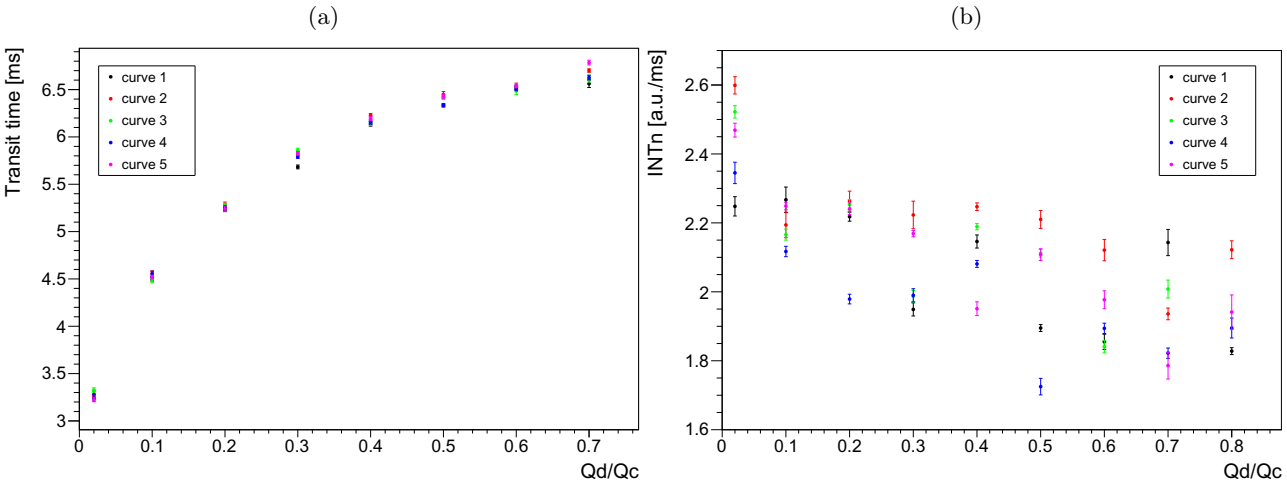

Figure A.8: The length of the droplets and the velocity as a function of the quotient between Q_d and Q_c, for the regime 2, for the double flow-meters controlled production method.

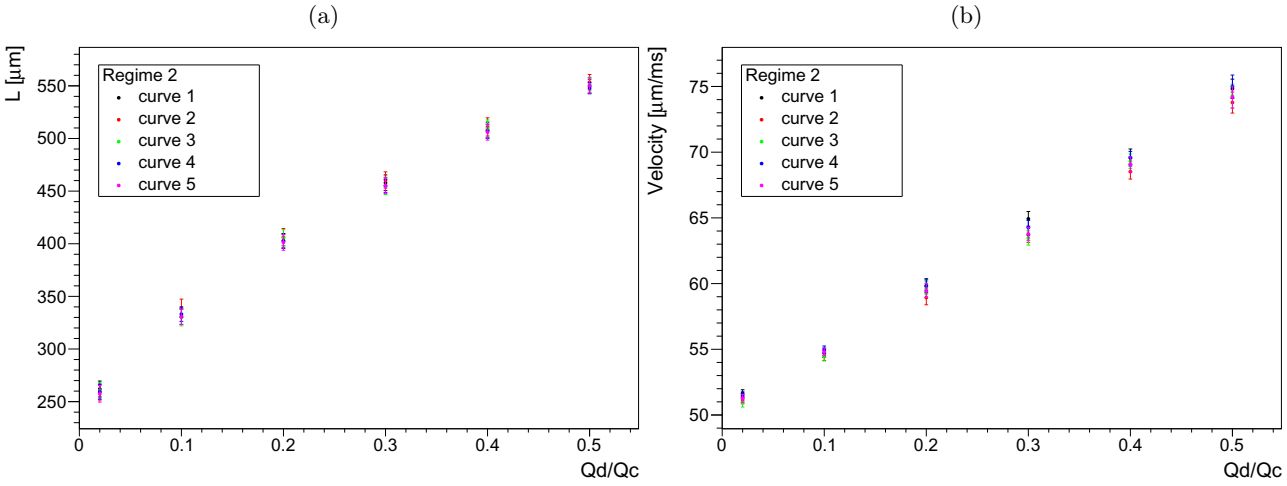

By taking a look at each single regime individually and also by comparing them (always with in mind the aim to find out both the best production method and the best conditions to take the final measurements) I observe briefly the following things.
The curves trending is similar to the one predicted by Garstecki [12] (talking about the length of the droplets, and so the transit time also, it increases almost linearly with the increase of Q_d/Q_c). The velocities follow the most rational trend after the last observation made. This said there is a big difference when looking at the normalized integral: it seems possible to extrapolate a trend in a much easier way by considering the regime 1 with respect to the regime 2, where the normalized integral manifests itself as a very scattered sequence of points as a function of Q_d/Q_c.
Next, focusing on the regime 1 only, we can also start identifying a range of Q_d where the INTn is almost linearly decreasing with respect to Q_d (with Q_c fixed): this, plus more others considerations, lead us later to take measurements for the detection of proteins in the range of Q_d = (2, 3, ..., 10) $\frac{\mu l}{min}$ in agreement with what we see here.
Just to mention, it is also helpful to observe the following graphs, in which we show the trend of INTn as a function of the length of the droplet both in micrometers and in milliseconds (transit time). Comparing the two regimes, it is again observed that the situation is more organized for regime 1.

Figure A.9: The normalized integral as a function of the transit time and the length of the droplets in micrometers (for the regime 1) for the double flow-meters controlled production method.

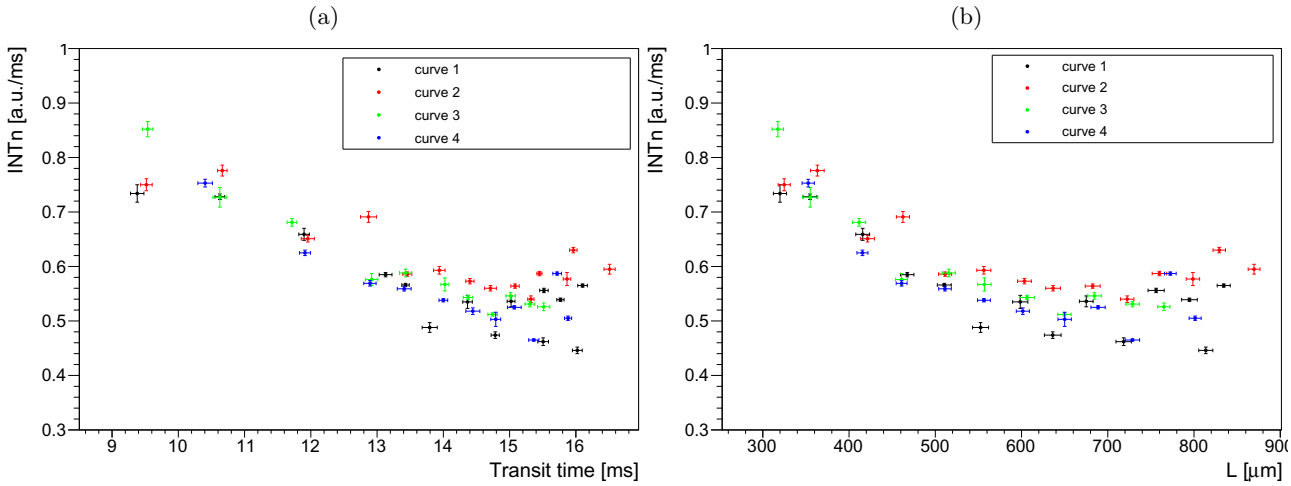

Figure A.10: The normalized integral as a function of the transit time and the length of the droplets in micrometers (for the regime 2) for the double flow-meters controlled production method.

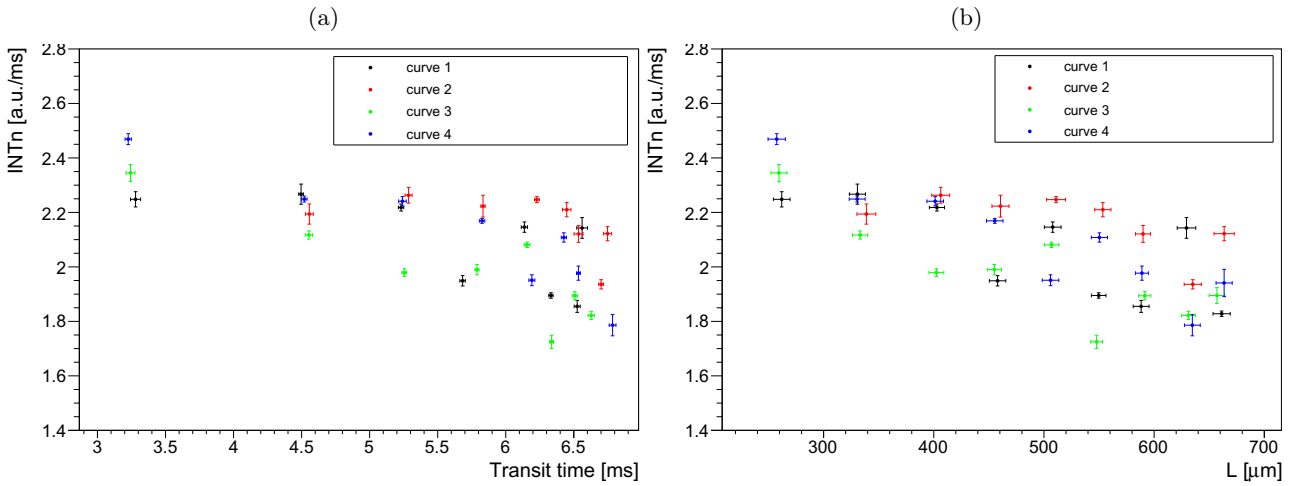

Measurements in time Measurements over time (60 minutes) without refilling the test tubes containing the fluids to compensate for the usage of those.
I had to estimate the evolution of the parameters of the droplets at fixed Q_c and Q_d flows: every four minutes, acquire with both photodiode and camera. Used two comparison regimes:

- $Q_c = 25\ \frac{\mu l}{min}$ and Q_d such that L is approximately two times the width of the channel ($12\ \frac{\mu l}{min}$).
- $Q_c = 50\ \frac{\mu l}{min}$ and Q_d such that L is about twice the width of the channel ($24\ \frac{\mu l}{min}$).

In the data analysis, I had to first determine the optical parameters (transit time, integral of the signal, etc...) associated with the signal from the measurements with the photodiode, and from the measurements with the CCD the length and the actual speed of the droplets associated with each train considered. Next plotting the parameters as a function of time, estimate the evolution of those in time.

Figure A.11: The transit time and the normalized integral as a function of time (for both regimes) for the double flow-meters controlled production method.

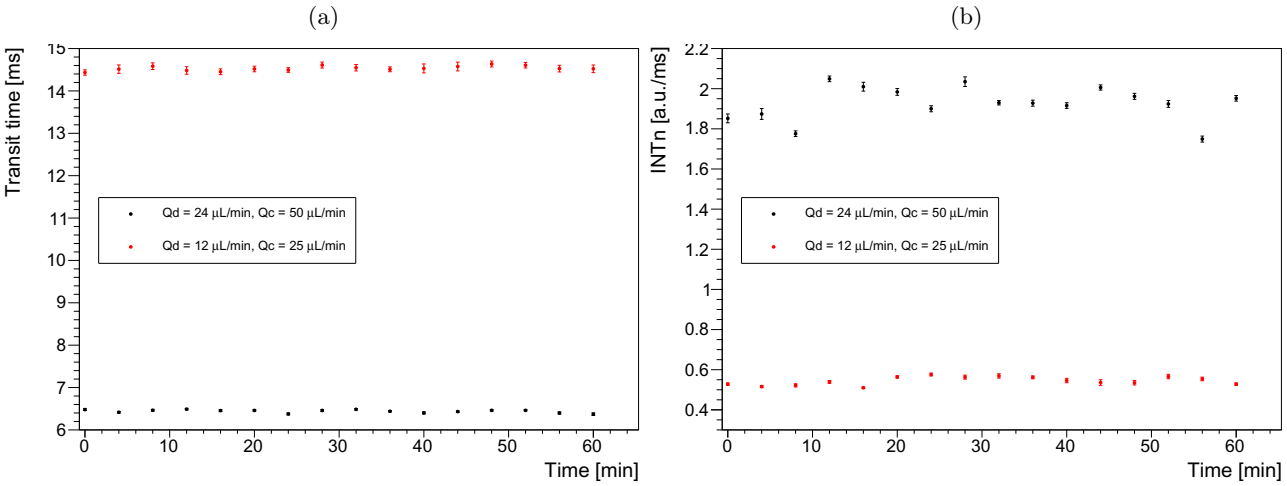

Figure A.12: The length of the droplets in micrometers and the velocity as a function of time (for both regimes) for the double flow-meters controlled production method.

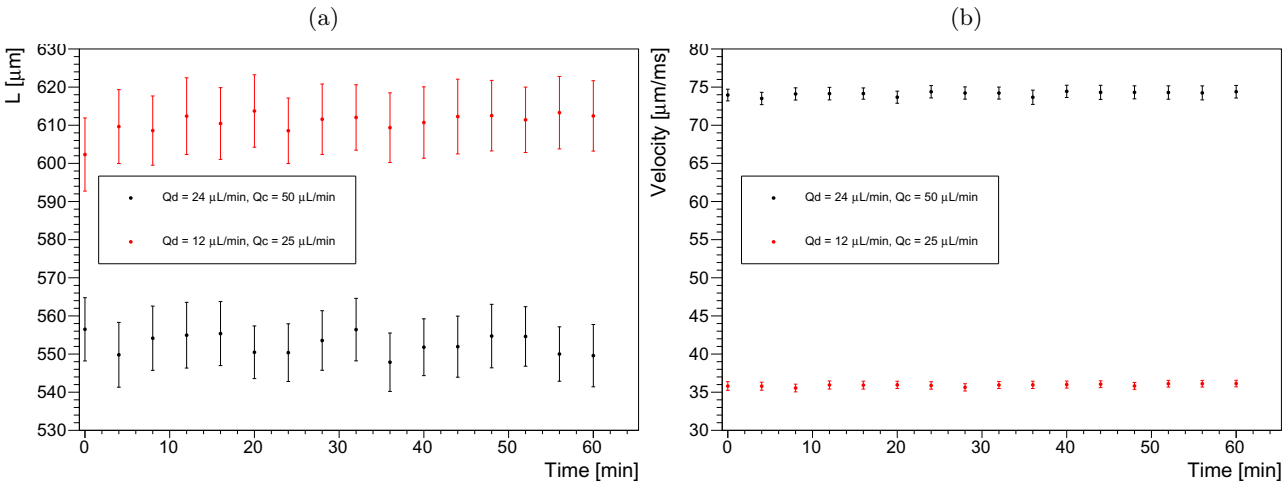

Figure A.13: The evolution in time of the frequency of the droplets.

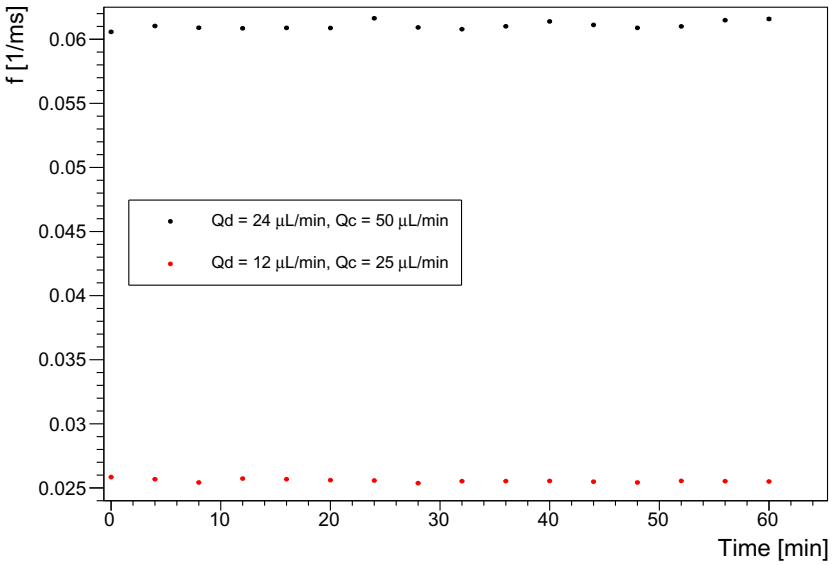

Talking about the regime one, it doesn't seem to be affected that much by the evolution in time of the system (considering all the parameters). The regime two, instead, seems to have some slight oscillations both for the length and the normalized integral.

Single droplet reproducibility With photodiode and camera, I had to study the reproducibility on a single droplet at different times and days, acquiring about twenty/twenty-five measurements at different times and days at fixed Q_c and Q_d flows and at the same levels in the tubes and height of the exhaust, estimating length and error associated with photodiode and camera. Used two comparison schemes:

- $Q_c = 25\ \frac{\mu l}{min}$ and Q_d such that the length of the droplets produced is approximately two times the width of the channel ($12\ \frac{\mu l}{min}$); this is called regime one.
- $Q_c = 50\ \frac{\mu l}{min}$ and Q_d such that L is about twice the width of the channel ($24\ \frac{\mu l}{min}$); this is called regime 2.

Regarding the data analysis, I had to determine the transit time associated with the signal and its dispersion, from the photodiode measurements, and also the effective length and its dispersion from the video measurements. Then I had to determine the cross video-photodiode scatter plots for each droplets' train acquired.
The measurements were spread over at least three subsequent days equally (three/four in the morning and three/four in the afternoon for three consecutive days), avoiding subsequent consecutive acquisitions.

Figure A.14: Here the cross video-photodiode scatter plot for the regime 1 is reported. The transit time is plotted in relation with the length of the droplets.

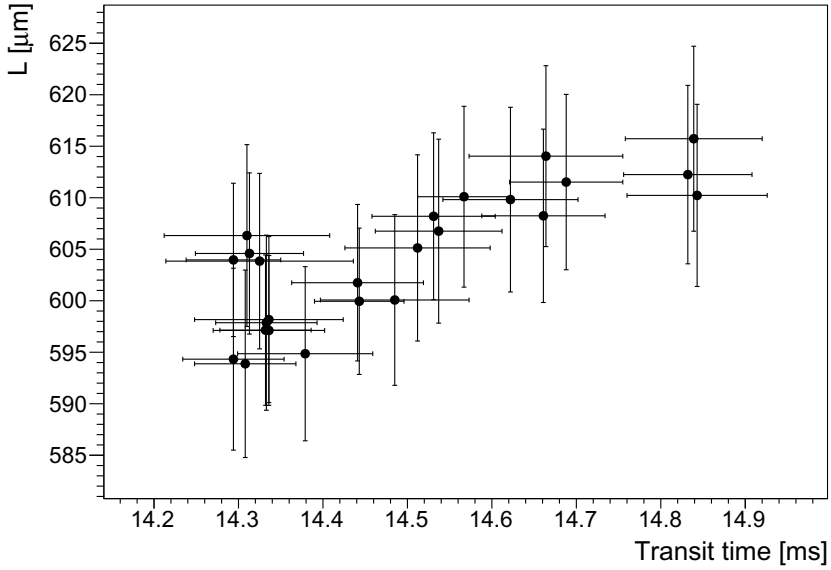

Figure A.15: Here the cross video-photodiode scatter plot for the regime 2 is reported. The transit time is plotted in relation with the length of the droplets.

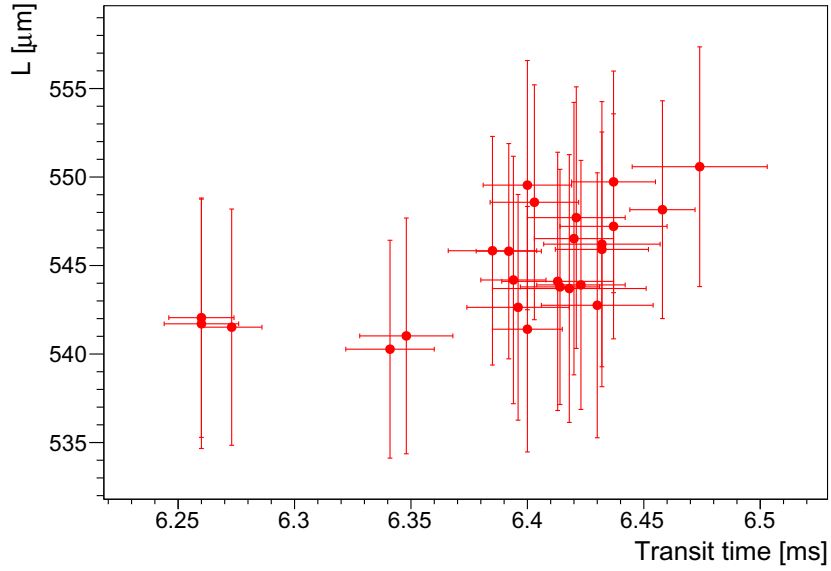

As can be seen from these plots, the reproducibility of the single droplet parameters is good . Almost all points seem to be concentrated in one region of the image.

A.1.3 Final observations

Let's summarize what we have seen:

- there is no noticeable effect on the L and v due to the variation of the amount of liquids during the measurements;
- there is no trending variation of L and v in time during a measurement;
- the exhaust height does not influences the dimension nor the velocity of the droplets;
- the curves trending is similar to the one predicted (L increase almost linearly with the increase of Q_d/Q_c);
- good reproducibility of the dimension of droplets.

This said, a problem emerge: although it seems that the apparatus, as it is, is suitable for measures to detect proteins, an obstacle for the moment is binding, i.e. concerning the fact that although the two flow meters are very reliable for measurements, they do not allow objects to be introduced inside due to how they are designed.
In this regard it was necessary to investigate, before finding a solution to solve the problem of this apparatus without discarding it, other methods of producing droplets that would allow the insertion of objects (such as proteins) into the dispersed phase by default.
These are: an apparatus based on pressure control such that the dispersed phase passes directly from the test tubes to the chip without requiring the use of flow meters; a control that uses a flow meter for the continuous phase (proteins or objects in general are inserted only in the dispersed phase) and a syringe pump for the dispersed phase which allows the injection into the chip of a fluid with possibly the presence of a particulate matter.

A.2 Pressure controlled production

A.2.1 Setup scheme

Figure A.16: Diagram of the experimental apparatus for droplet measurements with the pressure controlled configuration.

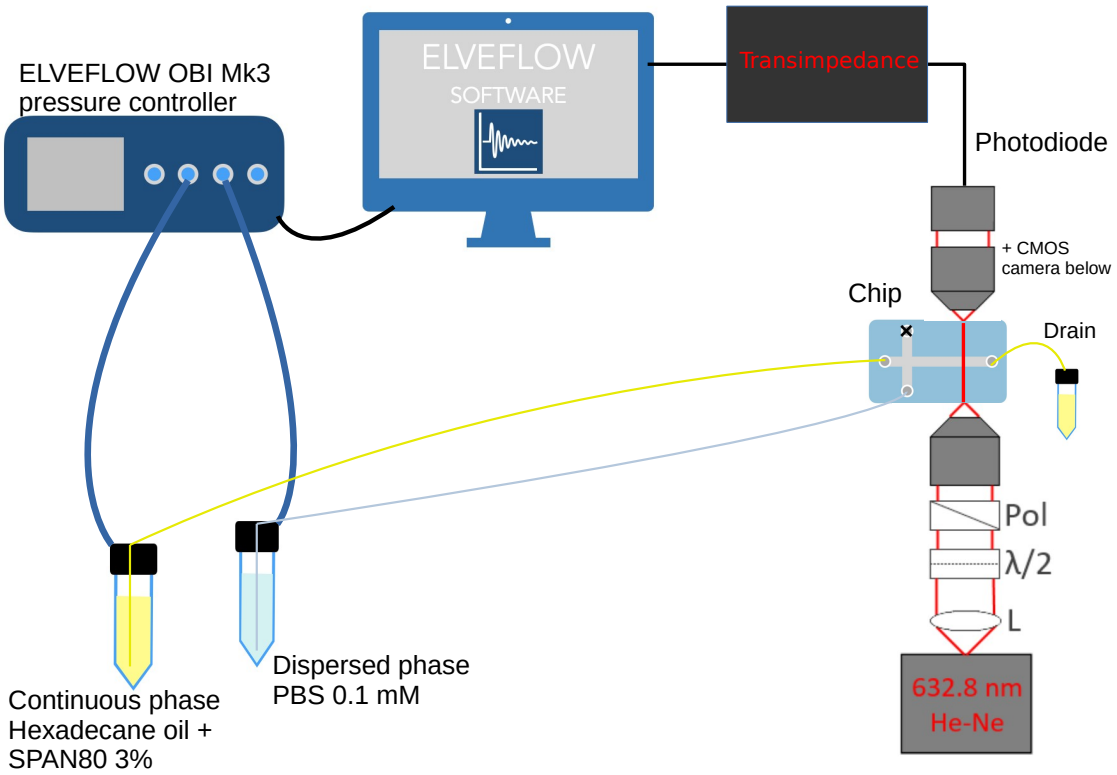

A.2.2 Characterization

With the sample in collinear guide configuration and using a T-junction as a droplet generator, I had to implement a droplet production control with optimal reproducibility at different times and days, comparing the production of droplets with a pressure controlled production method with other production methods. To this end, I had to check both the continuous phase (hexadecane oil with 3% surfactant) and the dispersed phase in pressure. Note that a functionalization of the channel has been done before the starting of this measurements session so I checked if any unusual effect happened due

to this.
Different measures have been carried on and I specify these in the following.

Dependence on the fluid levels in the test tubes Study the influence of the variation of levels in the oil and PBS test tubes with P_c and P_d fixed, with the same levels and height of the discharge, using two comparison regimes:

- P_c = 55 mbar and P_d = 35 mbar (regime 1).
- Pc = 100 mbar and P_d = 71 mbar; this is called regime 2.

Consider as levels for both schemes:

- Fixed oil levels (5 ml) with variable PBS levels: (8 - 7 - 6 - 5 - 4 - 3 - 2) ml
- Fixed PBS levels (2 ml) with variable oil levels: (8 - 7 - 6 - 5 - 4 - 3 - 2) ml

As a procedure to follow, I proceeded as follows:

1 I entered the desired levels;

2 I performed two consecutive measurements at fixed levels with P_d-P_c in the two regimes;

3 I replaced liquids in the tubes;

4 I performed again the measurements with new levels.

In the data analysis, I had to determine optical parameters from the measurements with photodiode (transit time, integral of the signal, etc...) associated with the signal, and from the measurements with the camera the length and actual speed of the droplets associated with each train considered. Plotting the optical parameters and L and v as a function of the levels of test tubes, estimate the rate of change due to the volumes of fluid (height) in the test tubes.

Figure A.17: The transit time and the normalized integral as a function of the level of the PBS in the test tube (for both regimes) for the pressure controlled production method.

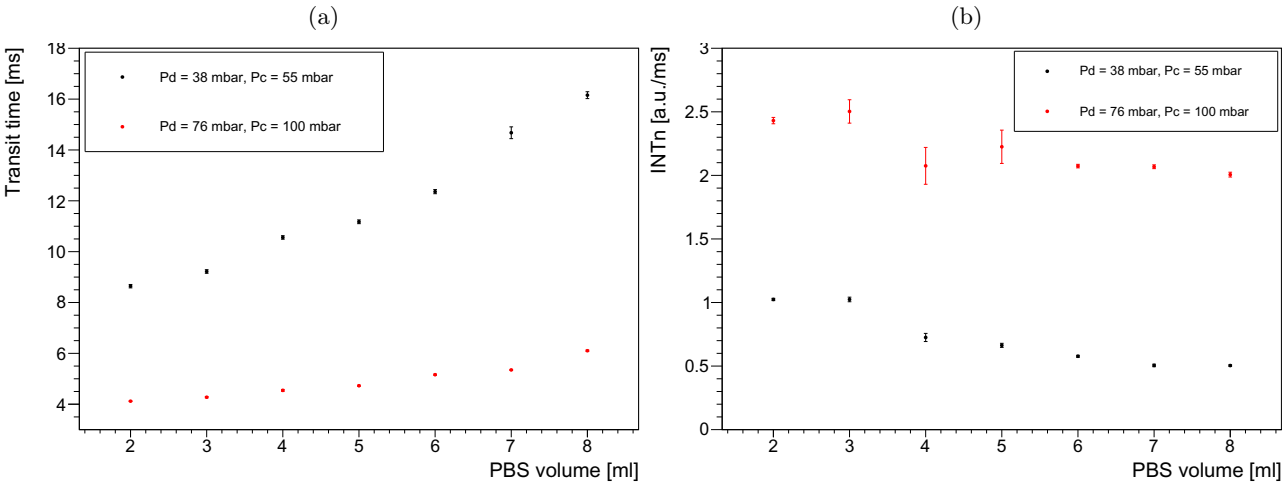

Figure A.18: The transit time and the normalized integral as a function of the level of the Hexadecane in the test tube (for both regimes) for the pressure controlled production method.

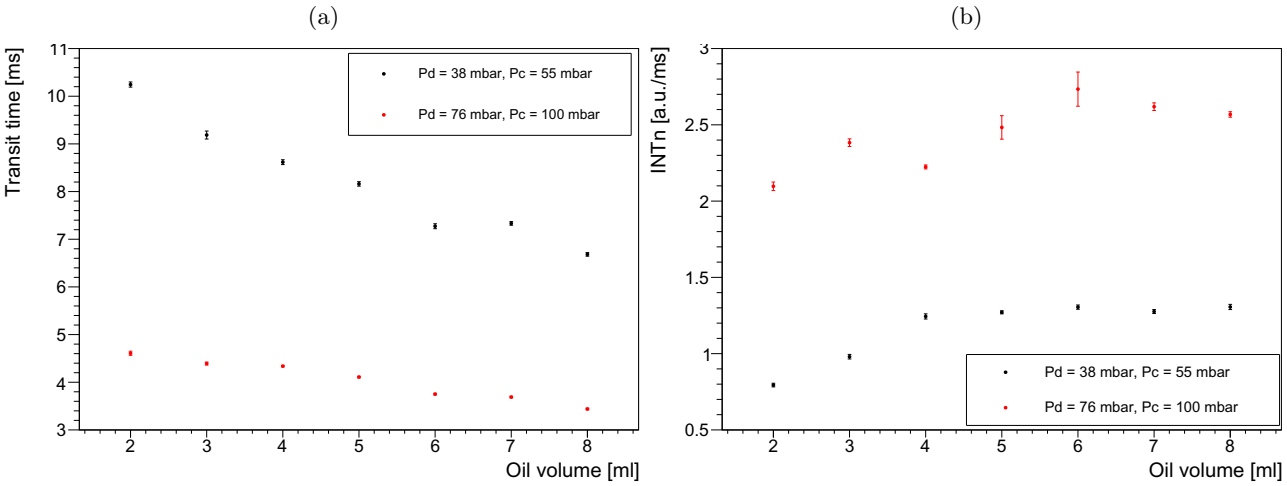

As expected, due to the contribution of the hydro-static pressure (that changes in time since the height of fluids are changing), a variation in the length of the droplets is observed in both regimes. Due to how is constructed, also the normalized integral is affected.

Curve study The study of the trend of the various parameters (both optical and geometrical) as a function of the pressure of the dispersed phase (so as a function, also, of the length of the droplets since the correspondence between them). Three curves spread over three days with both photodiode and camera, fixed P_c and varying P_d, with the same levels (starting) and height of the drain. Used the following regime: $P_c = 55$ mbar and varying P_d along the whole droplet production range. Regarding the data analysis, determine the optical parameters (transit time, integral of the signal, etc...) associated with the signal from the measurements with the photodiode. We saw that the measurements with the camera are redundant so I omit them. Then plotting the parameters estimate the rate of dispersion in the curve.

Figure A.19: The transit time and the normalized integral as a function of the ratio between P_d and P_c for the pressure controlled production method.

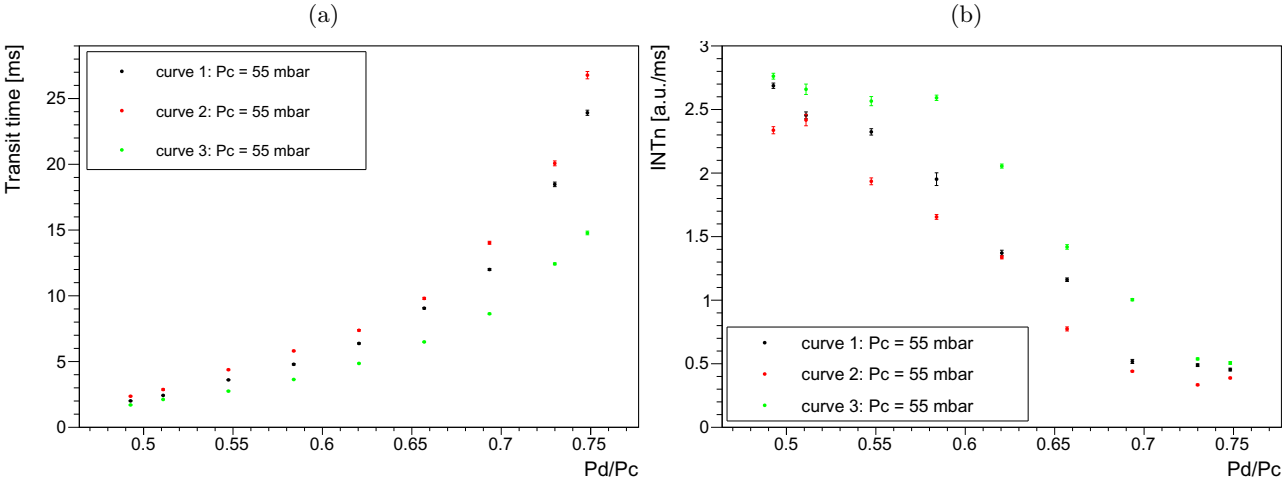

Since it is possible to relate the pressures with the fluxes, what we said already for the double flow meters production method is also true here: the curves trending is similar to the one predicted by Garstecki [12] (talking about the length of the droplets, and so the transit time also, it increases almost linearly with the increase of P_d/P_c). This time is also important to observe that the range

of L (transit time but also the length) is very big and this is probably also due to the phenomenon mentioned above (during the measurements, the levels of liquids decrease so the contribution of the hydro-static pressure does).

Measurements in time Measurement over time (60 minutes) (without refilling the solutions in the test tubes to compensate for the usage of those) to study the evolution of parameters in time at fixed P_c and P_d pressures: every four minutes, acquire both with photodiode and camera. Used two comparison regimes:

- $P_c = 55$ mbar and $P_d = 35$ mbar.
- $P_c = 100$ mbar and $P_d = 71$ mbar; this is called regime 2.

In the data analysis, determine the optical parameters (transit time, integral of the signal, etc...) associated with the signal from the measurements with the photodiode, and from the measurements with the CCD the length and the actual speed of the droplets associated with each train considered. Next plotting the optical parameters and L and v as a function of time, estimate the rate of changes in the shape of the droplet in time.
I report here just one regime (the first) for simplicity.

Figure A.20: The transit time and the normalized integral as a function of time (for regime 1) for the pressure controlled production method.

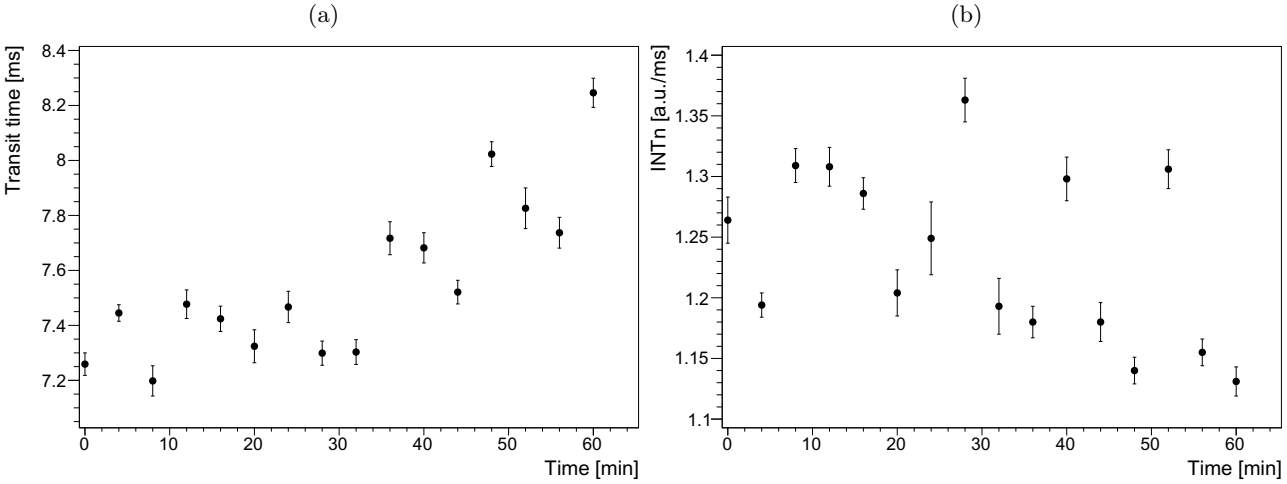

Figure A.21: The length of the droplets in micrometers and the velocity as a function of time (for regime 1) for the pressure controlled production method.

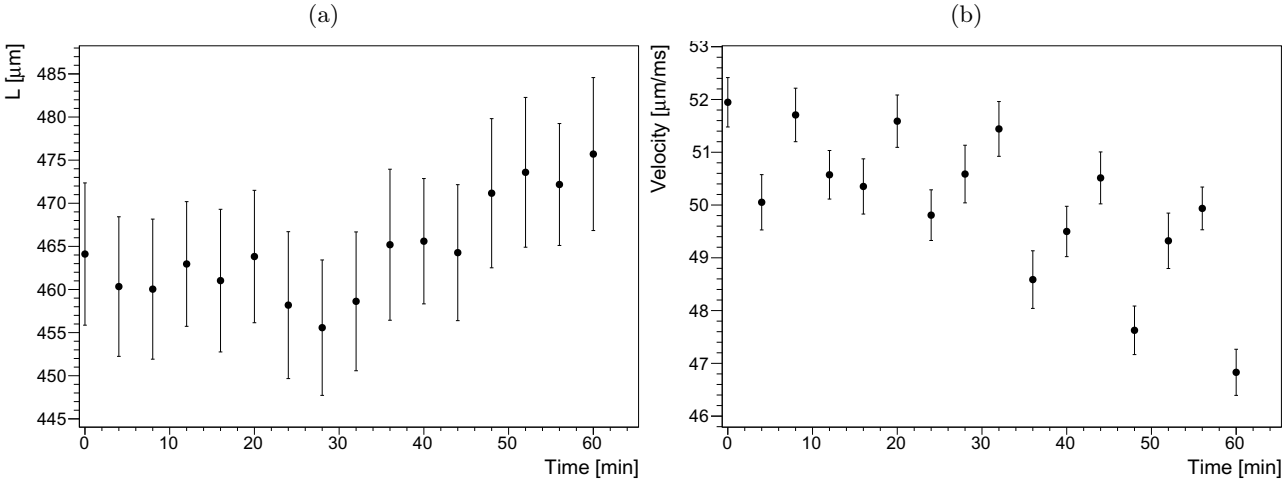

Once again, due to the contribution of the hydro-static pressure (that changes in time since the height of fluids are changing), a variation in the length of the droplets is observed and so also in the other parameters.

Single droplet reproducibility With photodiode and camera, study the reproducibility on a single droplet at different times and days, acquiring about twenty/twenty-five measurements at different times and days at fixed P_c and P_d pressures and at the same levels in the tubes and height of the exhaust, estimating length and error associated with photodiode and camera. Use two comparison schemes:

- $P_c = 55$ mbar and $P_d = 35$ mbar.
- $P_c = 100$ mbar and $P_d = 71$ mbar; this is called regime 2.

Regarding the data analysis, I had to determine the transit time associated with the signal and its dispersion, from the photodiode measurements, and also the effective length and its dispersion from the video measurements. Then I had to determine the cross video-photodiode scatter plots for each train of droplets acquired and the histograms relating L to the transit time.
Unfortunately it was not possible to carry out reproducibility measurements of the single droplet due to the fact that the same conditions could not be obtained on different days. In particular, a too large variation was observed from the point of view of the geometry of the droplet, setting the same pair of pressures, taking measurements on different days. The range of P_d within which we were distant from dripping and co-flow changed from day to day which means that to obtain droplets of similar length the pressures would have to be varied, which is not feasible from the point of view of the reproducibility study. We wondered about the cause of this problem, as it was probably linked to the chip and disappeared after a few days from the start of data taking (it should be noted that chronologically the method of production of droplets under pressure was first studied and then that in flow and no critical issues were observed for the latter). A probable cause is traced back to the functionalization of the microfluidic channel carried out shortly before the start of the measurements. In fact, there could have been some remnants or residues that could have altered, for example, the wettability of the channel and that with the flow of fluids inside have gradually decreased until no longer invalidating the following measurements once a condition of stability. Clearly this is only a hypothesis but it also seems a plausible cause based on the observed dynamics.

A.2.3 Final observations

Let's summarize what we have seen:

- the amount of liquid inside the test tubes vertically placed (both continuous and dispersed phase) influences greatly the longitudinal dimension of the droplets;
- looking at the curves, the range of L is very big also due to the previous effect (during the measurements the levels of liquids decrease);
- slight increase of L in time and decrease of v;
- very bad reproducibility in different days (the study wasn't carried on due to the big changes of range in Pressure from dripping to co-flow). Notice that this maybe was due to the recent functionalization of the channel since the pressure driven flow control was the first to be studied.

This said is important to mention that it was possible to introduce small particles/object in the dispersed phase with this type of control. Unfortunately the above results suggest that the flow control is much more reliable in order to guarantee repeatability and reproducibility conditions, necessary in the case in which the presence of proteins inside the produced droplets has to be revealed.

A.3 The usage of a syringe pump

A.3.1 Setup scheme

Figure A.22: Diagram of the experimental apparatus for droplet measurements with the usage of a syringe pump.

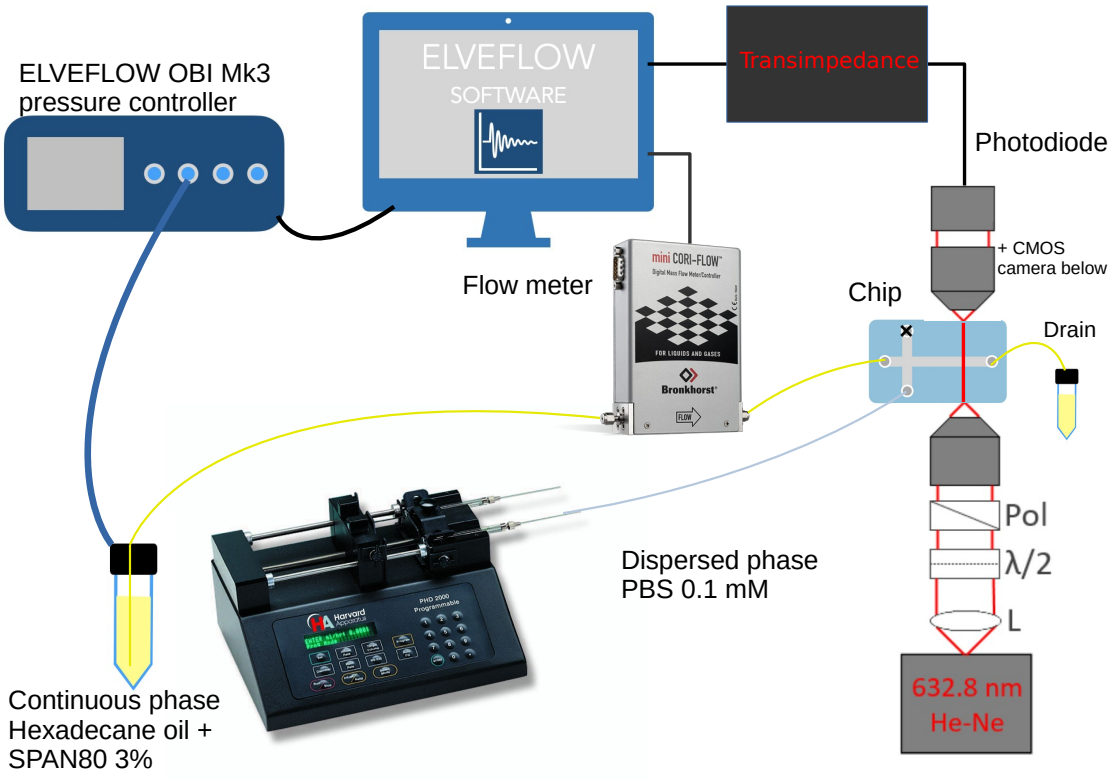

A.3.2 Characterization

With the sample in collinear guide configuration and using a T-junction as a droplet generator, I had to implement a droplet production control with optimal reproducibility at different times and days, comparing the production of droplets with flow control with one flow meter and one syringe pump (used for the dispersed phase) with other production methods. To this end, I had to check both the continuous phase (hexadecane oil with 3% surfactant) and the dispersed phase controlled in flow with one flow meter for the continuous phase and one syringe pump for the dispersed phase. Then check if the syringe pump allows good reproducibility of curves as a function of length.
Different measures have been carried on and I specify these in the following. Note that all the observations will be placed after the plots with the results for simplicity and to avoid repetition since at this time the pattern is clear.

Curve study Reproducibility of the normalized integral curves as a function of length: four curves spread over three days (two on a single day and another two on two different days) with both photodiode and camera, fixed Q_c and varying Q_d, with the same starting levels and height of the drain. Used a single regime: $Q_c = 50\ \frac{\mu l}{min}$ and varying Q_d along the whole droplet production range.
Regarding the data analysis, determine the optical parameters (transit time, integral of the signal, etc...) associated with the signal from the measurements with the photodiode. From the measurements with the camera, determine the length and the actual speed of the droplets associated with each train considered. Then plotting the optical parameters of the transit time sometimes expressed as L (ms) as a function of the parameters L and v, estimate the rate of dispersion in the curve.

Figure A.23: The transit time and the normalized integral as a function of the ratio between Q_d and Q_c for the syringe pump controlled production method.

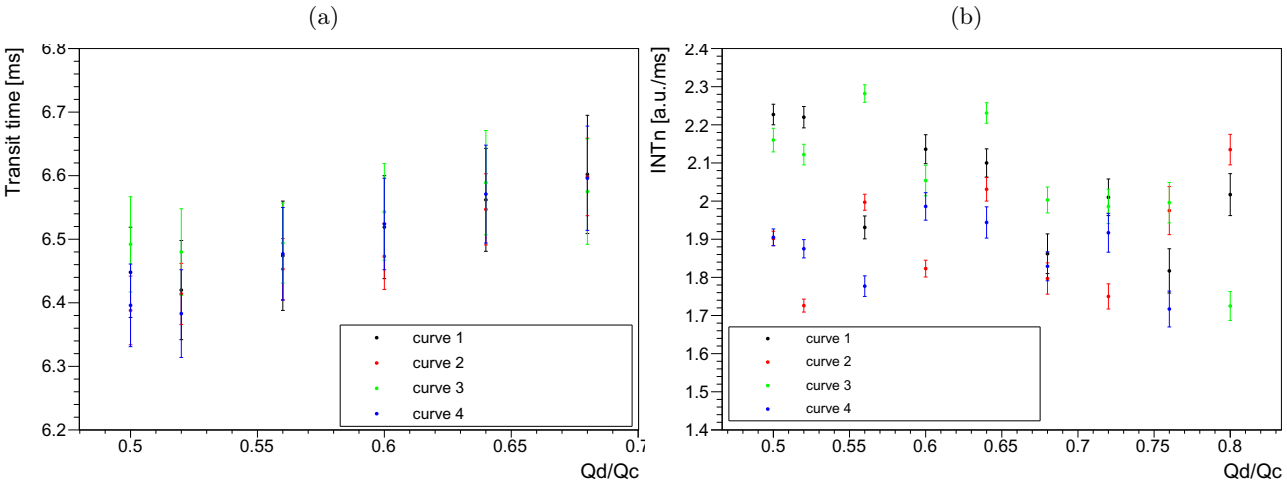

Figure A.24: The lenght of the droplets and the velocity as a function of Q_d for the syringe pump controlled production method. Here just the curve 3 and 4 are reported for simplicity since the redundancy of the camera-based information.

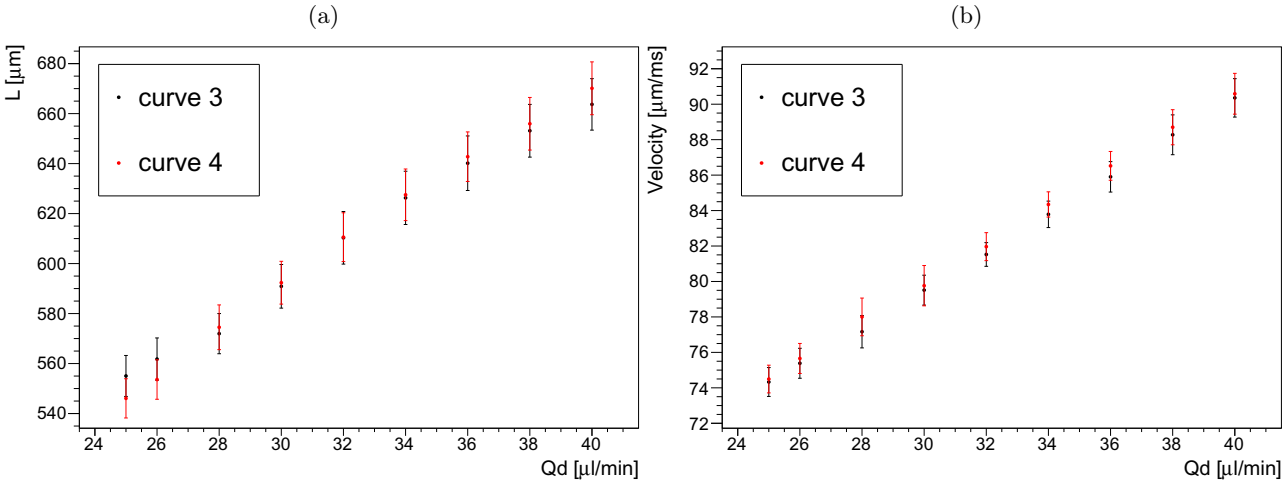

Measurements in time Measurement over time (60 minutes) (without refilling the solutions tanks to compensate for the usage of those) of the reproducibility of a single droplet at fixed Q_c and Q_d flows: every four minutes, acquire both with photodiode and camera. Used single regime: $Q_c = 50\ \frac{\mu l}{min}$ and Q_d such that L is approximately 2 times the width of the channel (35 $\frac{\mu l}{min}$). In the data analysis, determine the optical parameters (transit time, integral of the signal, etc...) associated with the signal from the measurements with the photodiode, and from the measurements with the CCD the length and the actual speed of the droplets associated with each train considered. Next plotting the optical parameters and L and v as a function of time, estimate the rate of changes in the shape of the droplet in time.

Figure A.25: The transit time and the normalized integral as a function of time for the syringe pump controlled production method.

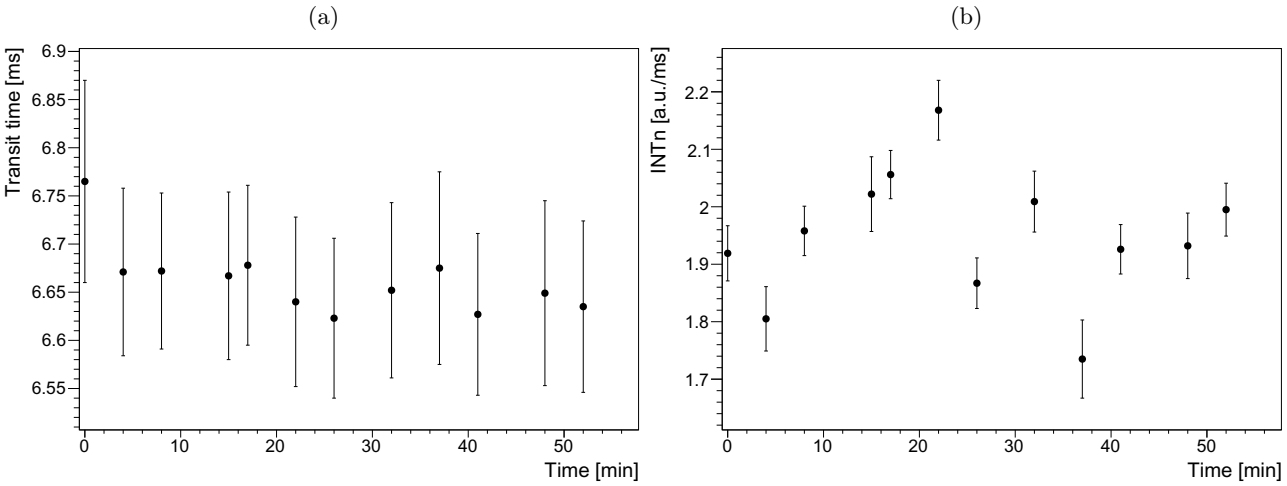

Figure A.26: The length of the droplets in micrometers and the velocity as a function of time for the syringe pump controlled production method.

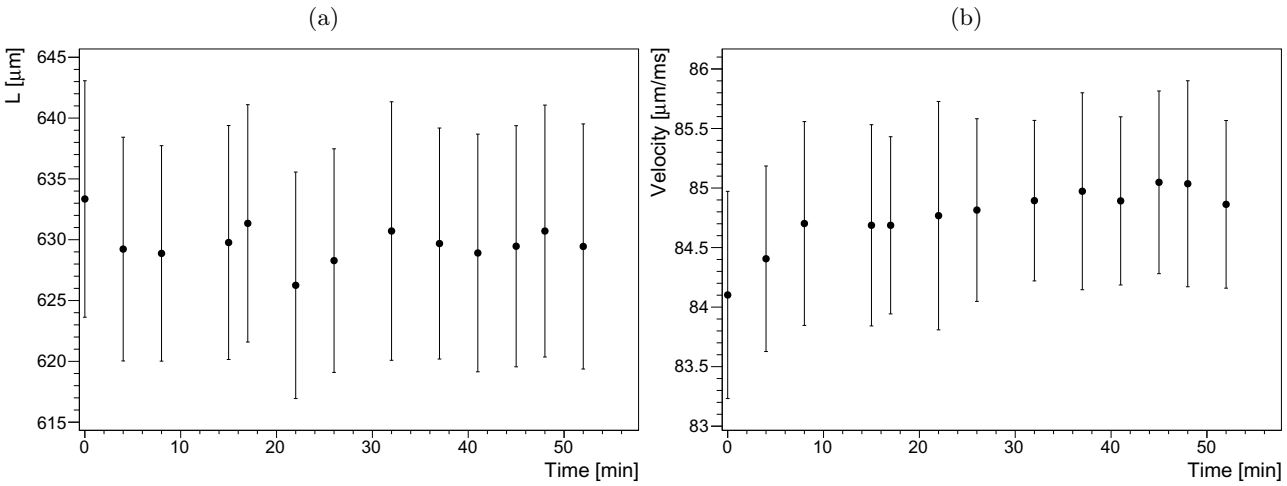

Single droplet reproducibility With photodiode and camera, study the reproducibility on a single droplet at different times and days, acquiring about twenty/twenty-five measurements at different times and days at fixed Q_c and Q_d flows and at the same levels in the tubes and height of the drain, estimating length and error associated with photodiode and camera. Used the regime: $Q_c = 50\ \frac{\mu l}{min}$ and Q_d such that the length of the droplets produced is approximately two times the width of the channel ($35\ \frac{\mu l}{min}$). Regarding the data analysis, I had to determine the transit time associated with the signal and its dispersion, from the photodiode measurements, and also the effective length and its dispersion from the video measurements. Then I had to determine the cross video-photodiode scatter plots for each droplets' train acquired and the histograms relating L to the transit time. The measurements were spread over three subsequent days equally (three/four in the morning and three/four in the afternoon for three consecutive days), avoiding subsequent consecutive acquisitions.

Figure A.27: Here the cross video-photodiode scatter plot is reported. The transit time is plotted in relation with the length of the droplets.

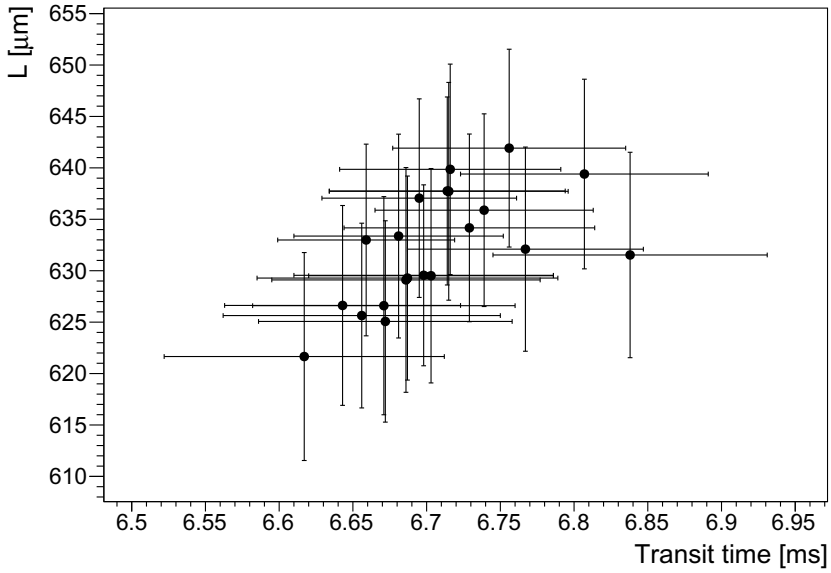

The problem of the oscillation of the fluxes Flow-rate fluctuations in microfluidic channels, where the flow rate is supplied by a syringe pump, are known phenomena. The flow-rate fluctuations come from the mechanical oscillations of the pump motor. In fact due to the presence of a screw (here I am considering just this type of syringe pumps) there are many and many microsteps. For this reason I observed qualitatively the behavior of the mass of liquid flowing out from PHD2000 Harvard Apparatus as a function of time to understand its viability as an experimental apparatus for my interests monitoring this phenomenon. Below I present some extremely qualitative data regarding the periods of oscillations as a function of Q_d, the amplitude of the oscillations as a function of Q_d and finally the relation between the period of oscillations and the diameter of the syringes. Indeed I used a set of three syringes with three different diameter as well as different material (glass and plastic) since both these factors are known in literature for affecting the system. A detailed study of this type of phenomenon was not part of my work of thesis but was carried in parallel to this work (L. Zanini, unpublished) so here I just present some qualitative trends that I had the possibility to observe by myself one day.

Figure A.28: The periods of oscillations as a function of Q_d.

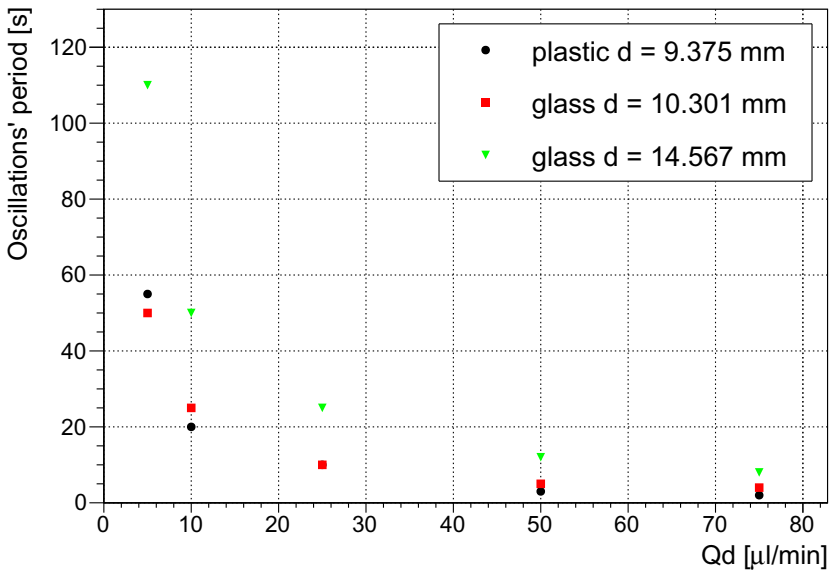

Figure A.29: The amplitude of the oscillations as a function of Q_d.

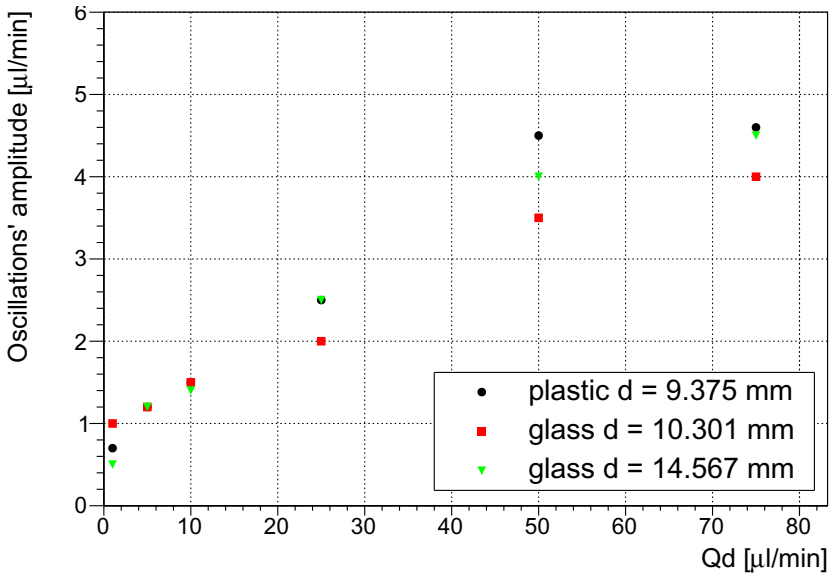

Figure A.30: The relation between the period of oscillations and the diameter of the syringes for a set of three syringes with three different diameter as well as different material (glass and plastic).

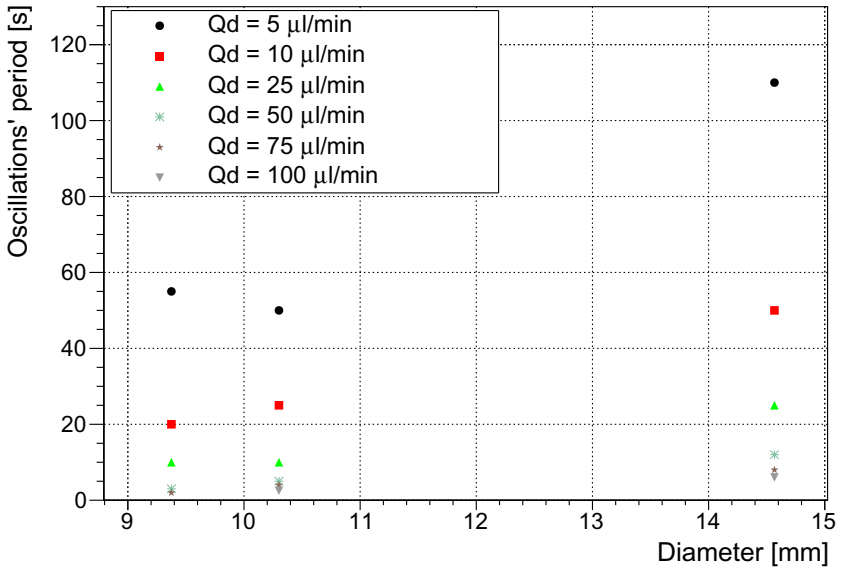

What I can observe is the following:

- there is a similarity with the result coming from a theoretical model: $T \approx \frac{d^2}{Q_d}$ where d is the diameter of the syringe and Q_d the flow of the dispersed phase controlled by the syringe pump;
- the observed periods are, actually, probably related to micro steps rather than the lead screw step, which should cause an oscillation of longer period than those reported here so far;
- for the plastic syringe, amplitude values have shown too much temporal evolution, so the preference for future usage will be glass (not very clear from these plots only);
- of the two available options for the glass ones, as expected, the one with a smaller diameter is preferable due to shorter period fluctuations (data can be taken by making the measurement last twice or three times longer than the periods such that after with the data analysis one can mediate the obtained values);
- no dependencies on the amplitudes as a function of diameter have been observed qualitatively.

A.3.3 Final observations

Let's summarize what we have seen:

- good curves trend as predicted;
- there is no trending variation of L and v in time during a measurement;
- there is the problem of the oscillations of the values of fluxes due to the step motor.

Despite it was possible to introduce small particles/object in the dispersed phase with this type of control we decided to use the double flow meter setup with a proper modification since the better reliability. This lead us the final configuration of the setup already discussed.

Bibliography

[1] G. Bettella. *Integrated Opto-Microfluidic Lab-on-a-Chip in Lithium Niobate for Droplet Generation and Sensing*. PhD thesis, PhD School of Physics, University of Padova, 2016.

[2] R. Zamboni. *Study of light driven phenomena for optofluidic applications in Lab-on-a-chip platforms in lithium niobate*. PhD thesis, PhD School of Physics, University of Padova, 2019.

[3] Marion Bradford. *"A Rapid and Sensitive Method for the Quantification of Microgram Quantities of Protein Utilizing the Principle of Protein-Dye Binding"*. Analytical Biochemistry 72 (1-2): 24-254,1976.

[4] Karolina A. Majorek, Przemyslaw J. Porebski, Arjun Dayal, Matthew D. Zimmerman, Kamila Jablonska, Alan J. Stewart, Maksymilian Chruszcz, Wladek Minor. *"Structural and immunologic characterization of bovine, horse, and rabbit serum albumins"*.Molecular Immunology 52 (2012) 174-182, 2012.

[5] S. Saoncella, *Applicazione optofluidica di uno spettrofotometro integrato in niobato di litio per misure di pH*, Tesi di laurea, Dipartimento di Fisica, Università degli studi di Padova (2016-2017).

[6] S. Saoncella, *Optical control of droplet motion on Fe-doped lithium niobate crystals via photovoltaic effect*. Master's thesis, Department of Physics, University of Padova, 2019.

[7] R. Zamboni. *Optofluidic application of a Mach-Zehnder interferometer integrated in lithium niobate for droplet sensing*. Master's thesis, Department of Physics, University of Padova, 2017.

[8] Lorenzo De Bortoli. *Study of light driven phenomena in integrated optomicrofluidic lithium niobate platforms*. 2017.

[9] Elena Izzo. *Studio della dinamica del viraggio di PH chimico mediante una piattaforma optomicrofluidica*. Laurea triennale, 2019.

[10] Giovanni Bragato. *Velocimetro per gocce microfluidiche basato su di un interferometro fotonico integrato in niobato di litio*. Laurea triennale, 2019.

[11] G. F. Christopher and S. L. Anna. *Microfluidic methods for generating continuous droplet streams*. Journal of Physics D: Applied Physics 40:319-336, 2007.

[12] P. Garstecki, M. J. Fuerstman, H. A. Stonec, and G. M. Whitesides. *Formation of droplets and bubbles in a microfluidic T-junction -scaling and mechanism of break-up*. Lab Chip, The Royal Society of Chemistry , 6:437-446, 2006.

[13] R. S. Weis and T. K. Gaylord. *Lithium niobate: Summary of physical properties and crystal structure*. Appl. Phys. A , 37:191-203, 1985.

[14] C. N. Baroud, F. Gallaire, and R. Dangla. *Dynamics of microfluidic droplets*. Lab Chip, The Royal Society of Chemistry , 10:2032-2045, 2010.

[15] Gordon F Christopher, N Nadia Noharuddin, Joshua A Taylor, and Shelley L Anna. *Experimental observations of the squeezing-to-dripping transition in t-shaped microfluidic junctions*. Physical Review E, 78(3):036317, 2008.

[16] L. Zanini. *Dispositivo opto-microfluidico in Niobato di Litio per la caratterizzazione di gocce con nanoparticelle d'Oro*. Tesi di laurea, Dipartimento di Fisica, Università degli studi di Padova, 2018.

[17] Patrick Tabeling. *"Introduction to microfluidics."*, OUP Oxford, 2005.

[18] Nam-Trung Nguyen, Steven T Wereley, and Seyed Ali Mousavi Shaegh. *"Fundamentals and applications of microfluidics."*, Artech house, 2019.

[19] `https://www.thermofisher.com/it/en/home/life-science/protein-biology/protein-assays-analysis/protein-assays/bradford-assays.html`

[20] `https://www.bio-rad.com/featured/en/bradford-assay.html`

[21] `https://en.wikipedia.org/wiki/Bradford_protein_assay`

[22] `https://www.sigmaaldrich.com/content/dam/sigma-aldrich/docs/Sigma/Bulletin/b6916bul.pdf`

[23] `https://en.wikipedia.org/wiki/Spectrophotometry`

[24] `https://root.cern.ch/download/minuit.pdf`

[25] `https://en.wikipedia.org/wiki/MINUIT`